INFORMATION TO USERS

This dissertation was produced from a microfilm copy of the original document. While the most advanced technological means to photograph and reproduce this document have been used, the quality is heavily dependent upon the quality of the original submitted.

The following explanation of techniques is provided to help you understand markings or patterns which may appear on this reproduction.

1. The sign or "target" for pages apparently lacking from the document photographed is "Missing Page(s)". If it was possible to obtain the missing page(s) or section, they are spliced into the film along with adjacent pages. This may have necessitated cutting thru an image and duplicating adjacent pages to insure you complete continuity.

2. When an image on the film is obliterated with a large round black mark, it is an indication that the photographer suspected that the copy may have moved during exposure and thus cause a blurred image. You will find a good image of the page in the adjacent frame.

3. When a map, drawing or chart, etc., was part of the material being photographed the photographer followed a definite method in "sectioning" the material. It is customary to begin photoing at the upper left hand corner of a large sheet and to continue photoing from left to right in equal sections with a small overlap. If necessary, sectioning is continued again — beginning below the first row and continuing on until complete.

4. The majority of users indicate that the textual content is of greatest value, however, a somewhat higher quality reproduction could be made from "photographs" if essential to the understanding of the dissertation. Silver prints of "photographs" may be ordered at additional charge by writing the Order Department, giving the catalog number, title, author and specific pages you wish reproduced.

University Microfilms

300 North Zeeb Road
Ann Arbor, Michigan 48106

A Xerox Education Company

73-2836

FOREST, George Joseph, 1944-
TUNNELING IN METAL-SEMICONDUCTOR JUNCTIONS.

The City University of New York, Ph.D., 1972
Physics, solid state

University Microfilms, A XEROX Company, Ann Arbor, Michigan

Tunneling in Metal-Semicnnductor Junctions

by

George J. Forest

A dissertation submitted to the Graduate Faculty in Physics in partial fulfillment of the requirements for the degree of Doctor of Philosophy, The City University of New York.

1972

This manuscript has been read and accepted for the Graduate Faculty in Physics in satisfaction of the dissertation requirement for the degree of Doctor of Philosophy.

8/2/72
date

Chairman of Examining Committee

7/26/72
date

Executive Officer

Professor Melvin Lax

Professor Arthur Paskin

Professor Oscar Lumpkin

Supervisory Committee

The City University of New York

PLEASE NOTE:

Some pages may have

indistinct print.

Filmed as received.

University Microfilms, A Xerox Education Company

Acknowledgements

I would like to gratefully acknowledge the help of Dr. Surender Puri during the early stages of this experiment. The technical assistance of Joe Lane, Jerry Cannella and the rest of the City College Shop made the construction of the equipment one of the most enjoyable aspects of the experiment. Randy Caton, who during his quest for a Ph.D., allowed me the use of his magnet should also be thanked, for his courage.

Of course, greatest thanks are due my thesis advisor, Dr. Erich Erlbach, for patience and encouragement in dealing with the numerous difficulties that were encountered.

Table of Contents

List of Figures	Page	1
Introduction	Page	5
Experimental Techniques	Page	34
Data Analysis	Page	66
Conclusion	Page	114
Tunneling Study of the Γ_2' level in Ge	Page	131
References	Page	150

Fig.	Page	Figure Title
1	24	Energy diagram of a simple metal with (b) and without (a) an applied electric field
2	26	Metal-Insulator-Metal junction without an applied bias (a) and with an applied bias (b)
3	28	Energy level diagram for a p-n junction without (a) and with (c) an applied bias Current vs Voltage for such a junction (b)
4	30	Incremental resistance (y axis) as a function of applied D.C. bias for Sn-Ge junction, $\mu_F \cong 25$
5	33	d^2I/dV^2 vs V for p-n junctions of Ge (a) and Si (b) and for m-s junctions of Ge (c) and Si (d)
6	52	Helium dewar and pumping lines
7	54	Cleavage device
8	56	Sample holder
9	58	Comparison of V vs I (c) and dI/dV vs V plots for determining the onset strength of process b compared to background a
10	60	Harmonic measuring circuit (a,c,d) and their equivalent circuits (b & e)

Fig.	Page	Figure Title
11	62	Harmonic measuring circuit (a) with D.C. bias and block diagram of our harmonic measuring circuit (b)
12	64	Harmonic measuring circuit of Thomas and Rowell
13	78	Incremental resistance (y axis) as a function of D.C. bias for Sn-Ge $\mu_F \cong 40mv$
14	80	Theoretical plot of incremental resistance vs D.C. voltage $\mu_F \cong 24mv$
15	82	Theoretical plot of incremental resistance vs D.C. voltage $\mu_F \cong 40mv$
16	84	Blow up of incremental resistance vs D.C. bias around the TA phonon energy
17	86	Incremental resistance vs D.C. bias for Sn-Ge $\mu_F \cong 29mv$
18	88	Blow up of incremental resistance vs D.C. bias for Sn-Ge $\mu_F \cong 40mv$ around the LA phonon energy
19	90	2nd Harmonic (y-axis) vs D.C. bias for Sn-Ge $\mu_F = 40mv$
20	92	Ratio of TO to LA phonon conductance (at onset) plotted against Fermi level

Fig.	Page	Figure Title
21	94	2nd Harmonic (y-axis) voltage vs D.C. voltage (forward bias) for Sn-Ge, $\mu_F = 40$ at 4.2^oK
22	96	2nd Harmonic voltage (y axis) vs D.C. voltage (forward bias) for Sn-Ge, $\mu_F = 40$ at 1.5^oK, $H \neq 0$
23	98	2nd Harmonic voltage (y axis) vs D.C. voltage (forward bias) for Sn-Ge, $\mu_F = 40$ at 1.5^oK, $H = 0$
24	100	2nd Harmonic voltage vs D.C. voltage (forward and reverse) for Sn-Ge, $\mu_F = 29$mv
25	102	Incremental conductance vs D.C. voltage for Au-Si
26	104	2nd Harmonic voltage vs D.C. voltage for Au-Si
27	106	Incremental Conductance vs D.C. voltage for Cr-Si
28	108	2nd Harmonic voltage vs D.C. voltage for Cr-Si
29	110	2nd Harmonic voltage vs D.C. voltage for low resistance Au-Si
30	112	2nd Harmonic data of Tsui and Dunkleburger on low resistance Au-Si
31	123	Ratio of TA to LA phonon conductance (at onset) is plotted against Fermi level
32	125	Schematization, following Davis and Steinrisser, of inelastic phonon-assisted tunneling

Fig.	Page	Figure Title
33	127	Absolute phonon conductance as a function of Fermi level
34	129	Magnitude of k=0 optical phonon as a function of Fermi level
35	138	Reverse bias plot of Incremental resistance vs D.C. voltage showing Γ_2' level
36	140	Reverse bias plot of 2nd Harmonic voltage vs D.C. voltage showing Γ_2' level in Ge
37	142	Fractional change in resistance (y axis) as a function of magnetic field for large reverse bias (-140 mv)
38	144	Position of Landau levels (for Γ_2' state) is plotted against D.C. voltage
39	146	Fractional change in incremental resistance is plotted against D.C. bias for various magnetic fields
40	148	Fractional change in incremental resistance plotted against D.C. bias for one magnetic field

Introduction

Tunneling experiments have been done on various types of junctions. The simplest type of junction is the metal-vacuum junction. Fig 1a shows an energy diagram of a simple metal. For an electron to leave the metal classically it must be given an energy equal to the work function of the metal. If now the electron is placed in an electric field the energy band structure changes as shown in Fig. 1b. If the electric field is made strong enough the energy band is bent over sufficiently so that the distance between the metal and the vacuum through the barrier is very small. In such a situation electrons in the metal see empty states in the vacuum separated from them by a small distance. They may tunnel through the barrier into these states. This type of tunneling is called field emission. It yields information about the surface properties of the material being studied. If another metal were to be brought close to the first metal the band structure of Fig 2a would result. Fig 2b shows the effect of creating a potential difference between the two metals. Now, once again electrons on one side of the junction see empty states on the other side and will tunnel into them. To get reasonable tunneling currents an appropriate barrier thickness must be used (of the order of 30 Angstoms). A much thicker barrier results in too small a tunneling current. Too thin a barrier results in a very small junction resistance and consequent experimental

difficulties. The barrier is formed by growing an oxide on one of the metals and evaporating another metal on top of it. By controlling the width of the oxide layer one can obtain a very thin insulating barrier. There are some problems associated with using this technique. Pinholes through the oxide and general lack of strength is one of them. The oxide may also add its own influence to the tunneling characteristics of the junction. For instance, there are large zero bias "anomalies" associated with Ta-Ta oxide-Al junctions.[1] These effects are due to the presence of magnetic scattering in the oxide[2] and not to the bulk properties of the tantalum. Perhaps the most famous use of metal-metal oxide-metal junctions was in measuring the superconducting density of states.[3] In this type of experiment one of the metals of the junction is a superconductor. If the electrons are tunneling into a large density of states, it would not be unreasonable for them to have a higher probability of tunneling than were they to tunnel into a low density of states. In superconducting junctions the tunneling current directly displays this dependence on the density of states. Actually though, the problem of using tunneling measurements as a probe of the density of states is not particularly clear.[4,5,46] If an analogy is made between tunneling of electrons and photons, a mismatch in the density of states causes a reflection of the incident electrons just as a mismatch in the index of refraction causes reflection of light. Tunneling into an

abnormally high density of states may not then reflect itself in a high conductance. Similarly, in the sense that tunneling is an overlap of the wave functions, the higher the mass the more tightly bound and less able an electron is to extend into the barrier. This reduces the overlap between left and right hand metals. Thus, although there is reason to believe that an increased density of states gives an increase in conductance, there are other effects which may cancel this. In all events, density of states effects are seen in superconductors but have not been seen in transition metals.

In order to study semiconductor properties metal-semiconductor or p-n junctions are used. A p-n junction in, for instance Si, is formed by alloying an acceptor impurity (i.e. Boron) into a heavily n type wafer of Si. Initially we can think of two different Fermi levels (one in the valence band of the p region, the other in the conduction band of the n region). In equilibrium these Fermi levels must be at the same energy. Thus the Fermi level in the n-region must be lowered in energy. This is done by the formation of an electric field in the junction caused by a migration of charge from the barrier region. Equivalently we can think of electrons on the n side wanting to migrate to the p side where they are in the minority and vice versa. The electrons that migrate from the n region to the p region leave behind a positive(from the impurity ions) carrier free region while the holes that leave the p region behind a negative region depleted of carriers.

Thus an insulating dipole layer is formed which resists further charge flow. Tunneling is then done through the insulating depletion region. The voltage current characteristic for a tunnel diode is given in Fig. 3b . The negative resistance region is caused by the uncrossing of the energy bands. We would expect the tunneling current to be zero when the bands are completely uncrossed. In fact, a current exists, This has been interpreted as being due to band tailing.[7] In other words the valence and conduction bands are not really sharp but may extend considerably into the forbidden gap. This explanation does not seem really unequivocal since alternate processes might account for such an excess current (photon emission in the barrier). We will return to this later since we have done some work in trying to identify band tailing in Ge. Notice though that the density of states does appear prominently in these junctions. P-n junctions have also been used to look at a host of other semiconductor properties. The Landau level structure of InSb[8] and Ge[9,10] (Γ_2' band) has been studied in this way. Phonon energies have been measured and the change in these energies with pressure have been found.[11] The band gap between L and Γ_2' bands in Ge has also been observed using p-n junctions. The difficulty associated with p-n junctions is that they are complicated. The type of barrier that is formed is not particularly well known. It may also be simpler to study n and p type semiconductors individually rather than together in a p-n junction.

Metal-semiconductor contacts answer these needs. In a metal semiconductor contact a metal is placed (evaporated, electroplated, etc.) on the semiconductor . Recently, it has been found that evaporating the metal onto a vacuum cleaved surface gives quite reproducible results. As a first guess, the barrier in metal-semiconductor junctions can be thought of a being formed by a difference in work function between the metal and the semiconductor.[12] The smaller the work function the greater the Fermi level of one relative to the other. Since in equilibrium there is only one Fermi level, electrons leave the metal and enter the semiconductor or vice versa. When the electrons leave the semiconductor they accumulate at the surface of the metal and a depletion region is formed. The build up of negative charge prevents the further flow of electrons out from the semiconductor. In Ge and Si the barrier is not quite formed in this way. In these semiconductors there is a large density of surface states. Even in the absence of a metal contact, electrons will fill those surface states which are below the fermi level. This will make the surface negatively charged and a depletion region will be formed. The addition of a metal contact may or may not make a difference depending on the density of surface states. In Ge the density of surface states is high enough so that changes in the barrier are very small when a metal is added. Thus in Ge one can expect the same barrier shape independent

of which metal is used (what its work function is). Basically the large number of electrons shields the depletion region from further loss of electrons. The barrier shape can be calculated, at least to a first approximation, by assuming that in the depletion region there are no electrons. Then Poisson's equation becomes $\nabla^2\phi = 4\pi e^2 n_0/\epsilon_0$ where the only charges are those from the ionized impurities. The solution is a parabola, of the form $V(z) = \frac{2\pi e^2 n_0}{\epsilon_0}(z-z_2)^2$ A knowledge of the barrier height (the potential at the surface) would be sufficient for us to find the constant z_2 in the formula for the barrier shape. This would then completely determine the barrier. The barrier height can be gotten by measuring the capacitance of the barrier. Viewing the barrier as a type of parallel plate capacitor of known charge and area (the junction area and impurity content of the sample is known) a knowledge of its capacitance relates the voltage between its plates to the distance between them. For a parabolic barrier this would determine z_2 as $z_2 = \left[\frac{\epsilon_0}{2\pi n_0 e^2} (V_B - V + \mu_F) \right]^{1/2}$ where n_0 is the carrier concentration, V_B is the barrier height and μ_F is the Fermi degeneracy of the semiconductor. Our initial assumption, that there are no electrons in the depletion region is not altogether true. Actually there are some electrons in the depletion region, particularly near the semiconductor. If these are taken into account they

change the shape of the barrier from parabolic to parabolic-exponential. That is, the parabolic assumption (no electrons) is worst where the barrier is greatest. In this region the solution has an exponential character. It has been shown that this refinement doesn't change the tunneling current very much,[13] and a parabolic barrier is commonly used. Actually the whole idea of tunneling through a barrier, in general, is an approximation. It is assumed that the ionized impurities do not form discrete charges but are actually a uniform positive charge distribution. As the impurity concentration increases the distance between impurities becomes comparable to the junction width(junction width $\sim n_0^{-1/2}$ distance between impurities $\sim n_0^{-1/3}$). It then appears that an electron can no longer be thought of as tunneling through a continuous barrier. Instead an electron may be though of as scattering off individual impurities.[14] A complete calculation of this type of tunneling has not been done for n-Ge (or as far as I know for other semiconductors). Recently, on the other hand, it has been seen that at low impurity concentration there exists resonanat elastic scattering off the impurities.[15] Defects in the junction have also been used to explain the tunneling current.[15]

When the assumption of some type of continuous barrier can be made, tunneling through this barrier is reasonably well understood, in Ge. Here, Conley, Duke, Mahan and Tiemann (CDMT)[16] have calculated the tunneling current as a

function of bias. They have assumed a parabolic barrier and used an effective mass approximation to solve exactly for the transmission coefficient through this barrier. They have further assumed that the Ge is really a semiconductor with one zone centered conduction band at k=0. They claim that the generalization to the case of many valley structure and arbitrary tunneling direction is trivial. Further, they assume that the boundary is smooth and that the component of momentum in the plane of the junction is conserved.

In Ge the conduction band minima are located in the <111> direction and have both transverse and longitudinal effective masses. The theory is compared with experiment for tunneling in the <100> direction. In this direction, all the tunneling masses are the same. The large size of the Fermi sphere (containing all k up to k_{Fermi}) enables the electron to conserve k in the plane of the junction. This theory was compared with the experimental work of Conley and Tiemann[17] on electroplated contacts of indium on Ge. Although the agreement between theory and experiment was reasonably good, even better agreement was later gotten by Davis and Steinrisser[18] using vacuum cleaved junctions.

The theory of CDMT can be thought of as a one band approximation. The electron is thought not to be affected by the valence band in Ge. Instead, the electron is thought only to tunnel under the conduction band. Whereas this

approximation may be fine for tunneling into the L conduction band in Ge it is not necessarily a good assumption to make if there is tunneling into the Γ_2 band of Ge. The barrier height in a vacuum cleaved junction is in the neighborhood of .6 ev. The band gap between the Γ_2 band and the valence band is about .9 ev. An incomming electron would be much closer to the valence band state in Ge than the conduction band state and we would expect to see its tunneling properties modified by the valence band. If a one band approximation is bad for tunneling into the Γ_2 band of Ge it is even worse when used to explain the results of elastic tunneling in p-n junctions. In these junctions an electron leaves the valence band of a semiconductor and ends up in the conduction band. Clearly just looking at the effect of the conduction band on the tunneling will be inaccurate.

There is one major qualitative consideration of the one band model that we should consider. Fig. 4 is a plot of incremental resistance (dV/dI) as a function of applied bias. The major thing that is noticed is that there exists a maximum in the curve. The origin of this maximum can be seen by qualitative considerations. First, assume that the barrier does not appreciably change as the bias voltage is changed. The incremental resistance is then a measure of the number of new electrons that tunnel, for a small increase in voltage, at a given bias voltage. The maximum that is seen occurs for electrons tunneling out of the

semiconductor. At low bias the electrons tunnel from near the Fermi level of the semiconductor. As the bias is increased the new electrons that tunnel, do so from nearer the bottom of the conduction band. Since the density of states is getting progressively smaller the incremental conductance is also decreasing. Finally at a bias equal to the Fermi degeneracy of the semiconductor the bottom of the band is reached. At this point, further increases in bias do not result in any new electrons. The downward swing of the curve is now due to barrier effects. The incremental current through the junction is decreased due to a decrease in barrier height. This qualitative argument locates the position of the maximum at the Fermi degeneracy. This is what the calculation predicts for Ge. Although the position of the maximum would not change for a 2 band model in Ge it is not a universal truth that the maximum reflects the Fermi degeneracy in all metal-semiconductor contacts.[13] If for instance, the Fermi degeneracy is large, electrons at the bottom of the band see a far greater barrier than those at the Fermi level. If these electrons are not important in tunneling, our qualitative considerations concerning the position of the maximum break down

As stated before, the one band model is inadequate for describing tunneling in a p-n junction or tunneling in a Ge m-s junction, backward biased so that there is tunneling into the Γ_2' band. One approach, that is qualitatively easy

to see, is to use a WKB approximation. For a WKB approximation the transmission probability is defined as $e^{-2\kappa x}$ where κ is the decay constant. For a one band model $\kappa = \sqrt{2m^*(V-E)}$ for a two band model κ must be suitably generalized. In a one band WKB approximation the E(k) relation is known. $E(k) = \hbar^2 k^2/2m^*$ and this is identified as the kinetic energy of the electron. As the electron goes into the barrier the kinetic energy becomes negative and the k turns into a κ or attenuation constant. That is $E-V(x) = \hbar k^2/2m^* = E(k)$, so that $k = \sqrt{2m^*(E-V(x))}$. To use a two band model[19] we must first find the two band E(k) relation. Once this is found we find the attenuation constant just as was done for the one band case.

We write the Schroedinger equation

$$(p^2/2m + V(r))\psi = E\psi$$

where ψ is either $\psi_{conduction}$ or $\psi_{valence}$

now $\psi = U_k(r)e^{ik\cdot r}$

and we have

$$[(\hbar k^2/2m + V(r)) + \hbar k\cdot p/m]\,U_{kc}(r) = E\,U_{kc}(r)$$

now

$$U_{k\pm}(r) = U_{oc}(r)\,a_\pm(k) + U_{ov}(r)\,b_\pm(k)$$

then we get the following hamiltonian

$$\begin{pmatrix} E_G + \hbar^2 k^2/2m & \hbar/m\, kp \\ \hbar/m\, kp & \hbar^2 k^2/2m \end{pmatrix}$$

then

$$E_{\pm} = E_G/2 + \hbar^2k^2/2m \pm \frac{\sqrt{E_G^2 + 4\hbar^2k^2p^2/m^2}}{2}$$

given E (k) we can find m_+ and m_- (upper and lower band effective masses) in terms of p. If we then define a reduced effective mass as

$$\frac{1}{m_{reduced}} = \frac{1}{m_+} + \frac{1}{m_-}$$

then

$$E_{\pm}(k) = E_G/2 + \hbar^2k^2/2m \pm (E_G^2 + E_G\hbar^2k^2/m_r)^{1/2}$$

and

$$-\hbar^2k^2/2m_R = E_{\pm}(E_G - E_{\pm})/E_G$$

Now we assume that $E_{\pm}$ is the kinetic energy

and $k = i\kappa$

Finally we have

$$\chi = \sqrt{2m_R/\hbar E_G\,(V(x)-E)(E_G - V(x)+E)}$$

Notice that this reduces to the one band case when $E_G \to \infty$ Also notice that the attenuation constant is much smaller for a two band calculation than would be the case for a one band model. A two band calculation of this nature has been done for tunneling into the L conduction band of Ge. The results agree with the one band model of CDMT.

Another way to do a two band calculation is to write the electric field as eX [20]. Then a zero order hamiltonian can be written as $(p^2/2m + V(r) + X)\psi_c = E\psi_c$ Band to band transitions can be introduced through the matrix element $\langle\psi_c|x|\psi_v\rangle$ connecting valence and conduction bands.

So far we have been dealing with elastic tunneling properties. Most of our experimental work has, however, dealt with phonon assisted tunneling. The importance of phonon-assisted tunneling is most clearly seen in a study of Ge or Si p-n junctions. In Ge for instance the conduction band is located at the Brillouin zone boundary. The valence band is located at the zone center. In going from the valence to conduction band (as a tunneling electron must do in a p-n junction) the electron's quasi-momentum must go from <000> to <111>. The junction eledtric field is considered to be weak compared to the periodic potential.[21] If this is so K is still a good quantum number. To some degree k in the direction of tunneling is not conserved but k perpendicular to this direction should be conserved. Since k must be more or less conserved we would not expect any tunneling between valence and conduction bands in a Ge p-n junction. In Ge junctions of arsenic it turns out that the arsenic impurity elastically scatters the tunneling electrons enabling them to acquire sufficient change in momentum to go from <000> to <111> states. In antimony junctions phonons are required to supply the necessary momentum to the electrons. The phonons that participate are naturally the Brillouin zone boundary phonons (with momentum <111>). The participation of these phonons is very clearly seen in a tunneling experiment. Ideally at very low bias there is no current. As soon as the bias is increased sufficiently a tunneling electron has enough energy

to emit a zone boundary phonon. When this is done the phonon takes up the momentum necessary to allow the electron to tunnel from valence to conduction band a current flows. There are four zone boundary phonons in Ge: the TA,LA,LO, and TO phonons. These occur at about 8 mev, 28 mev, 30 mev and 36 mev respectively. If the tunneling experiment is done at low temperatures only phonon emission processes are important. At low enough temperature thermal smearing is eliminated and each of these four phonons can be clearly resolved. The exact energies of these phonons have, in fact, been found by the use of tunneling.

Phonon structure has also been found in metal-semiconductor junctions of Ge[18] and Si.[22,23] The existence of this structure is somewhat surprising since elastic tunneling from the metal can start in any k state (up to k_{Fermi}) and phonons are thus not needed to conserve k. However, phonon-assisted tunneling is also allowed and is sufficiently strong to be seen. The first question that presents itself is the mechanism for these phonon processes. Do p-n junctions of Si and Ge share the same mechanism? Do metal semiconductor contacts behave in a similar way to p-n junctions? Do any calculations give quantitative results that agree with experiment?

One of the first attempts to describe phonon-assisted tunneling was made by Kane[24] to describe tunneling in p-n junctions of Ge. Roughly, he considered two bands as participating in the tunneling. The electron tunneled from the n-side

into the forbidden gap under the conduction band (L band). During this tunneling it could emit a phonon and make a transition to the valence band (Γ_{15}). This process was only used to explain the TA phonon. The participation of the other phonons was not calculated. The phonon-assisted tunneling predicted by this process turned out to be several orders of magnitude smaller than the experimental tunneling current. Kleinman[20] pictured a different tunneling process which he claimed was much more probable. In the Kleinman process the tunneling electron started out in the L conduction band. It emitted a phonon either prior to or shortly after entering the junction. Uponnemiting the phonon the electron made a transition to the Γ_2' upper band conduction state. Once in this state the electron tunneled into the junction. The tunneling between the upper conduction band at (Γ_2') and the valence band at (Γ_{15}')was described by Kleinman as being due to induced transitions caused by the electric field in the junction. We will later discuss this whole process in some more detail.

The Kleinman process could account for the approximate magnitudes of the TA and LA phonons. Yet the Kleinman process could not be extended to Si. His explaination of the results seen in Ge depended on the detailed band structure of Ge. It was necessary to have a small zone centered upper conduction band (Γ_2'in Ge) close in energy

(154 mv in Ge) to the lower conduction band. In Si the upper conduction band is of the order of volts higher than the lower conduction band. It would seem very unlikely that this band could be expected to participate strongly in the tunneling process. Thus in Si another tunneling process must be called upon. Phonon structure has in fact been observed in metal-semiconductor junctions of both Ge and Si. In Ge the phonon-assisted tunneling that appears seems to be similar to that which had been observed in p-n junctions. The calculation of Kleinman for p-n junctions was extended by Davis and Steinrisser[18] to explain the results that were seen in metal-semiconductor junctions. These calculations agreed with their data on the absolute magnitude of the phonon-assisted tunneling conductance due to the LA phonon. They extended their calculation to the TA,LO, and TO phonons. The relative magnitudes of the LA, TA and LO phonons seemed to agree with their theoretical predictions at their impurity concentration. The TO phonon observed, however, was much stronger than expected theoretically. Phonon structure has recently also been observed in silicon m-s and mos junctions. In contrast to germanium the relative magnitudes of the phonon-assisted structure that was observed in these junctions differed strongly with the relative magnitudes that had been observed in p-n junctions of silicon.[25] Fig. 5 is a comparison of the data taken on

p-n junctions of germanium and silicon with the data taken on m-s junctions of these materials. The phonon-assisted structure in m-s junctions is now thought to occur at the maxiumum in the phonon density of states and to be due to impurity mediated phonon emission.[26,28] Lambe and Jaklevic[27] have shown that a tunneling electron may excite vibrational modes in molecules which have been added to the barrier region of the junction. In a metal-semiconductor junction the junction itself posses vibrational modes in the form of phonons. The tunneling electron excites these phonons (without necessarily conserving k) primarily at energies equal to a maximum in the phonon density of states. Further work by Schein and Compton seemed to indicate that impurities might play a major role in mediating this interaction. As an electron tunnels into the m-s junction from the metal it first sees a very strong barrier. In this region there are very few electrons. As the electron tunnels further into the barrier it comes upon a region where there are a few electrons. These electrons then lightly screen the impurities in this part of the junction. Schein and Compton[26] claim that these impurities located in this "reserve region" of the junction are responsible for the electron phonon interaction. They feel that if the tunneling electron were to be just scattering off maxima in the phonon density of states then strong phonon-assisted tunneling should be seen in p-type

as well as n-tye silicon. That this is not the case implies that the process is impurity mediated. To prove that the impurities of importance come from the reserve region, Schein and Compton have used compensated semiconductors. Thus they can form a p-type semiconductor which has a great many n-tye impurities. For a p-type semiconductor there is no reserve region for the n-type impurities. The fact that phonons are not seen in this type of junction is taken by them as evidence that the electron-phonon interaction is caused by reserve region impurities.

At the time that we were planning our experiment not all these experimental facts were available. The situation concerning phonon-assisted tunneling at that time however still appeared sufficiently dubious to warrant further experiment. Our original idea was to cleave samples of germanium and silicon along different principal directions. If not all the phonon-assisted tunneling could be traced to one process, we expected the different processes to have a different dependence on the tunneling effective mass. By cleaving in different directions and thereby introducing different tunneling masses we hoped to gain information concerning the various mechanisms. We were, however, unable to cleave in all those directions which would have been necessary to pursue this experiment. A nearly equivalent procedure is to change the width of the tunneling barrier. This is not difficult to do. Increasing the carrier concentration

of the semiconductor causes the width of the m-s barrier to become narrower (just as increasing the charge on a cpapacitor causes a strong electric field). Our experimental aim was then to measure the phonon-assisted tunneling conductance for the four Brillouin zone boundary phonons in germanium as a function of carrier concentration. During this experiment we came upon other properties of tunneling junctions. These will be discussed when we explain our data.

Figure One

Energy diagram of a simple metal with (b) and without (a) an applied electric field

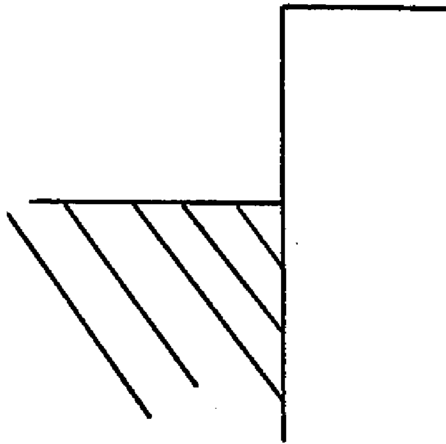

(a)

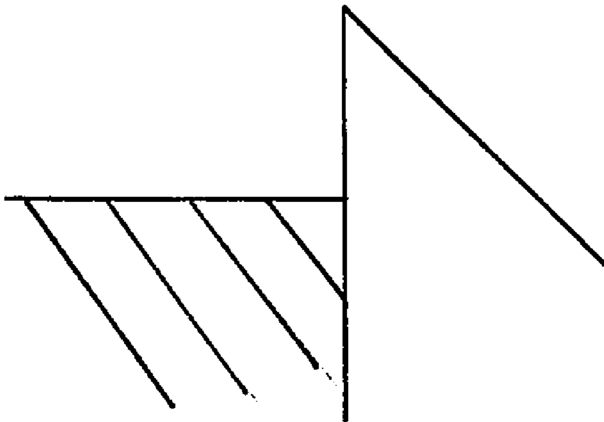

(b)

Figure Two

Metal-Insulator-Metal junction without an applied bias (a) with an applied bias (b)

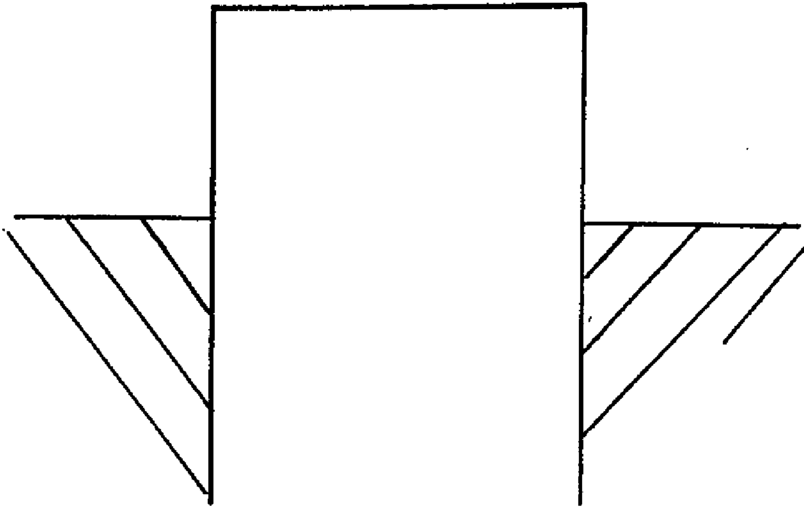

(a)

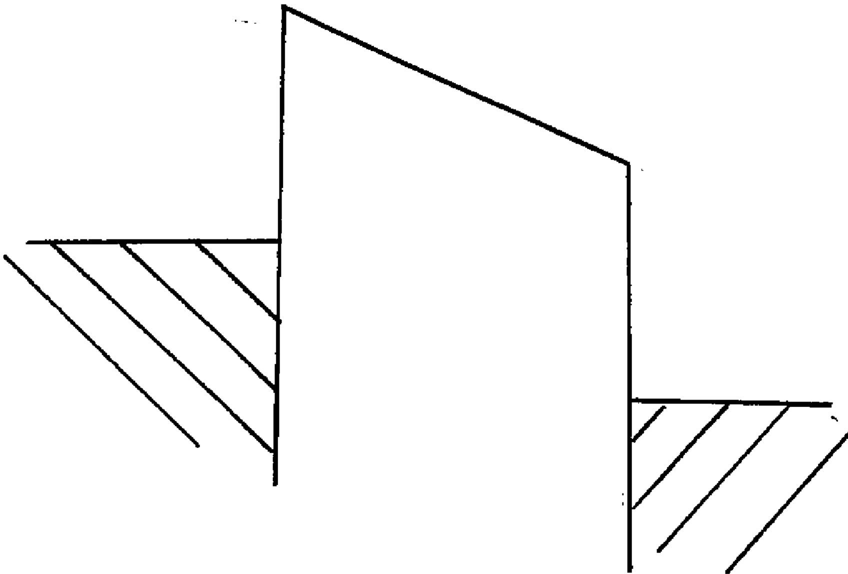

(b)

Figure Three

Energy level diagram for a p-n junction without (a) and with (c) an applied bias

Current vs. D.C. voltage for such a junction (b)

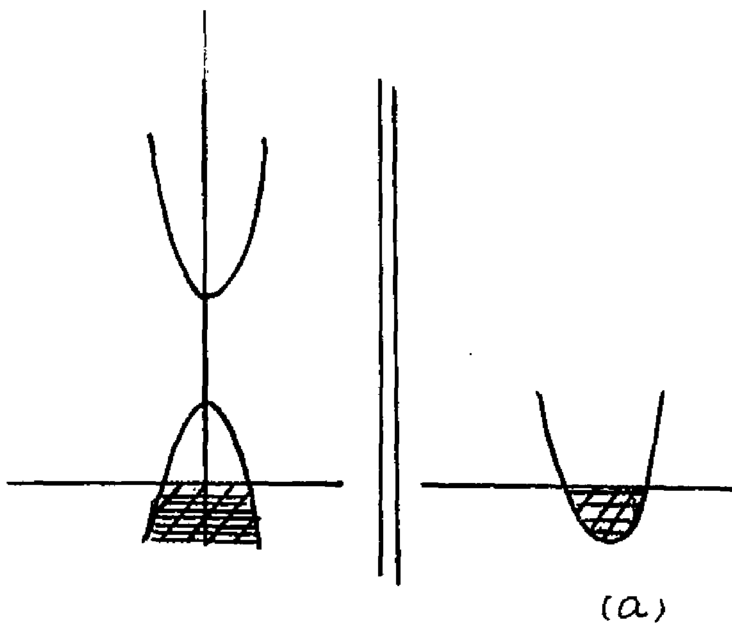

(a)

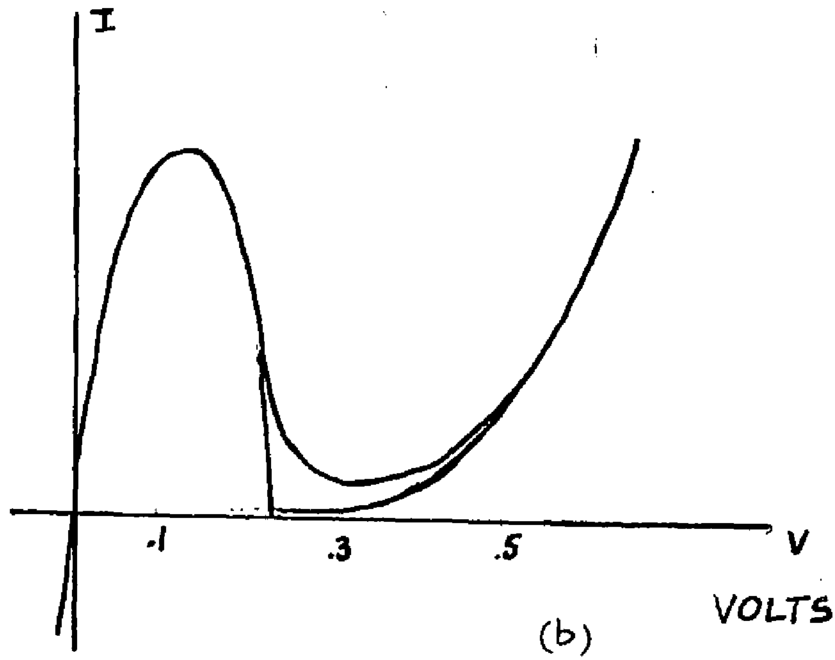

(b)

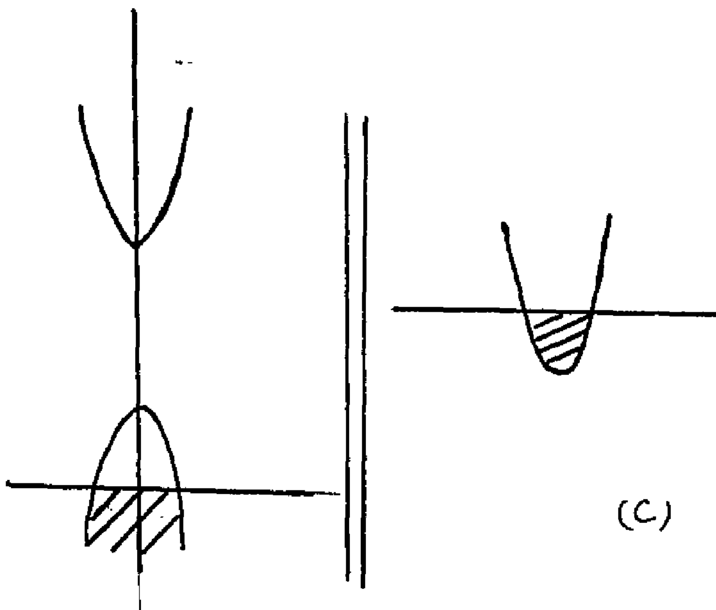

(c)

Figure Four

Incremental resistance as a function of applied D.C. bias (x axis) for Sn-Ge junction, $\mu_F = 25$mv.[a] The arrows denote the positions of the phonon onset voltages.

In (a) the vertical scale is the voltage across the sample (A.C.) and is 20 microvolts per box. In (b) the vertical scale is 200 microvolts per box and is the voltage across a 10K resistor in series with the sample. The horizontal scale in both (a) and (b) is 5 mv per box.

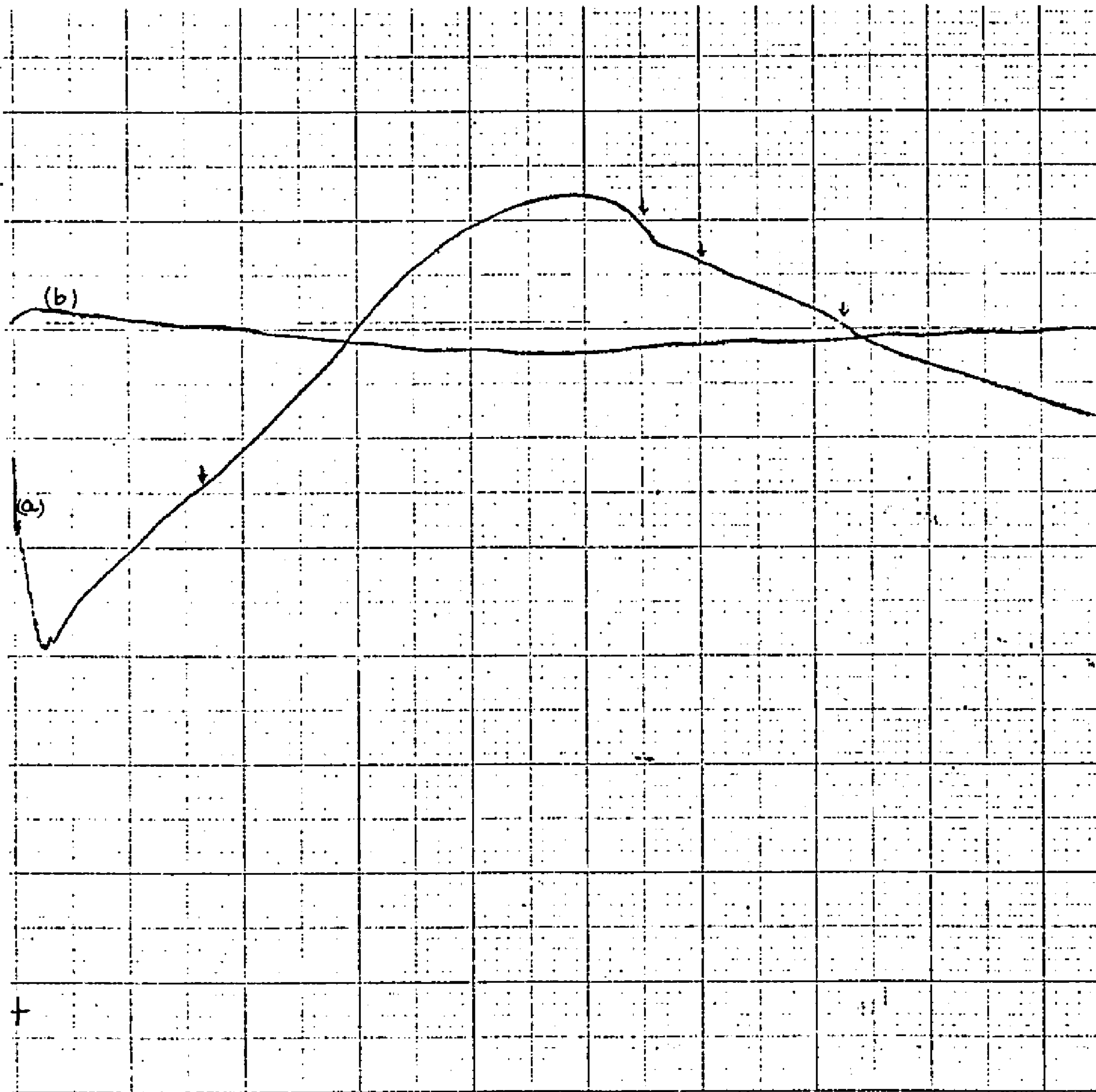
(b)
(a)

Figure Five

Forward bias plot of d^2I/dV^2 vs V for p-n junctions of (a) Ge[48] and (b) Si[48]

Forward and reverse bias plots of d^2I/dV^2 vs V for m-s junctions of (c) Ge[18] and (d) Si[22]

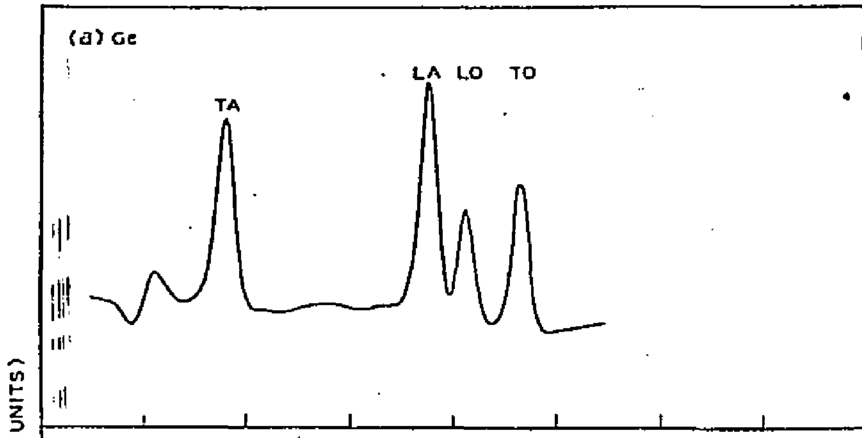

(a)

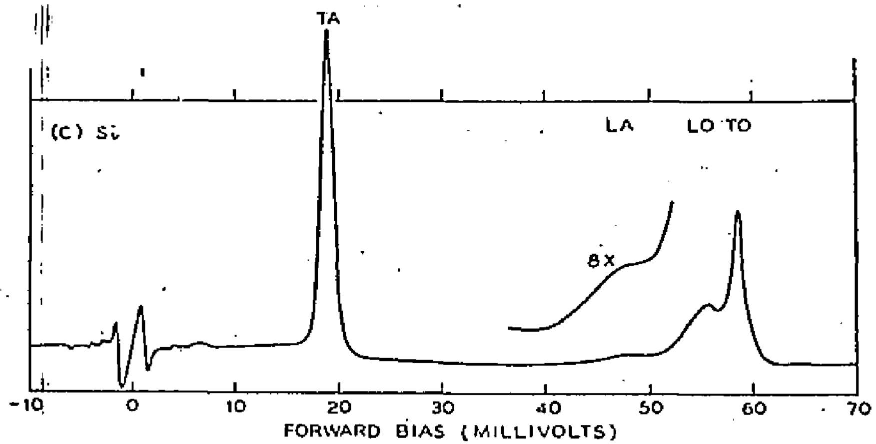

(b)

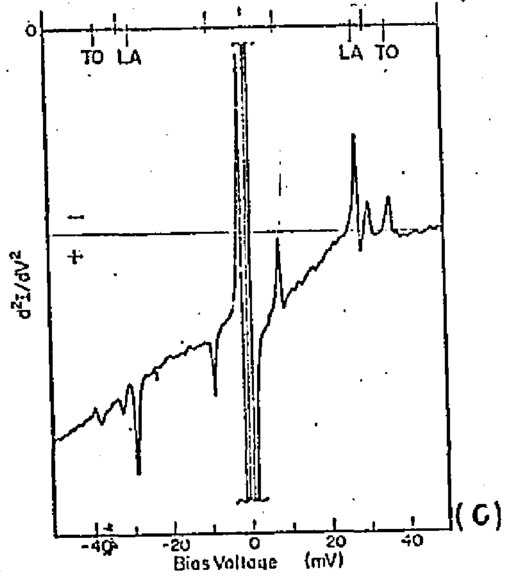

(c)

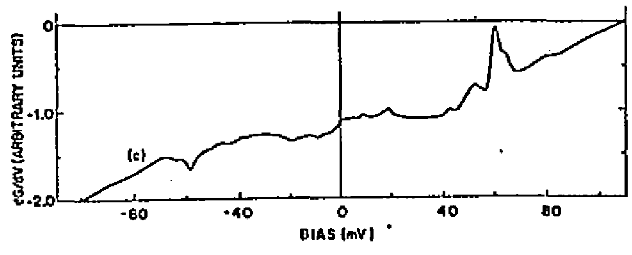

(d)

Experimental Techniques

The experimental techniques we used enabled us to fabricate metal-semiconductor contacts and make measurements on these at temperatures ranging from 1.5^0K to 300^0K. We were able to apply a magnetic field up to sixty kilogauss parallel to the tunneling current. We could measure the current through the sample as a function of the bias voltage across it, and also the incremental conductance (dI/dV) and its derivative (d^2I/dV^2) as a function of applied bias.

The cryogenics needed for this experiment were simple. Our original setup (see Fig. 6) consisted of a 20 Kg Westinghouse superconducting magnet in its own cryostat. The original cryostat did not have provision for pumping on helium and the bore diameter of the magnet was only 1". We decided to put our sample in the same helium space as the magnet. We added the flanges appropriate for pumping on this helium space and a manometer to measure the helium vapor pressure (essentially to measure the temperature). In order to automatically control the temperature below 4.2^0K we put a manostat in the pumping line. One point gave us some concern. Since both the sample and magnet were in the same helium space the magnet would be at the same temperature as the sample. If the magnet quenched (the superconducting wire in it went normal) at maximum field and low temperature we were afraid that, at this low vapor pressure, the magnet would be unable to dissipate the heat that would be generated and might be open circuited. To guard against this we put

a level detector in the cryostat. We used a level detector described by White.[29] This consisted of a 1000 ohm resistor in series with a 12 volt battery and an ammeter. When the resistor was immersed in helium it was able to dissipate much of the power that was being fed into it. As soon as the helium level dropped below the resistor it could not dissipate the power as effectively. The temperature of the resistor rose and its resistance dropped. Several resistors at different heights in the cryostat were used. We monitored the current through these resistors in order to determine the level of helium.

We found it convenient to pre-cool the cryostat by partially filling its vacuum jacket with nitrogen gas and immersing it in a dewar of liquid nitrogen. We then backfilled the sample space with helium gas and monitored the drop in pressure of this gas as the sample space cooled down toward liquid nitrogen temperature. When the sample space had cooled sufficiently we pumped out the vacuum jacket and were ready to transfer helium. A thermocouple gauge was used to monitor the pressure in the vacuum jacket. For pre-cooling this pressure was kept at 100 microns and when the jacket was pumped out again the pressure fell to about 30 microns. Only a mechanical pump was use for this.

We had one problem with pre-cooling that might be worth mentioning. Originally we found that the dewar would not hold helium. We traced this to the fact that we pumped out

the cryostat's vacuum jacket with the same pumping lines that had been used to pump on helium. Some of the helium from these lines had migrated into the vacuum space and was not frozen out when the liquid helium was transferred. In other words it prevented us from getting a hard vacuum. We overcame this by pumping on the vacuum jacket with somewhat different pumping lines as well as repeatedly flushing the jacket with nitrogen through a pipe distinct from the helium pumping lines.

For other experiments we used a 60 Kg superconducting magnet, which came complete with it cryogenics.

Originally we attmepted to make metal-semiconductor contacts on etched Ge surfaces by electrodeposition of either gold or tin. The whole sample expept for a large area junction was masked by nail polish. The area that was not masked was the one on which the tin was deposited. Contact to the electrodeposited metal was then made by using conducting epoxy to bond wires to the junction. Although electrodeposition had been used elsewhere, we had all sorts of problems depositing a uniform adherent film. Besides these problems our whole technique depended upon having a large area junction. Unfortunately we wanted to measure junctions which had a whole range of resistances. Using large area junctions would confine us only to those junctions which had high resistances (only Ge where carrier con - centrations of less than $5x10^{18}$ could be used). We

therefore had to be able to make small junctions and bond wires to them. The junctions were made by vacuum deposition on freshly vacuum cleaved surfaces in a manner similar to that of Wolf and Losee.[23] We designed an apparatus that could cleave a bar of Ge in vacuum in a stream of evaporating metal. Before the evaporated metal was able to strike the cleaved surface a mask was interposed which would define 5 mil metal dots on the sample. We used an Edwards vacuum coating unit which can achieve a vacuum of less than 10^{-6}mm Hg in a vacuum space of some 18" in diameter. We tried to make sure that the film thickness was sufficiently thick to reflect the bulk properties of the metal that we were evaporating. By measuring the amount of the tin that was evaporated and calculating the total area over which it was evaporated we could get a measure of the film thickness. As a rule of thumb criterion we put a glass slide next to the sample. If the glass slide was opaque at the end of the evaporation we judged the film to be sufficiently thick. Most of evaporations were done with Pb, Sn or Au and for these evaporations there was little problem.

Our cleavage device was in some measure patterened after Archer for use on Si. The sample was mounted in a small clamp Fig. 7 directly opposite an air core solenoid. The center of the solenoid contained a magnetic hammer the front half of which was brass, the back half steel. A mask made up of an array of 5 mil dots was mounted on a spring piece of copper. The

mask was then pressed up against the sample. A small scribe mark was used to initiate cleavage along the correct plane. When the assembly was mounted in the evaporator and cleavage was desired a current was passed through the air core solenoid. The current level which gave best cleavages had been pre-set and regulated with a variac. The current caused the back of the magnetic hammer to be drawn into the solenoid. The front of the hammer then protruded sufficiently to hit the sample and hopefully to. cleave it. The mask was in contact with that part of the sample that fell away after cleavage. The mask was then free to spring in front of that part of the sample that was still held in the vise. The metal was evaporated through holes in this mask. Since a whole array of dots was used it was not necessary to have large surfaces of good cleavage. Usually at least one dot could be found under the microscope that appeared to rest on a well cleaved area of the sample.

After taking measurements on dots that appeared on well cleaved surfaces as well as dots that didn't I am not sure that the nature of the cleavage plane is a dominant consideration. Wolf and Compton[31] have described their cleavage apparatus, which they have used for Si. Part of their discussion concerns itself with the amount of contamination of a vacuum cleaved evaporated junction. They conclude that it was easy to get less than one percent contamination. We experimentally determined that contamination was not a

major effect in our measurements by varying the pressure at which evaporations were made. Although a sample cleaved in air showed different properties than a sample cleaved in vacuum, we did not see any systematic difference in sample properties between samples cleaved at pressures of 10^{-5} and at pressures of 10^{-6}.

At one point we were taking data on Si which gave us strange and irreproducible results. We feared that the irreproducibility might have come from impurities getting into the junction before the evaporated metal. To try to get a better vacuum in the area of the sample we built a special liquid nitrogen trap which we fitted into the vacuum system. We found that the added vacuum produced by this trap had no effect on our junctions.

There is perhaps one technical point about the construction of the cleavage device. Initially we were afraid that the magnetic hammer would strike the sample and lodge itself in the way of the evaporated beam. We found this not to be the case. The magnetic hammer in fact struck the sample, overshot it slightly and was then drawn back, out of the way of the stream and into the air core solenoid.

There is another surprising point. We had been led to believe that Ge would only cleave perpendicularly to a <111> direction.[32] As a consequence of this information we cut our samples into bars of 2mmx1mmx15mm with the long axis along the <111> direction. Cleavage was to be made

perpendicular to the long axis. As it turned out, cleavage was not particularly successful. We then changed the direction of the long axis to the <110> direction. We got a much higher percentage of good cleavages in this direction. We were further hoping to be able to cleave perpendicular to the <100> direction. We found this altogether impossible. In fact the sample would preferentially cleave in some direction other than the <100> direction when they would not shatter outright. The wafers we bought were 1mm thick, 1" round and had a 100 surface. The 100 surface was chosen because we could cut bars giving us <111>, <110>, and <100> directions from it. These bars were cut with a wire saw and oriented by use of x-ray diffraction.

In the course of our work on Si junctions some strange results that we got caused us to want to evaporate metals other than tin, gold or lead. We tried evaporating copper, platinum, chromium and indium. Chromium adheres to glass so well that it was very difficult to clean the bell jar of the evaporator after using it. Platinum on the other hand alloys with refractory materials (i.e. W baskets used for evaporation). Besides being unsure of the purity of the platinum film we evaporated (because of this alloying) we had great difficulty evaporating the film at all. The fact that the platinum alloys with the basket used to evaporate it results in the destruction of the basket before sufficient platinum has been evaporated. The way to overcome this problem we found was

by a sort of flash evaporation technique in which a fine wire of platinum is wound between several heavy wires of tungsten. Thus, in no one spot is alloying heavy enough to break the tungsten wire, while all of the platinum gets quickly and uniformly hot. The best way to do this type of evaporation would be with an electron beam gun. But this was not available to us.

After evaporating the metal contacts it was necessary to make electrical connection to them. Initially we tried using conducting epoxy to bond a wire to the junctions. This approach failed. For small junctions the epoxy just didn't have enough strenth. We then tried to use a thermo-compression bonder to make these contacts. Although this technique had also been used before it did not work for us. We found that although the gold wire would make fine contact to the deposited metal, somehow during the formation of the bond it would tend to pull this metal off the junction. Although this in itself was not encouraging there was another problem with the thermocompression bonder. There was a fear that since this machine depended on heat to form the bond, this heat would influence the properties of the junction. We then tried pressure contacts as suggested by Wolf and Losee.[23] A 5 mil gold wire was bent in the shape of an S and attached to the upper half of what looked like a vise (see Fig. 8). The sample sat on the lower half of the vise on a brass block. We used the 5 mil gold wire to make contact with one of the 5 mil dots on the sample. This was done by using

a stereo zoom microscope capable of 60 power magnification. With the aid of the microscope it was possible by hand to adjust the position of the sample until it was directly under the gold wire. When this position was reached the vise was tightened in order to have the gold wire exert light pressure against the deposited metal. The sample was fixed in this position with Duco Cement. We did not take any special precautions to clean the gold wire except for the fact that prior to bringing it into contact with the junction we would cut off the old tip with a scissors exposing what was hopefully a clean piece of gold. The sample was on a holder which originally was a long dowel stick which was immersed directly into a helium storage dewar. When it proved necessary to go to lower temperature and to use magnetic fields the sample holder had to be put inside the magnet in the cryostat. This necessitated making the sample holder out of non-magnetic materials and introducing vacuum feed-throughs. The original wooden dowel stick used for immersing the sample was replaced with thin walled stainless steel tubing. None of these changes caused any particular difficulty.

So far we have concerned ourselves with the fabrication of the metal-semiconductor junction. The sample must also however have an ohmic contact. Ideally one would like to be able to feed the current (for the D.C. bias) through an ohmic contact, through the bulk semiconductor and then lastly through the junction of interest (the metal-semiconductor

contact). If either the bulk semiconductor or the ohmic contact has appreciable resistance compared to the junction then the D.C. bias will not appear solely across the junction. It will also then be unclear what bias is across the junction and what properties are due to it. Initially we made junctions on high resistivity degenerate Si. We tried to make ohmic contacts to these semiconductors by alloying antimony doped gold into the Si at a temperature of about 375^{0}C. Alloying was done, in an evaporator, using a molybdenum strip heater. The temperature of the strip heater was monitored by use of a copper-constantin thermocouple gauge. Although the eutectic temperature for silicon-gold is around 375^{0}C we could not get any alloying at this temperature. The Si had a thin layer of oxide which prevented the gold from alloying with it. By raising the Si to a higher temperature (550^{0}C) we could actually see the gold alloy into the silicon. If the silicon was raised to too highaa temperature the gold would completely disappear into it.

We found these contacts unsatisfactory at liquid helium temperature for our relatively low concentration samples. We then tried a phosphorous diffusant sold by the Transene company. This product is painted on the silicon. The phosphorous diffuses out of it when the silicon is baked at a temperature of 1100 to 1200 degrees centigrade. Contact resistance was measured by making two "Ohmic contacts" close together on a bar of silicon and immersing it in helium. If the contact resistance was less than 1% of the

expected resistance for the metal-semiconductor contact it was felt that the ohmic contacts were good enough.

When making ohmic contacts to germanium we did not have to use this paint-on diffusant. We tried essentially two techniques. One was the electrodeposition of anitmony doped gold onto a cleaned surface of germanium while the other was the evaporation of this gold onto the germanium surface. In both cases the gold was alloyed into the germanium and produced satisfactory ohmic contacts. The more convenient of the two methods was the evaporation of antimony doped gold and that is the one that we chose to use. Since this ohmic contact was of large area there was no real problem bonding wires to it. We found that the most convenient way was to solder directly to the evaporated gold layer.

We were basically interested in studying the voltage vs. current characteristics of our Schotky barriers. Although the voltage vs. current plots contained essentially all the information that we wanted from our data it was not easy to extract the information from these plots. The main reason for this is that our experiment concerned itself mostly with the phonon induced structure in the tunneling current of these junctions. To illustrate this point consider a linear V vs. I curve (fig 9). At some voltage on this curve assume that some other tunneling process also begins to participate. Let this process be small but also linear. The final V vs. I curve will show a small

change in slope where the new process first appears in voltage. The strength of the process will be reflected by the change in slope of the V vs. I curve. This change in slope however will be difficult to measure. It would seem much better to measure the slope directly. In other words, instead of plotting V vs. I it might be better to plot dI/dV vs. V. This technique was used by Hall[33] to resolve weak phonon-induced inflections in the V vs. I curves of a variety of compound semiconductors. Subsequent to this it was found that structure could be even more prominently displayed by plotting d^2I/dv^2 vs. V. Our experimental apparatus was originally patterned after the equipment of Thomas and Rowell.[34] I will try to describe the electronics which enabled us to directly measure dI/dV and d^2I/dV^2.

For generality assume that the total voltage across the junction is $V=V(I)$. For a resistor $V(I)=IR$. Now assume that the current through the junction is the sum of a D.C. current and an A.C. current. Then $V=V(I_{dc}+I_{ac})$. If the A.C. current through the junctions is assumed small compared to the D.C. current $V(I_{dc}+I_{ac})$ may be expanded in a taylor series about $I_{ac}=0$. Then $V(I_{dc}+I_{ac}) =$ [35]

$$V(I) + I_{ac}\, dV/dI + [I_{ac}^2/2!]\, d^2V/dI^2 + [I_{ac}^3/3!]\, d^3V/dI^3$$

Let us say that the A.C. current is sinusoidal. Then $I_{ac} = i_0 \sin\omega t$

and

$$V(I_{Dc}+I_{ac}) = V(I_{Dc}) + (i_0^2/4)\,d^2V/dI^2 + (i_0^4/64)\,d^4V/dI^4$$
$$+ \left[i_0\,dV/dI + i_0^3/8\,d^3V/dI^3 + \dots \right] \sin\omega t$$
$$- \left[i_0^2/4\,d^2V/dI^2 + i_0^4/48\,d^4V/dI^4 + \dots \right] \cos 2\omega t$$
$$- \left[i_0^3/24\,d^3V/dI^3 + i_0^5/384\,d^5V/dI^5 + \dots \right] \sin 3\omega t$$

This expansion tells us how to make derivative measurements. If an A.C. current of frequency w is fed through the sample along with the D.C. current we can find dV/dI by measuring the A.C. voltage of frequency w appearing across the sample. The expansion also tells us that there is a voltage of frequency 2w appearing across the sample. Measuring the magnitude of this voltage gives us the magnitude of d^2I/dv^2.

Part of the problem involved in this expansion is determining how large an A.C. current can be passed through the sample. Since the magnitude of the coefficients of dV/dI and d^2V/dI^2 go as i_0 and i_0^2 it would seem that a larger signal is best. On the other hand the validity of the expansion depends upon a small signal. We experimentally determined the size of the A.C. current that could be used. We varied the size of this current and noted the change in the experimental (either d^2V/dI^2 or dV/dI vs. V) curves. If higher order terms were important, varying the A.C. current through the sample should produce wide

variations in the nature of the curves. Experimentally it appears that using too high an A.C. current results in a smearing of the structure. We kept reducing the A.C. current until we no longer could see differences in the curves by further reduction. As a further check we took both first and second derivative measurements and compared them.

In order to directly measure dI/dV and d^2I/dV^2 we must develop a circuit capable of applying a sinusoidal current to the sample and measuring the first and second harmonic voltages across it.

The simplest of all circuits is shown in fig 10a. In this circuit an oscillator provides a voltage of frequency w across some small resistor. This causes a current of frequency w to travel in the loop shown by an arrow in the figure. The amount of current in the loop is determined by measuring the A.C. voltage of frequency w across the resistor R. If now the A.C. voltage of frequency w is measured across the sample it (by our taylor series expansion) is equal to $i_0 \, dV/dI$. If the resistor is made large compared to the A.C. resistance of the sample (dV/dI) changes in sample resistance will not affect the A.C. current level in the circuit. Then i_0 can be taken as constant and a measurement of the A.C. voltage across the sample is proportional to the A.C. resistance. Similarly we can

measure the A.C. voltage, of frequency 2w, across the sample. The Taylor series expansion allows us to think of the sample as a voltage generator of 2nd harmonic. We then can redraw the circuit as in fig 10b with this in mind. Now a voltage measurement (of frequency 2w) across AB gives us $\frac{i_0^2}{4} \frac{d^2V}{dI^2}\left[1-\frac{R_s}{R+R_s}\right]$. There are several things that could be improved upon in this circuit. The oscillator, although it is supposed only to put out frequency w also puts out some 2w signal. If this 2w signal were interpreted as comming from the sample it would give us erroneous values for d^2V/dI^2. Perhaps a better way of feeding the current (frequency w) into the sample might be to proceed as in fig 10c. In this figure we use a tuned L-C circuit which has small impedance for the frequency w but high impedance for frequency 2w. Thus, spurious 2nd harmonic from the oscillator is discriminated against. Also, when a 2nd harmonic measurement is made the size of the signal being measured is small. It is important to get the best signal to noise ratio. Fig 10d is an addition to the previous diagram which increases the signal to noise ratio. The added portion of the circuit is tuned to the 2nd harmonic frequency. If the total 2nd harmonic current flow in this loop, then the voltage measured across L_2 is $\frac{i^2}{4} \frac{d^2V}{dI^2}(\omega L)/(R_s+R_{L_2})$ If R_s is small compared to R_{L_2} we have increased the measured signal level by the ratio wL/R_{L_2} over the measured value for our simple circuit (by the Q of the inductor). For a high Q inductor thisamounts to a factor of better than

200. It is true that as the signal is increased so is the noise associated with it. The noise generation of the sample is quite small. The white noise goes as $\sqrt{RT}$, where R and T are both small. On the other hand, the shot noise at the input stage of the frequency selective voltmeter is high. The increase in signal noise is negligible compared to this shot noise. Thus the signal level has been increased by a factor of 200 while the noise has remained unchanged. This added L-C circuit also serves another purpose. Initially both first and second harmonic measurements were made across the sample. The first harmonic signal (which goes as i_o) is some 1000 times larger than the second harmonic signal (which goes as i_o^2). If the frequency selective voltmeter has a Q of 20 the first harmonic signal will swamp the second harmonic signal even when the voltmeter is set to read second harmonic. This added LC circuit eliminates this difficulty. It amplifies the second harmonic voltage while blocking the first harmonic. Basically it acts as an additional filter of high Q. Additionally, we want to take all our A.C. measurements as a function of applied D.C. bias. Fig 11a shows a D.C. source biasing the sample. The variable D.C. sourve was gotten, for us, by a motor driven potentiometer connected to a resistance programmable power supply. A frequency sensitive voltmeter is not as good as a voltmeter that is also phase sensitive. This type of instrument requires a reference from the oscillator. The signal to be measured and the reference have a definite phase relation-

ship while random noise of this frequency is not coherent with the reference. It is then possible to discriminate against random noise even at the signal frequency. A circuit incorporating these ideas is the circuit of Thomas and Rowell shown in fig 12. This circuit had certain disadvantages for us. The only resistance in loop 1w, is the resistance of the inductor L_1. For sample resistances of roughly this size, the first harmonic current will no longer be constant as the sample resistance is changed (D.C. bias is varied). This would mean that a plot of our measured signal ($i_0 dV/dI$) as a function of D.C. voltage would not have the same shape as the plot of interest (incremental resistance vs. D.C. bias). If further, the sample resistance were high a degradation in the performance of loop 2w could be expected. In order to get d^2I/dV^2 from the measured lineshape large corrections had to be made.

The final circuit that we used is shown in fig 11b. Although in some ways the noise performance of this circuit was not as good as other designs, we were able to use it for a wide range of sample resistances.

We have covered most of the experimental considerations of this project. It might be reasonable to say something about the actual data taking.

For dV/dI, and d^2V/dI^2 vs. V measurements the output of the phase sensitive voltmeter (PAR HR-8) and the output of the D.C. voltmeter (Kiethley) were fed into Y and X channels respectively of an x-y recorder. As the power

supply was swept through its voltage range the x-y recorder produced a continuous curve of incremental resistance or its derivative as a function of D.C. bias. The phase sensitive voltmeter had a time constant associated with it. The sweep rate of the D.C. voltage had to be slow enough not to obscure the structure we were looking at. For instance, if we wanted to observe structure whose width was 1 millivolt we would not want to sweep the D.C. voltage faster than 1 millivolt every 5 seconds for an integration time of 1 second. Similarly the A.C. voltage was kept small enough not to obscure the structure. Sweep rates were occasionally checked by running at slower speed and noting any difference. For the most part there was no particular difficulty associated with taking data.

We also took dV/dI vs. H measurements. For some reason we would get large bursts of noise every 30 seconds or so with the junctions used in these measurements. This made it impossible to take a continuous plot of their characteristics and forced us to take measurements point by point. Although this was very time consumming it did not form a basic problem.

Figure Six

Helium dewar and pumping lines

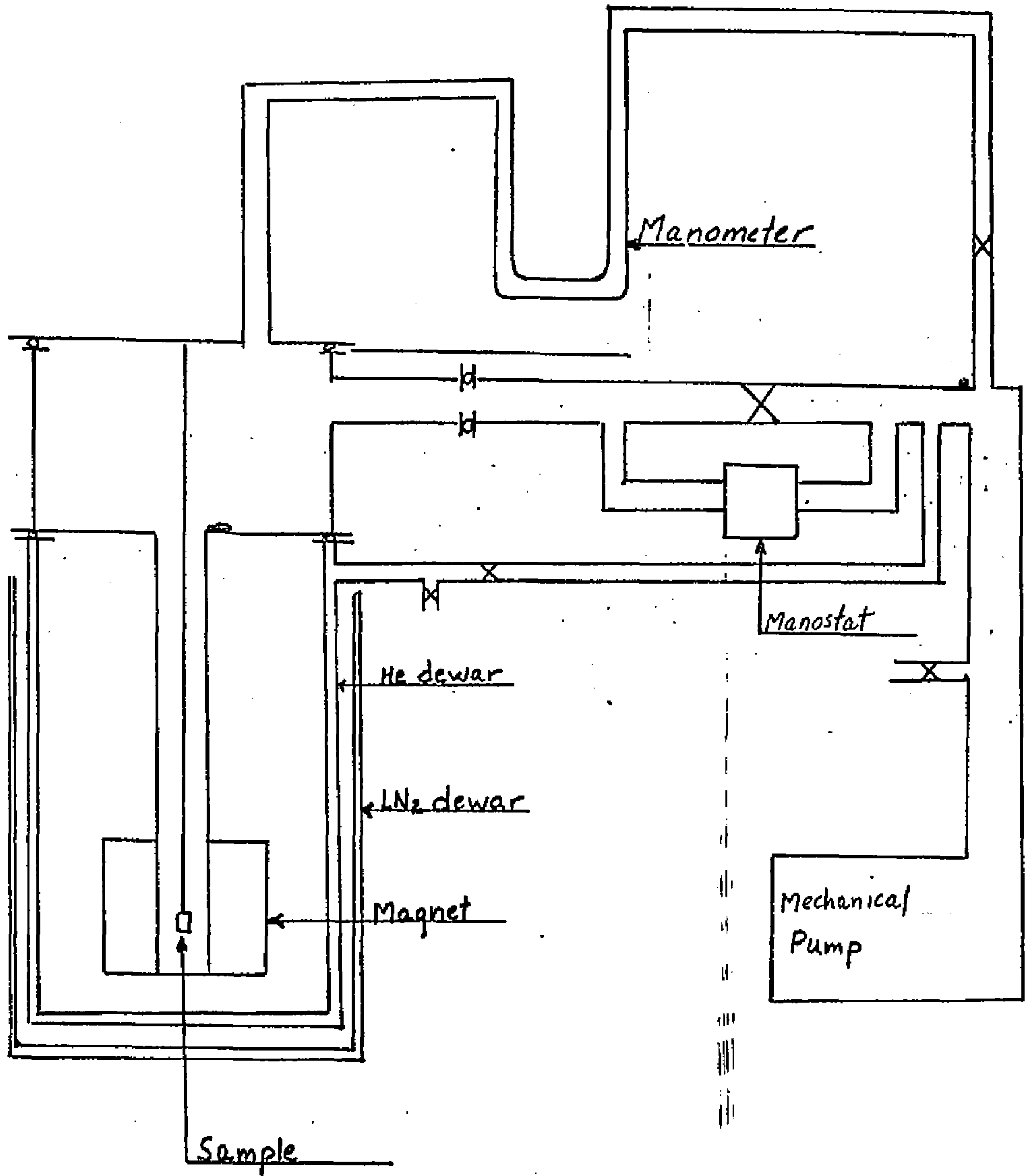
Manometer
Manostat
He dewar
LN2 dewar
Magnet
Mechanical
Pump
Sample

Figure Seven

Cleaveage device

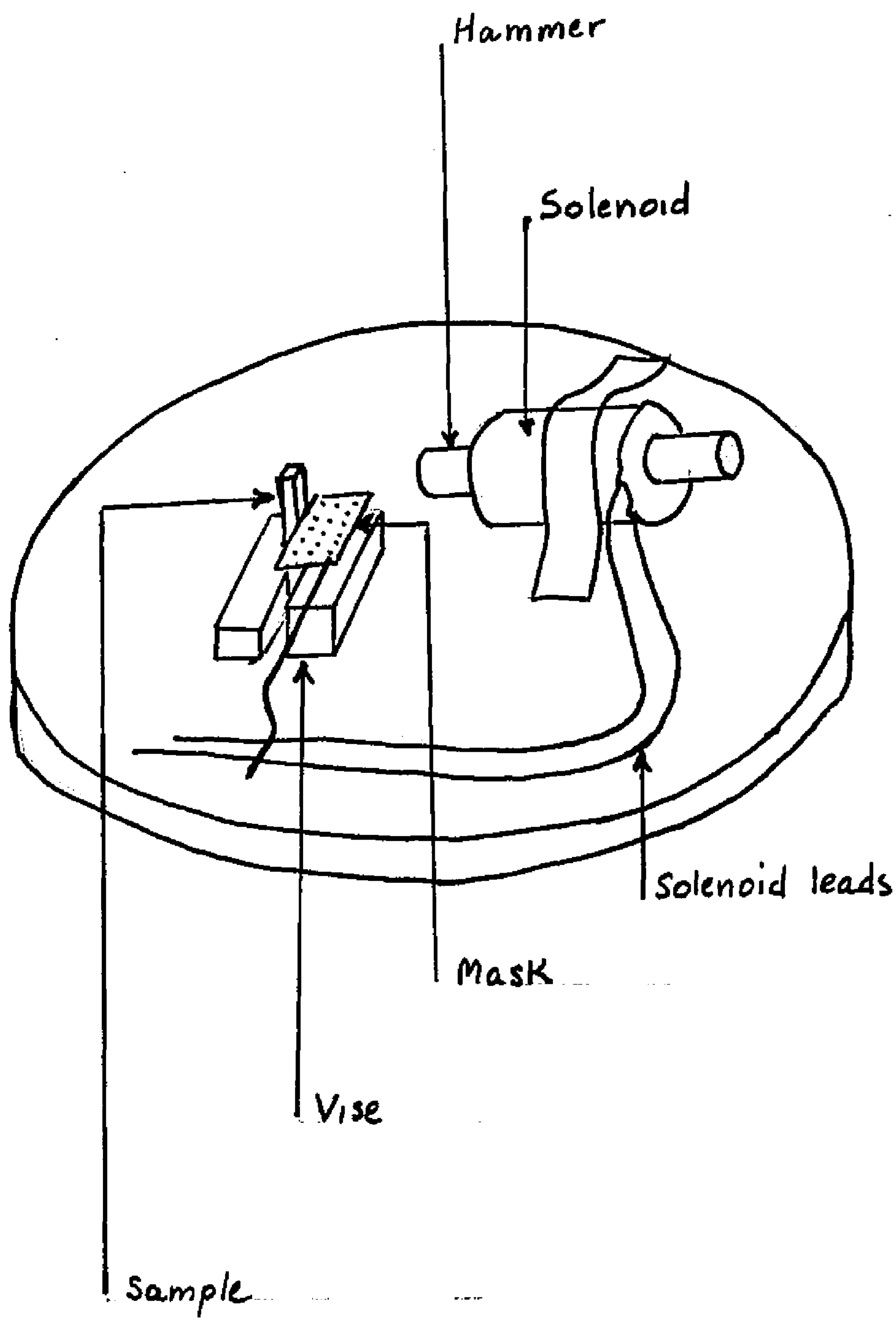
Hammer
Solenoid
Solenoid leads
Mask
Vise
Sample

Figure Eight

Sample holder

This sample holder did not have the capability of rotating the sample. This feature was later added.

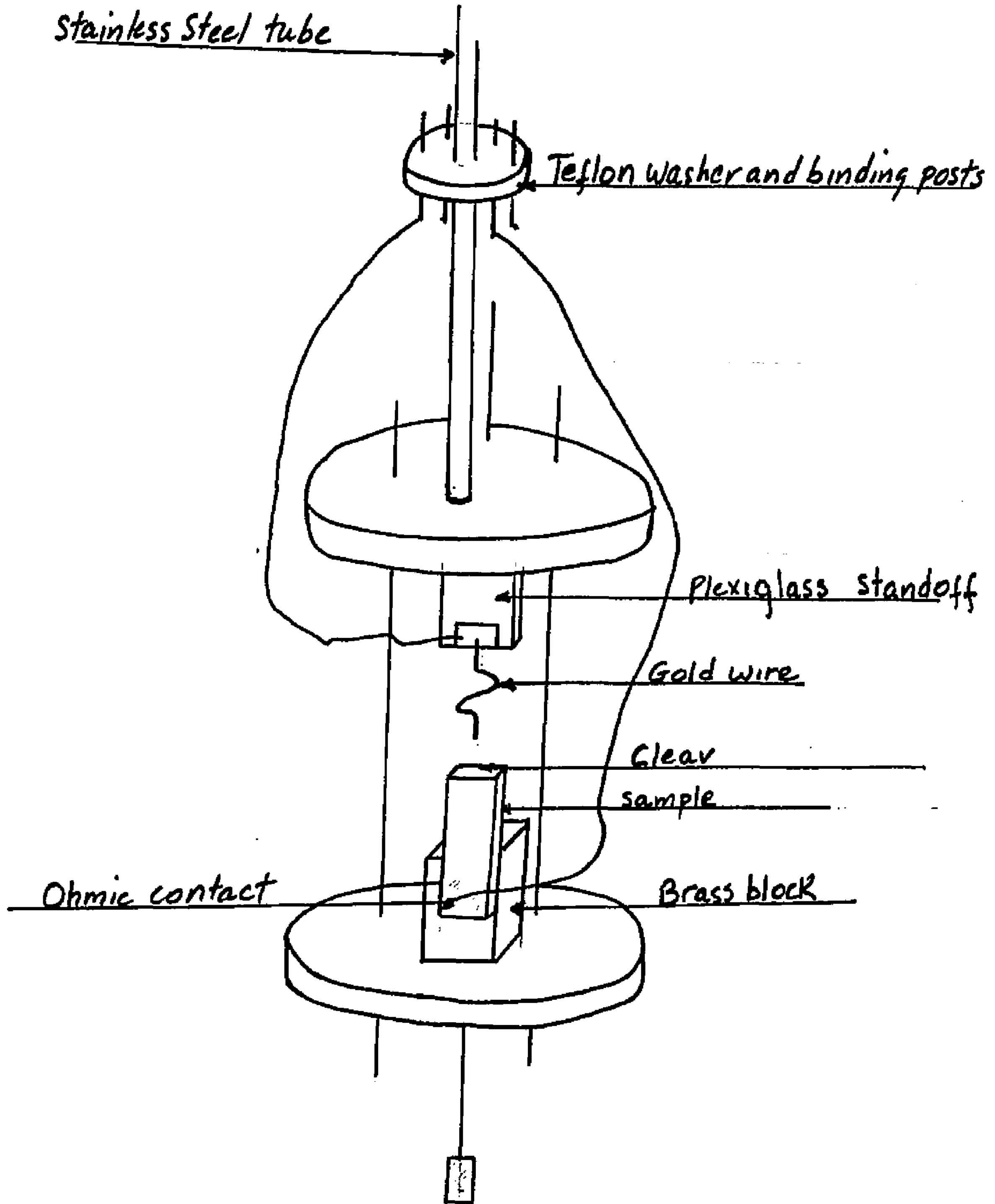
Stainless Steel tube
Teflon washer and binding posts
Plexiglass standoff
Gold wire
Cleav
sample
Ohmic contact
Brass block

Figure Nine

Figure (a) is some I vs V plot. Fig (b) is an I vs V plot which has some onset voltage. Fig. (c) is the sum of (a) and (b). Fig. (d) is the derivative of (c) plotted against D.C. voltage.
The figures are meant to show the greater clarity with which a dV/dI vs V plot (rather than a V vs I plot) displays the onset of a new process.

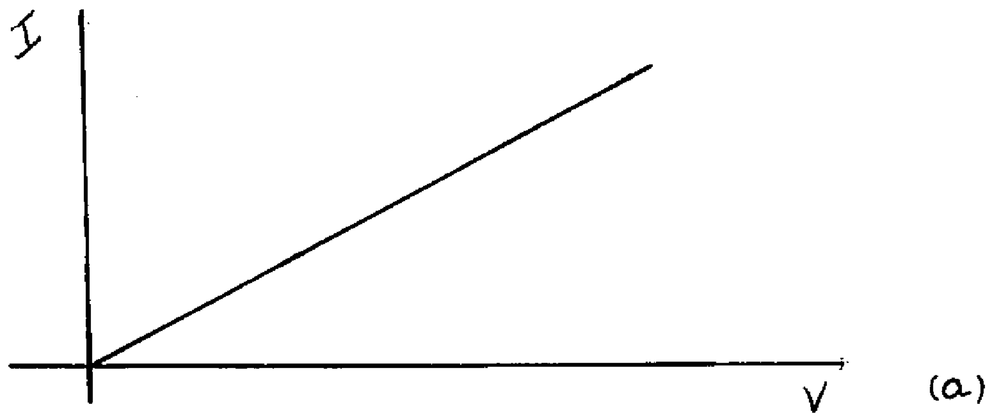

(a)

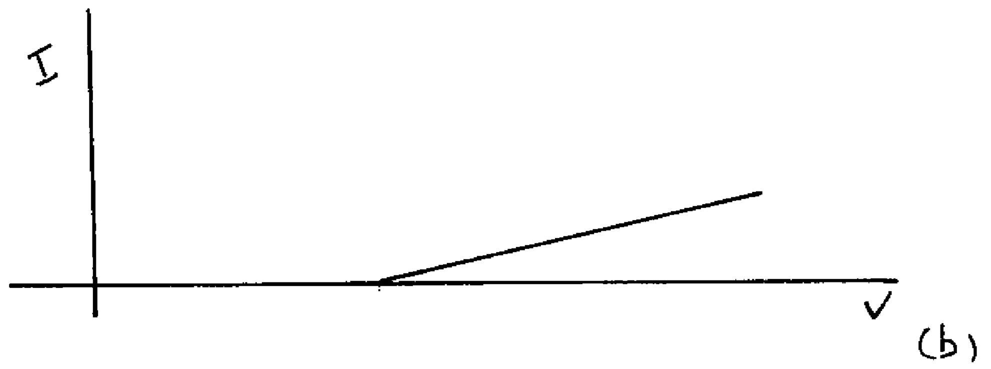

(b)

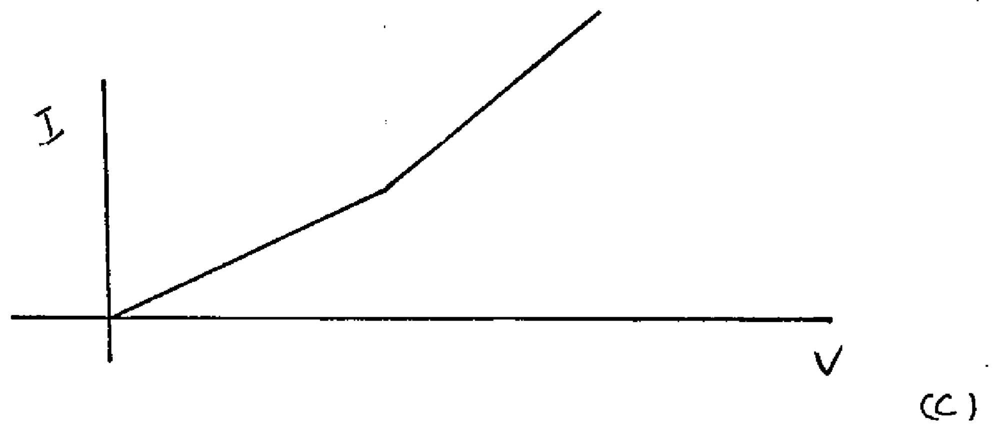

(c)

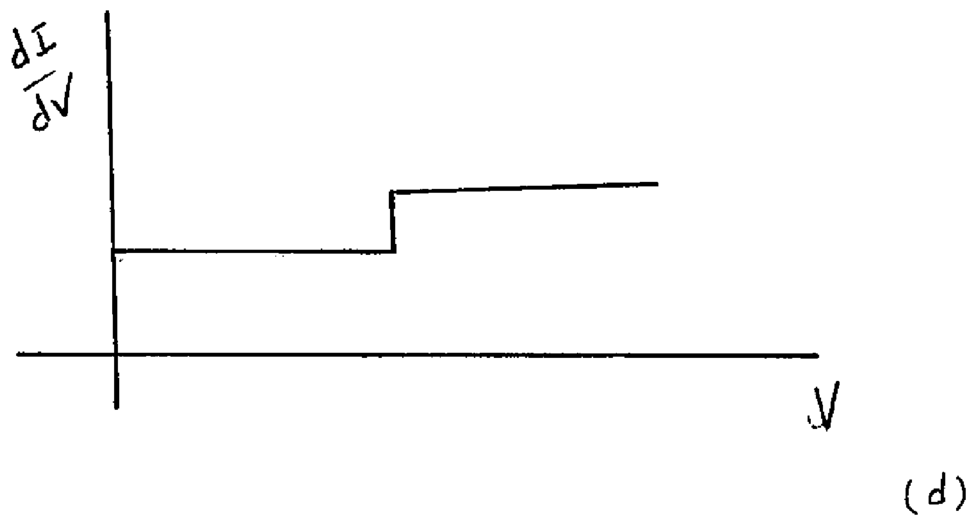

(d)

Figure Ten

Figures a,c and d are harmonic measuring circuits. Figures b and e are their equivalent circuits. The figure shows an evolution from a simple circuit to a more complicated but useful one.

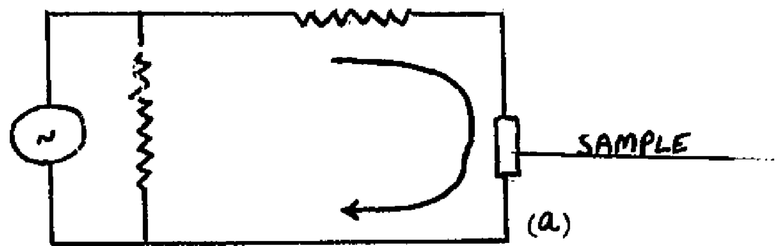
SAMPLE
(a)

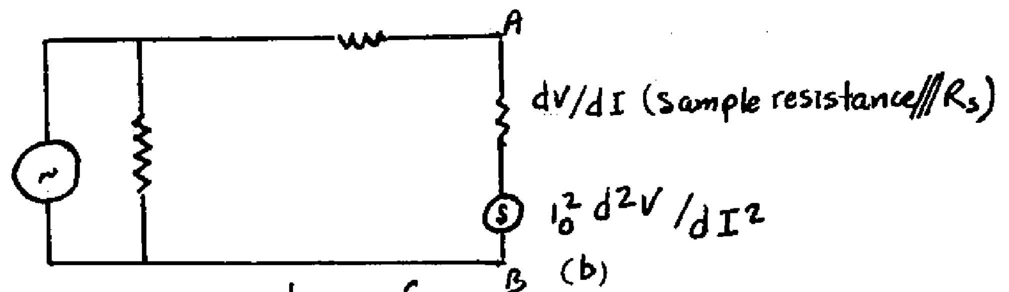
A
dV/dI (Sample resistance//Rs)
i0² d²V/dI²
B
(b)

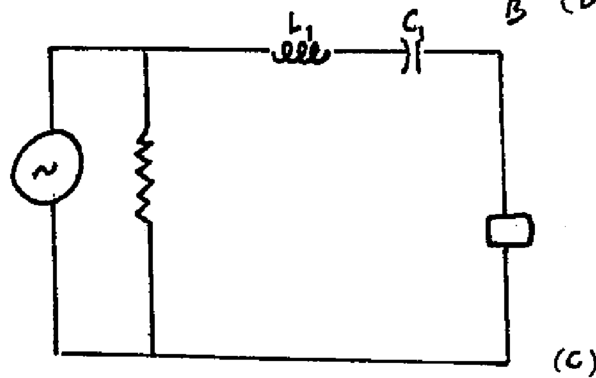
L1
C1
(c)

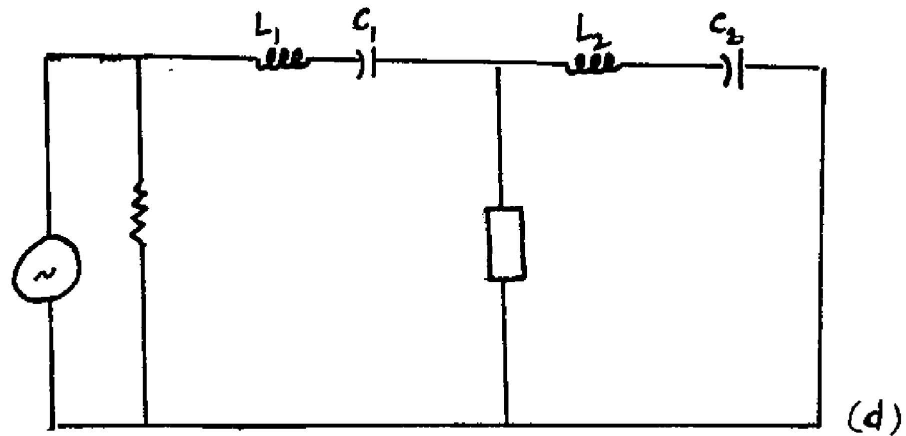
L1
C1
L2
C2
(d)

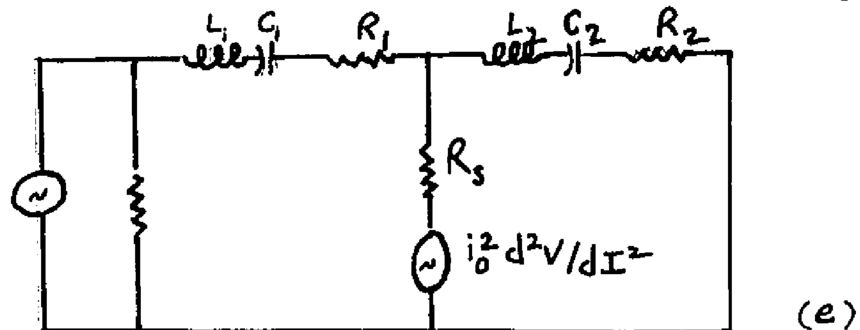
L1 C1
R1
L2 C2
R2
Rs
i0² d²V/dI²
(e)

Figure Eleven

Fig.a is a harmonic measuring circuit with a D.C. biasing arrangement.

Fig. b is a block diagram of the measuring circuit that we used.

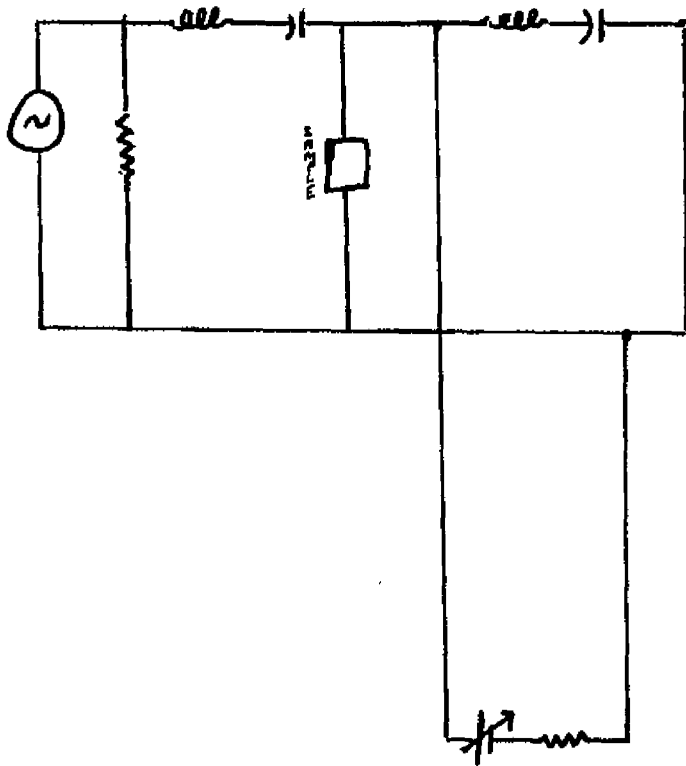

(a)

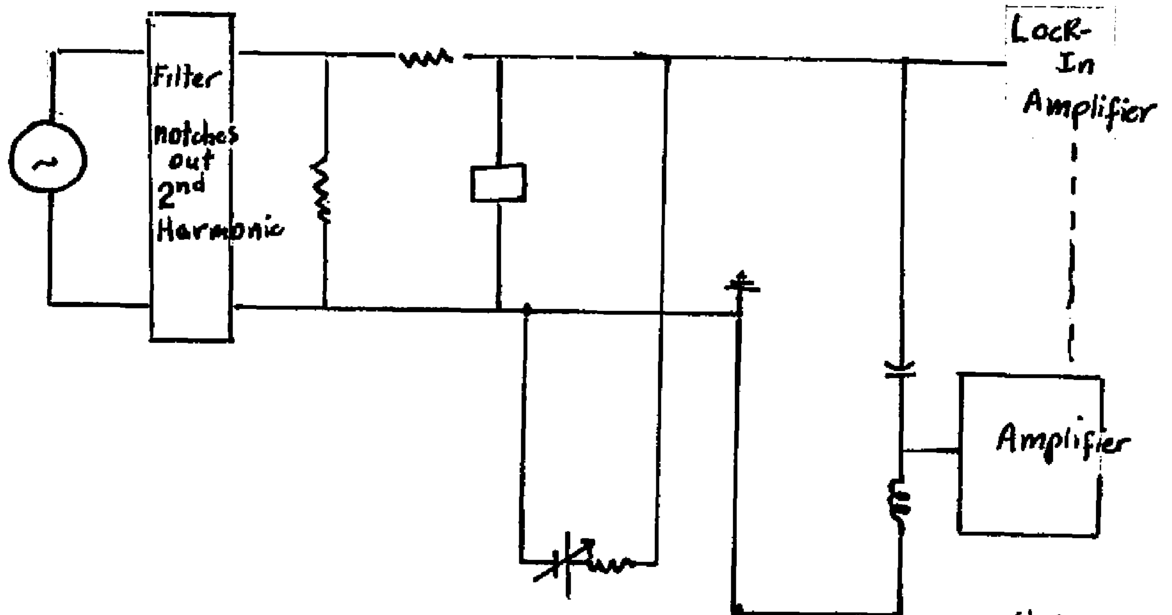

(b)

Figure Twelve

Harmonic measuring circuit of Thomas and Rowell [34]

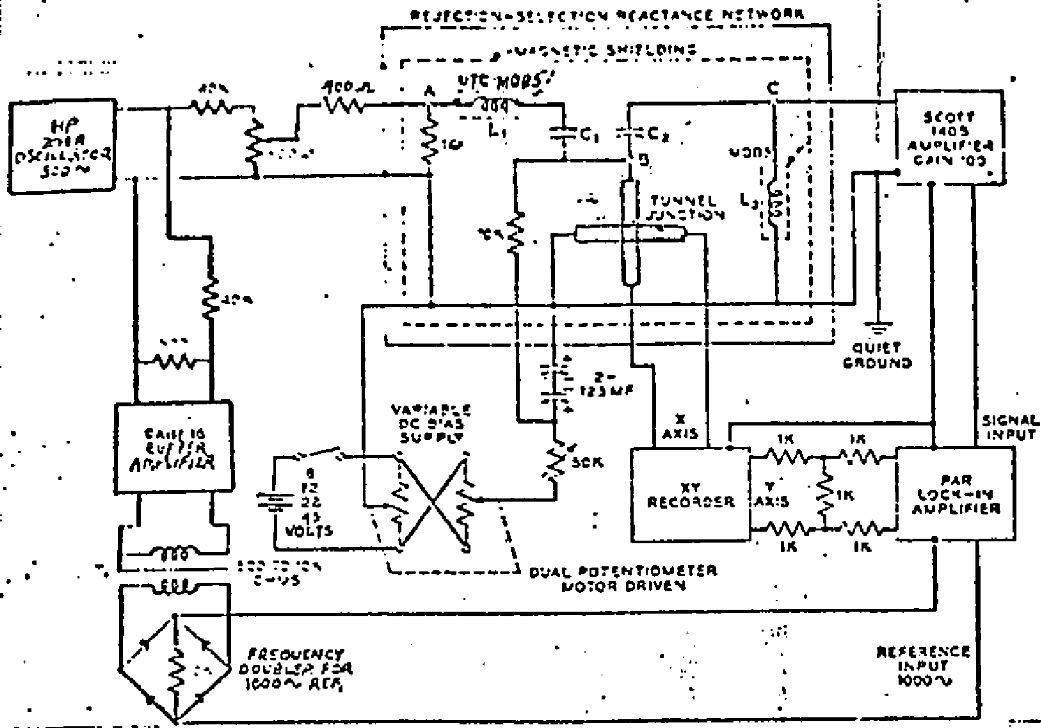

FIG. 1. Hybrid [...] circuit schematic [...] monic second deriv[...]

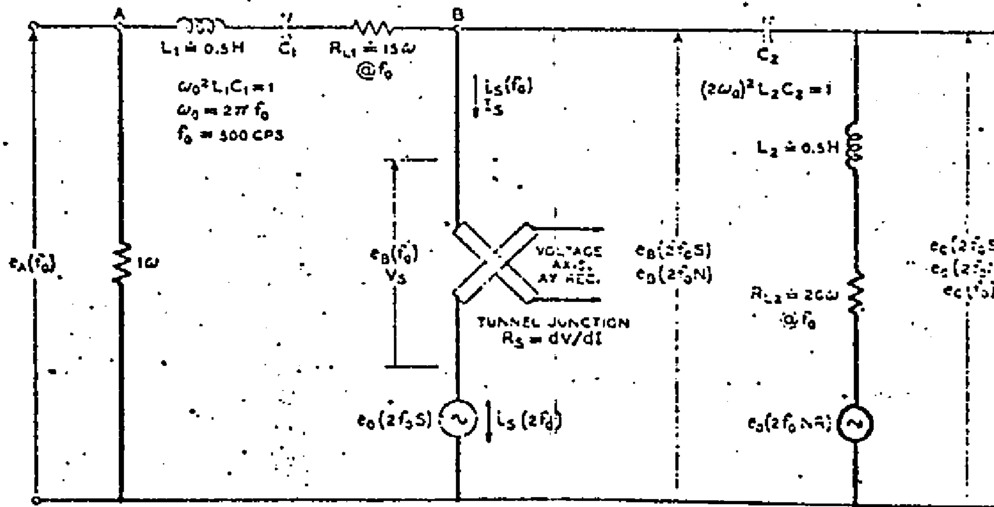

[...] Rejection-selection in[...] transformation reactance

Data Analysis

The primary information we wish to extract from the data is the relative and absolute magnitudes of the various phonon-assisted tunneling conductances. This can be done by using either the data for dI/dV vs. V or d^2I/dV^2 vs. V. For dI/dV data we measure the step height. For d^2I/dV^2, we measure the area under the resulting "bell shaped" curve. In either case we have to estimate the shape of the background due to direct tunneling.

Fig. 13 shows an experimental plot of incremental resistance (on the Y axis) as a function of applied bias. Also shown on that plot is a straight line somewhat above the incremental resistance plot. This is the measured A.C. current in the circuit. In this case we have kept the circuit current constant so that our measure voltage is directly proportional to the incremental resistance. The D.C. bias scale is 5mv/box. A maximum appears in the neighborhood of 40mv. This maximum reflects the Fermi degeneracy of the semiconductor and was used by us as a direct measure of the carrier concentration at the junction. Also, there is some very pronounced structure at zero bias. Our junctions were made out of tin evaporated on Ge. When the temperature is reduced below 3.7°K, tin becomes superconducting. The junction shown was taken at a temperature of about 1.5°K. The sharp structure shown at zero bias reflects the superconducting density of states of the tin. It disappears when the tin is driven normal by a magnetic field. If

tunneling through the barrier was not the main path of current transport this superconducting density of states would not be seen. For metal-oxide-metal junctions, for instance, it is often unclear whether the characteristics being measured are real or just due to a short or some other non-tunneling type of junction. The observation of a superconducting density of states is taken as proof that the junction is a good one (tunneling junction).[36] For our junctions, then, this superconducting density of states is also some evidence that our junctions are good. It is not however particularly strong evidence. Many junctions that showed superconducting structure produced irreproducible results. An example of this is shown in the junction in the figure. There is pronounced structure past the maximum in the incremental resistance. This structure had not been seen before or since. There is other evidence, however, to support our belief that our junctions are good, namely the presence of phonon structure. These junctions agree with what is expected theoretically and are reproducible within bounds. In figures 14 & 15 we show plots of theoretically derived graphs. Figs. 4, & 13 show the experimental graphs. The experimental graphs show not only the elastic background current but also show the phonon-assisted inelastic current. The theoretical graphs only contain the elastic part of the tunneling current. The theoretical graphs have been normalized to read 5 scale divisions (vertical) at 8 mv. This puts them into roughly

the same scale as the experimental graphs without having to redraw the experimental curves. The type of theoretical computation that was done does not give absolute magnitudes but line shapes. These lineshapes are not in bad agreement experiment when it is remembered that the experimental junctions themselves are not absolutely reproducible. It will be noticed, however that the theoretical curve appears worse for low carrier concentration junctions. There are various possible explanations for this. One explanation is that the junctions do not have uniform impurity concentration. Some of the current would then go through the low doping region while other current would go through the more highly doped region of the junction. If these currents are of comparable magnitude we would expect that the posion of the maximum should be smeared. Similarly the theoretical curve would be expected to lose its sharpness. We have done some computer analysis of this idea and it seems reasonable. On the other hand recent work indicates that resonant elastic impurity scattering at low carrier concentration can greatly affect the tunneling characteristics.[15] We have not tried to analyze our data with respect to this new work.

The theoretical curves were derived using a two band WKB model, following closely the work of Conley and Mahan. The WKB approximation is worst near the band bottom where the potential is rapidly varying. Thus we do not expect the theoretical and experimental curves to agree in this region.

Upon examining the data in Fig. 13 one can see inflections in the graph at the places where arrows are drawn on the figure. On the next figure we have blown up the first of these inflections. The vertical scale here is enlarged by a factor of ten, the horizontal scale by a factor of 5. We can, on this plot, measure with reasonable accuracy the step changes in resistannce caused by the participation of the phonon. The data shown has a Fermi degeneracy in which these measurements are particularly difficult. The thinner the barrier width, the smaller the fraction of tunneling current that participates through phonon assisted tunneling. This reflects itself in very small steps in the incremental resistance curve. Fig. 17 show the incremental resistance curve of another sample whose Fermi degeneracy is about 29mv. The phonon structure here is much more pronounced, and consequently easier to measure. In spite of the small size of the phonon participation we can still get a reasonable idea of its strength. The data is analyzed as follows. From Fig. 14 we find the A.C. voltage across the sample to be 10.2×10^{-5} volts, since the vertical scale is 20 microvolts per box. The A.C. current through the sample is measured from the curve of voltage across a series 100 ohm resistor and is 4.65×10^{-5} amps. The incremental background resistance, at the D.C. voltage corresponding to this phonon, is thus 2.2 ohm. The change in incremental resistance is derived by extrapolating the (nearly linear) background voltage, above and below the voltage at which the phonon-assisted tunneling appears. This is

shown in the expanded figure. The difference between the two extrapolated curves is the amount which we ascribe to the incremental phonon-conductance. Actually this particular data gives us the change inresistance, from which we can easily derive the change in conductance. The change in resistance for the above data is(.3 boxes)x(2. microvolts/box) x(1/4.65x10^{-5} amps) = .0129 ohms. The fractional change in resistance is .0059 or .59%. This is the conductance for the first phonon (the TA) and we proceed similarly to find the conductance for the other phonons. Fig. 18 is an expanded graph for the LA phonon. We find that the resistance of the junction at the LA phonon energy is 3.4 ohms and the incremental conductance of the phonon is 1.9x10^{-3} mhos. The ratio of the conductance of the TA phonon to the conductance of the LA phonon is a little over 1.4.

This analysis contains several possible sources of error. It does rely on an extrapolation of the elastic current as well as on a measurement of a small quantity. The change in resistance due to the phonons is only .6% of the background. It would be nice to have a consistency check on our measurements. Second harmonic measurements provide this check. Fig. 19 is an experimental curve in which the second harmonic has been measured. The quantity of interest is the area under the peaks of the d^2I/dV^2 vs. V curve. The experimental curve, as was mentioned in the last section does not measure d^2I/dV^2 directly. The value of d^2I/dV^2 can be gotten by multiplying the measured values by Vac^{-3} and a constant (containing the

gain of the L-C circuit, the current etc.). What we want to compare is the area under the peak for the TA curve with the area under the area under the peak of the curve for the LA curve to get the relative strengths. Although V_{ac} is very different as we go from the TA to LA phonon it remains about constant over the range of each phonon. We then must multiply the experimental area under the peak of the TA phonon by V_{ac}^{-3} at the TA phonon energy and do a similar thing for the LA phonon. The experimental area that we measured are .014 square boxes for the TA phonon and .033 square boxes for the LA phonon. As can be seen from Fig. 13 Vac is much bigger for the LA phonon than the TA phonon. The ratio of $V_{ac_{TA}}^{-3}/ V_{ac}^{-3}$ 3.65. Then the ratio of the conductance of the TA to LA phonon is 3.65 x .14/.33 = 1.5. This is in reasonable agreement with the answer that we got from use of just the first derivative, and is a measure of the accuracy of our analysis of the data.

Another source of error, which, by the way, limits the impurity concentrations on which we can make accurate measurements, is the spreading resistance in the semiconductor. This source can be seen by referring to Fig. 19 . Here we can measure the voltages at which the various phonons participate. We find that the LA phonon occurs at a voltage reading of about 30 mv. Since the LA phonon has an energy of about 27.5 mv there must be some cause for this shift. Part of the answer is that the superconducting energy gap of tin shifts all the structure by an amount equal to ½ the

energy gap of tin or .6mv. This is not nearly enough to account for the discrepancy. The remaining shift is due to this spreading resistance. As the Fermi degeneracy is increased the resistance of the junction drops. The resistance of the sample also drops, but not as fast. The result is that for high carrier concentrations the resistance of the bulk semiconductor and the junction may be comparable. This will introduce further corrections into our calculations. The voltage drop is no longer completely across the junction. In order to find out what part of V_{ac} is across the junction and what part is across the spreading resistance it would be necessary to determine the spreading resistance. By looking at Fig. 13 we see that the TA phonon which should appear at 8mv. appears at 9 mv. This means that when we put 9mv. across the combination, junction plus bulk sample we are only getting 8 mv. across the junction. If we knew the D.C. current in the sample at V_{dc} = 9mv. we could calculate the spreading resistance. The easy way to do this is to take V vs I curves, but, unfortunately, this was not done for this sample. The same information can be gotten by inverting the dV/dI vs. V curve to give a dI/dV vs. V curve. Integrating this curve graphically can be used to generate the V vs. I curve. By doing this it is found that the spreading resistance is something like .2 ohms. Now $\Delta\sigma_{TA}/\Delta\sigma_{LA} = (\Delta R_{TA}/\Delta R_{LA})(R_{LA}^2/R_{TA}^2)$ where we must use corrected values for R_{LA} and R_{TA}. The corrected factor $R_{LA}^2/R_{TA}^2 = (3.2/2.0)^2 = 2.6$. The ratio of $\Delta\sigma_{TA}/\Delta\sigma_{LA}$ is thus

increased to 1.5 instead of the old value of 1.4. Similarly thethe factor $V_{ac_{LA}}^3 / V_{ac_{TA}}^3$ in the equation $\frac{\sigma_{TA}}{\sigma_{LA}}$ = Area TA/Area LA: $(V_a(V_{ac_{LA}}^3 / V_{ac_{LA}}^3)$ is now $(3.2/2)^3=4.1$ instead of $(3.4/2.2)^3= 3.7$ this gives as the value of σ_{TA}/σ_{LA} = 1.7 instead of the previous value of 1.5. A similar analysis can be carried out for the other phonons. Fig. 20 is a graph of the relative magnitude of TO to LA phonon-assisted channels. The determination of a proper background is more difficult for the TO phonon, since there is additional structure near it which partially overlaps the TO phonon assisted structure. This is easily seen by consulting figures 21, 22, 23. Fig. 21 is taken at 4.2°K, Fig. 22 at 1.5°K but with a magnetic field, while Fig. 23 is taken at 1.5°K with H=0.[37] Notice that the TO zone boundary phonon is progressively sharpened in appearance and separated from the structure near it at a higher bias. It is reasonable that a decrease in temperature results in a decrease in thermal smearing. Another way of saying this is that the Fermi level is sharpened. Since a phonon is emitted when the Fermi level of the metal is a phonon energy below the Fermi level of the semiconductor (and vice versa) the onset is sharper if the Fermi level is sharper. If the metal is superconducting the onset of phonon-assisted tunneling is further sharpened. In this case (ideally) there can be no phonon-assisted tunneling until the difference in Fermi levels (between metal and semiconductor) is equal to the phonon energy added to ½ the superconducting energy gap. Once this energy is achieved

the tunneling electron sees a large density of states in the metal. Thus the onset of phonon-assisted tunneling is sharpened.

The additional structure previously mentioned at a bias of about 39 mv is also interesting. Fig. 24 is a graph of the uncorrected second derivative data which shows the four zone boundary phonons as well as the additional structure at 39 mv. Notice that the phonon-structure is anti-symmetric about zero bias (peaks on one side, dips on the other). The structure at 39 mv on the other hand is symmetric (dips on both sides). In Fig. 34 we plot the strength of the structure at 39 mv as a function of Fermi degeneracy in the Ge. The derivation of these plots from the experimental curves proceeds in a very similar way to our determination of the strengths of the various phonon channels. As we just mentioned, this structure is difficult to separate from the TO structure. Thus, in some sense, the values on the plot (Fig. 34) are not too accurate. It is clear, however, that there is no structure below a Fermi degeneracy of about 29 mv. The fact that the structure appears at the k=0 optical phonon energy, is symmetric about zero bias and has a threshold, all point to the fact that this structure is due to an electron-phonon self energy effect. This is discussed elsewhere.

We also took data on vacuum cleaved junctions on n-Si. Since phonon structure had been seen in p-n junction of Si we wanted to try to find phonon structure in Si ms junctions. At the time we made our measurements on Si the only published

work on n-Si ms junctions was done by Hsia and Tao.[38] They had made only first derivative measurements. They did not cleave the silicon but etched it and thenttried to avoid oxidation by quickly placing it in an evaporation unit, pumping down and evaporating. The result is that they certainly got some oxide between the evaporated metal and the bulk silicon. On looking at their first derivative plots we could see structure but couldn't determine if it was real or noise. We felt it would be worthwhile to take first and second derivative measurements of vacuum cleaved metal-silicon junctions (the silicon we used was antimony doped with a resistivity of .005-.010 ohm-cm). One of our experimental curves is shown in Fig. 25 . The phonons of Si that participate in Si p-n junctions have energies of 17.9 mv (TA), 43.7 mv(LA), 53.2(LO) and 58.5mv (TO).[39] The TA and TO phonon are the most prominent in p-n junctions. Naturally we were hoping to find structure at these energies on our data. Fig. 25 is a plot of incremental conductance as a function of applied bias. The minimum in incremental conductance corresponds to a sample resistance of about 22 K ohms. The fact that the minimum in conductance now lies to the left of zero bias is just due to the way data was taken. The second derivative plot is shown in Fig. 26 The horizontal scale is 10 mv/inch. There is certainly noticeable structure appearing at the TA and TO phonon energies. Unfortunately there is also structure at almost every other energy. A second (upper) plot was taken later to see whether the

structure was time dependent. It shows almost identical structure. Unfortunately these plots were not reproducible from sample to sample. In fact the same sample would show changed structure upon warming it up to room temperature and then re-immersing it in the helium. We tested to see if the structure was magnetic-field dependent. We found that up to field of 15 Kg, it was independent of magnetic field. Different dots evaporated at the same time on the same sample were compared. Even for these data, the structure was not reproducible, except that the structure corresponding to the TA and TO phonons was more reproducible than any other structure. We thought that this structure might be due to strains at the junction due to a mismatch in thermal expansion between the silicon and the evaporated metal. To explore this possibility we evaporated different metals. Fig.27 is a plot of a Cr-Si junction. This curve is uncorrected data of VdI/dV and Fig.28 is a second derivative plot. The A.C. voltage across the sample was not kept constant and thus the plots do not directly reflect the incremental conductance. The minimum in incremental conductance corresponds to a sample resistance of 64.5 ohms. This implies that the barrier height for Cr-Si junctions is lower than the barrier heights for Au-Si junctions. Notice also in these junctions the appearence of structure at zero bias (similar structure was seen with the other metals as well). This structure has been seen in various semiconductors and has been studied extensively in silicon by Losee and Wolf.[23]

We also made an attempt to evaporate platinum-silicon junctions but after some hardship in the evaporation itself, we were unable to get good junctions. These experiments were not conclusive in determining whether the thermal mismatch played a major role in producing this structure.

Another possible source of the added structure might be some type of sensitivity to surface contamination. To see if this was the case we cleaved a bar of silicon and delayed evaporation for some 60 seconds. We felt that if oxides or adsorbed gas was responsible for the structure this technique would cause a great difference in the nature of the structure. It didn't. We finally decided to go to higher carrier concentrations (.002-.003). Amazingly we saw no structure at all. Even the phonon structure was gone. We had so much spreading resistance with these samples that we couldn't put a large enough voltage across the sample. Most of the voltage would always appear across the bulk semiconductor. We felt that putting in even more power into the semiconductor would cause further problems. At this time we became aware that others had recently seen phonon structure in silicon. We can compare our data taken on vacuum cleaved, low resistance junctions with the data of Tsui and Dunkleburger[22] taken on silicon-oxide-metal junctions. There is close correspondence in the region where our respective data overlap but our data does not go out far enough in bias to see the phonons (Fig. 29 , 30) We still do not know where the original structure came from, in the high resistance samples.

Figure Thirteen

This figure is essentially a plot of incremental resistance as a function of D.C. bias for Sn-Ge $\mu_F = 40$ mv. The arrows denote the position of the onset voltages for phonon assisted tunneling.

Fig. a is the A.C. voltage across the sample. The vertical scale is 20 microvolts per box. The horizontal scale is 5 mv per box.

Fig. b is the A.C. voltage across the resistor in series with the sample (100 ohms). The vertical scale here is 500 microvolts per box. The horizontal scale is 5 mv per box.

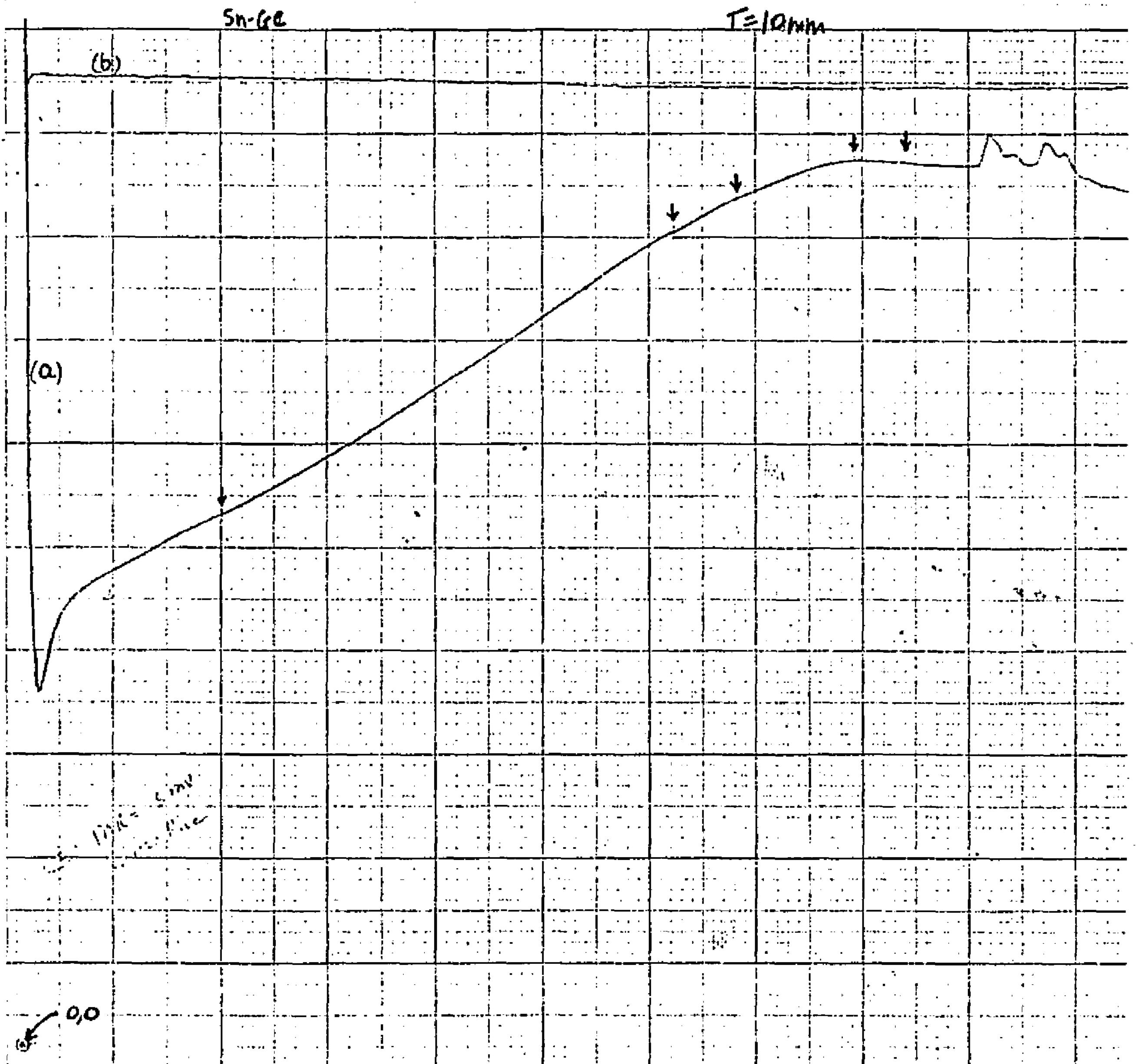
Sn-Ge
T=10mm
(b)
(a)
0,0

Figure Fourteen

Theoretical plot of the incremental resistance line shape as a function of D.C. bias. The horizontal scale is 5 mv per box. The vertical scale has been adjusted to read 5 scale divisions at 8 mv.

$\mu_F = 24$

HEWLETT-PACKARD

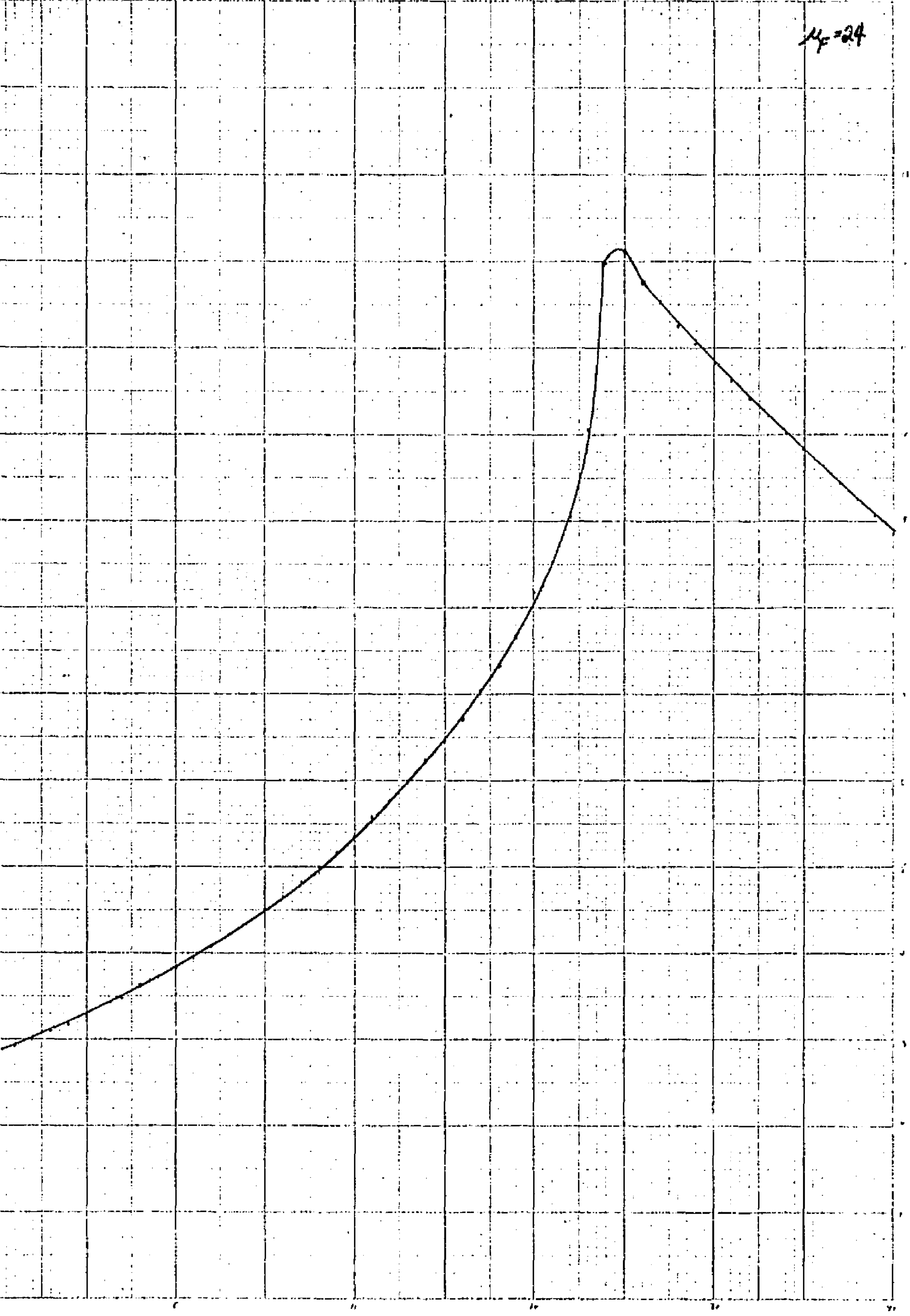

Figure Fifteen

Theoretical plot of the incremental resistance line shape as a function of D.C. bias. The horizontal scale is 5 mv per box. The vertical scale has been adjusted to read 5 scale divisions at 8 mv. $\mu_F = 40$.

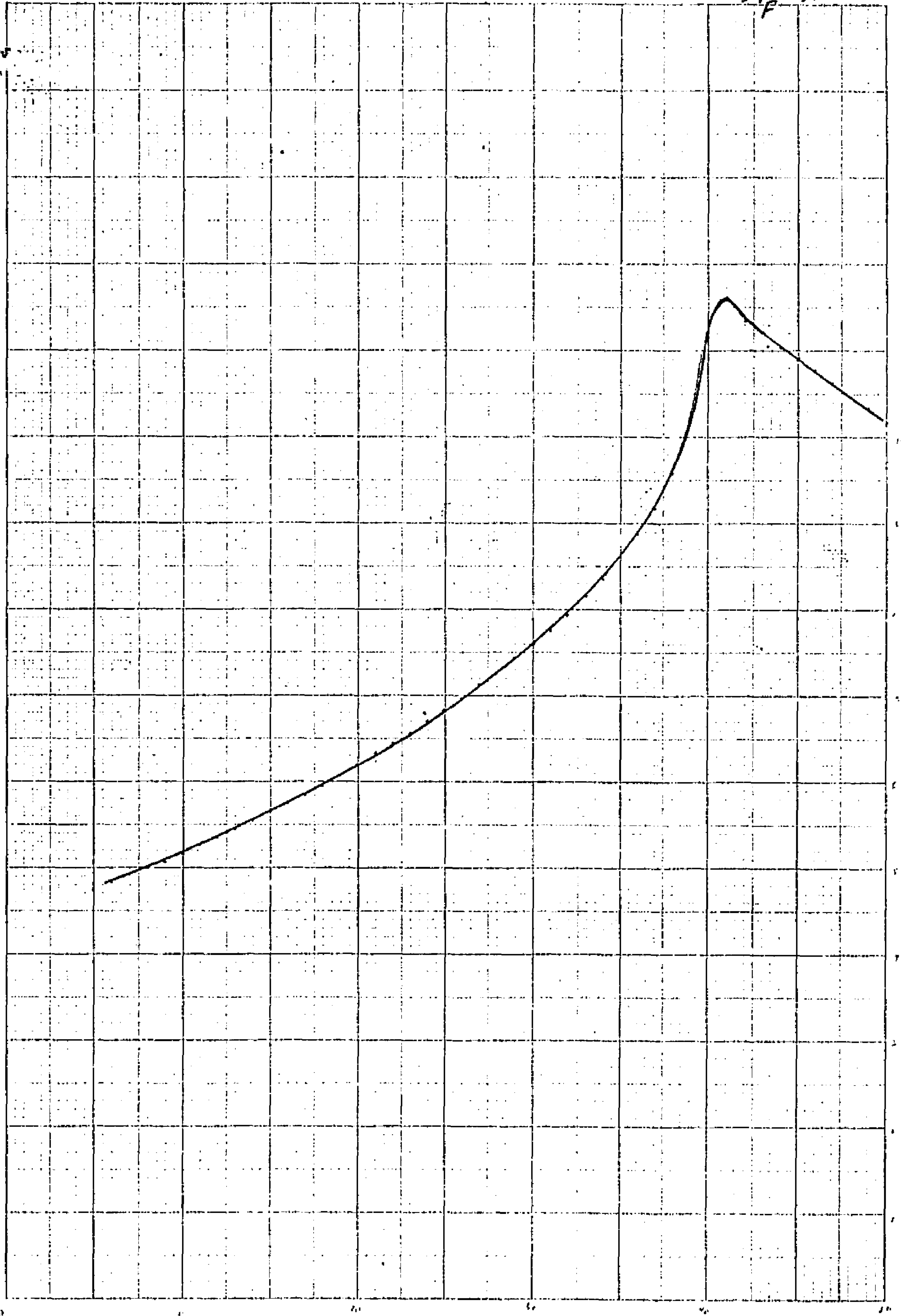
$\mu_F = 40$

Figure Sixteen

Blow up of incremental resistance (y axis) vs D.C. bias for μ_F=40mv. The vertical scale is 2 microvolts per box. The horizontal scale is 1 mv per box. The A.C. current through the sample is the same as in Fig. 13.

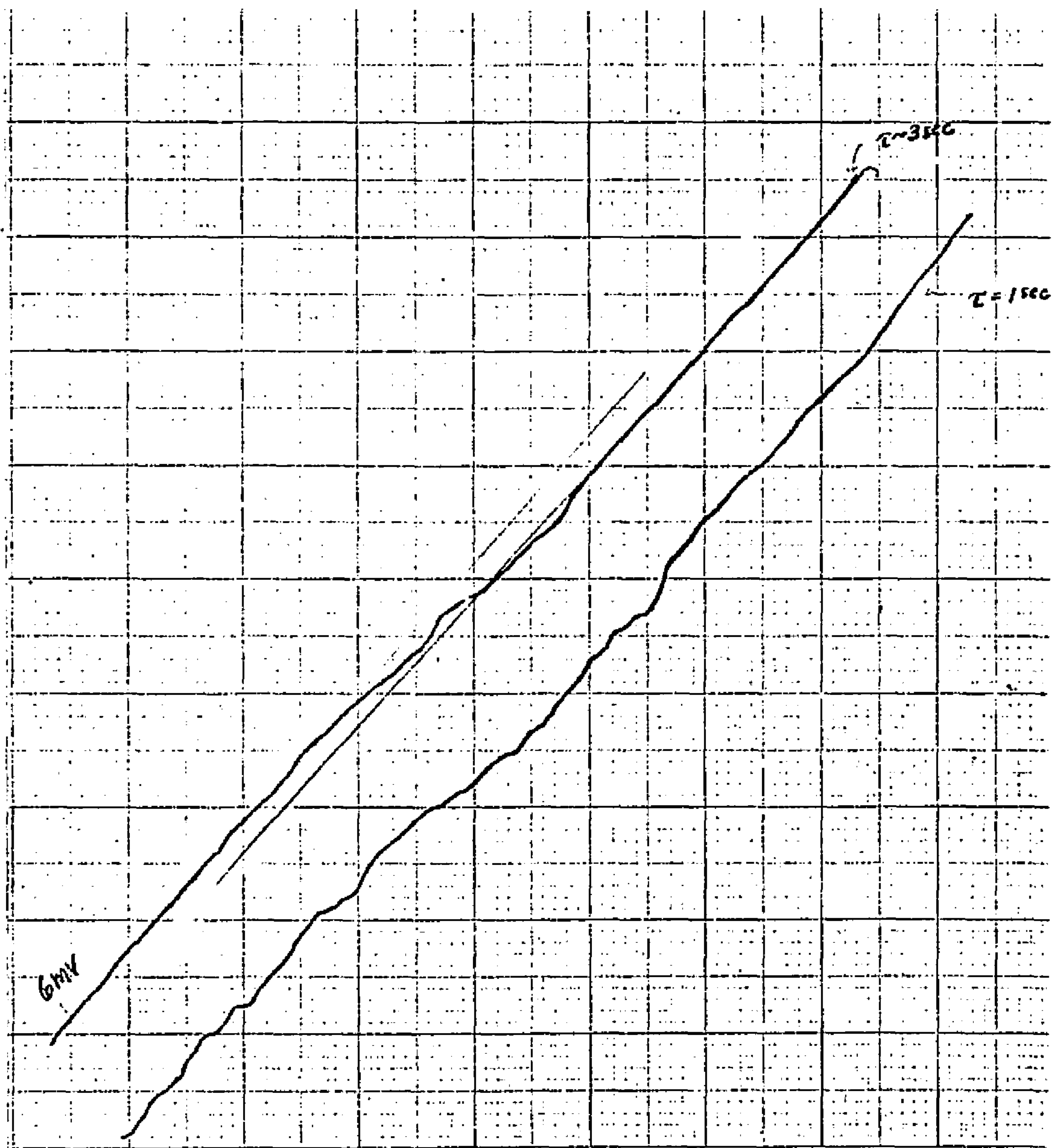

Figure seventeen

Fig. a is essentially a plot of incremental resistance as a function of D.C. bias. Fig. b is a plot of the A.C. current through the sample.

The vertical scale for Fig. a is 20 microvolts per box and measures the A.C. voltage across the sample.

The vertical scale for Fig. b is 50 microvolts per box and measures the A.C. voltage across a 100 ohm resistor is series with the sample.

The horizontal scale is 5 mv per box for both a and b .

$\mu_F = 29 mv$ Sn-Ge

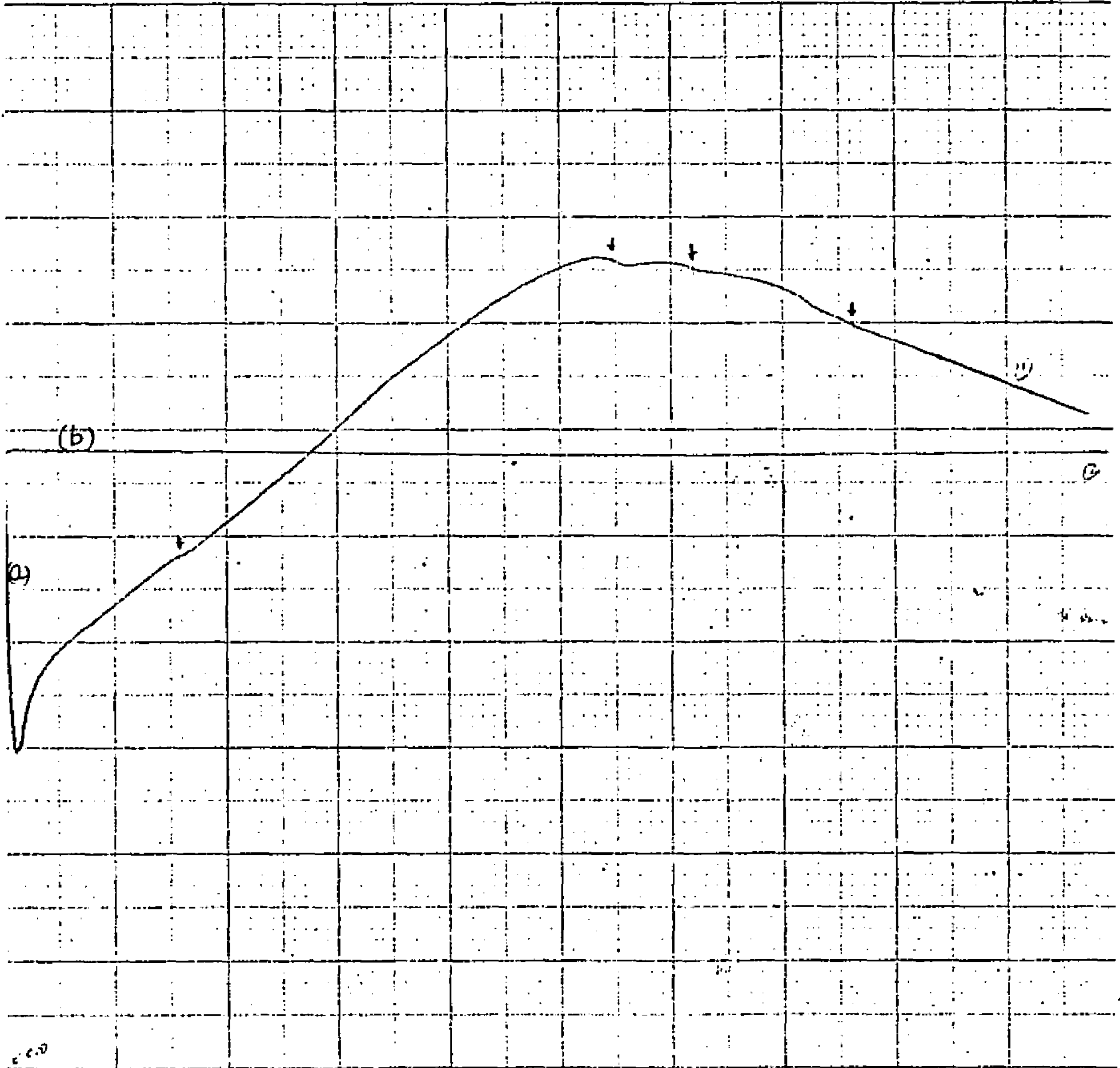

Figure Eighteen

Blow up of incremental resistance (y axis) vs D.C. bias for Sn-Ge, $\mu_p = 40$ around the LA phonon energy The vertical scale is 2 microvolts per box. The horizontal scale is 1 mv per box. The A.C. current through the sample is the same as in Fig. 13.

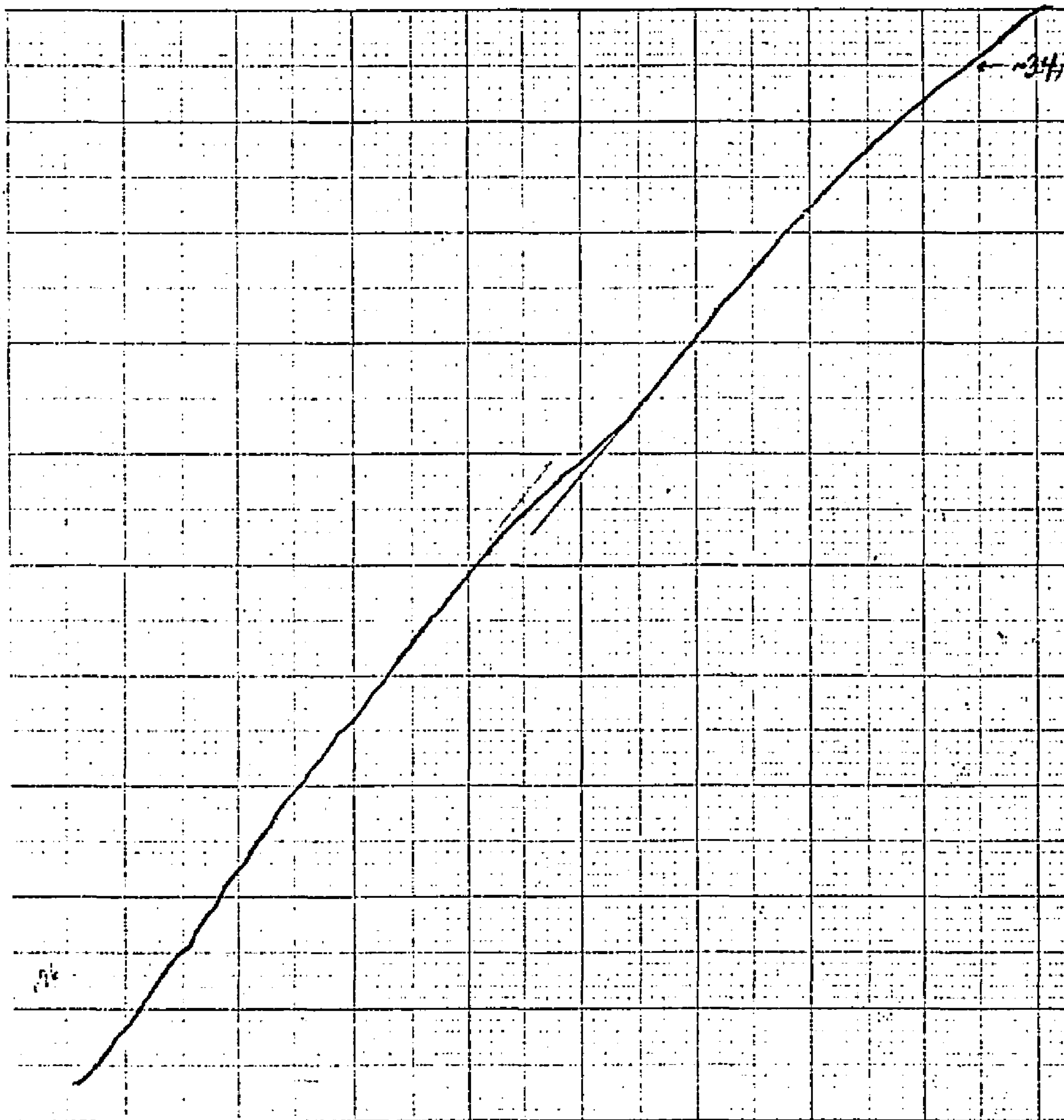

Figure Nineteen

2nd harmonic voltage (y axis) vs D.C. bias for Sn-Ge μ_F=40mv. To get d^2I/dV^2, corrections to this curve must be made.

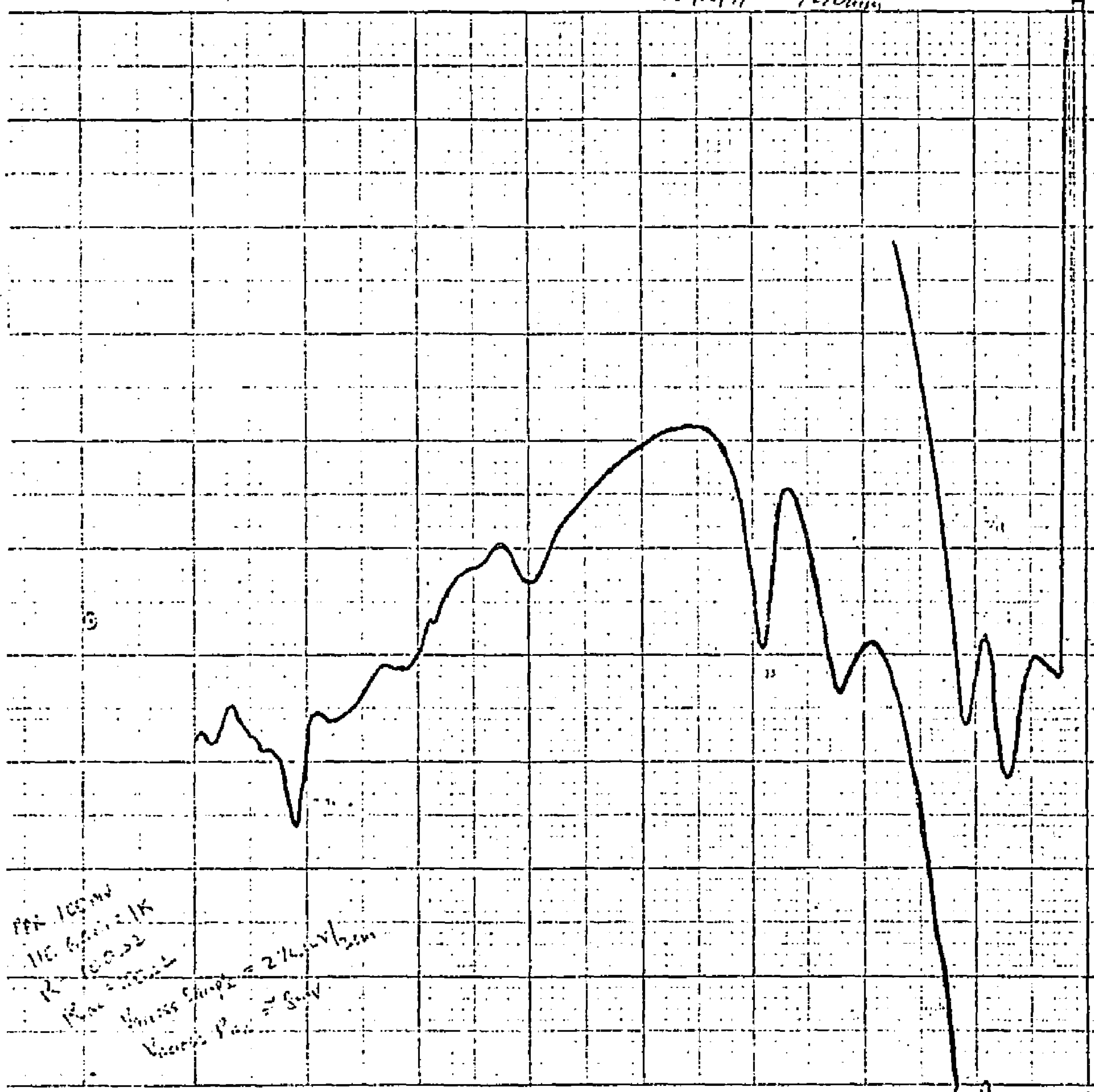
12/10/71

Figure Twenty

Ratio of To to LA phonon conductance (at onset) is plotted against Fermi level (x axis)

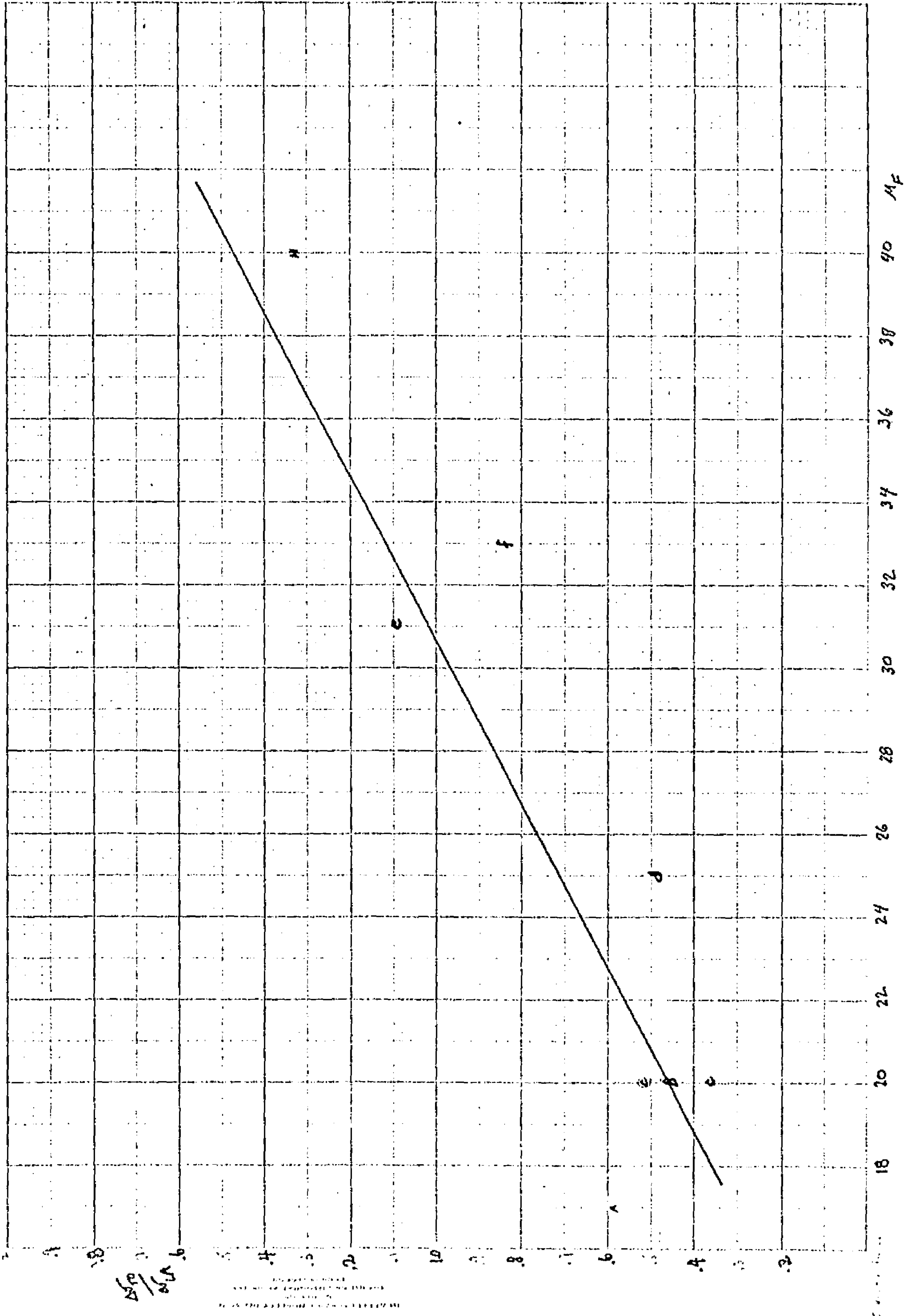

Figure Twenty One

2nd harmonic voltage (y axis) vs D.C. voltage (forward bias) for Sn-Ge, $\mu_f = 40$ at 4.2^{o}K

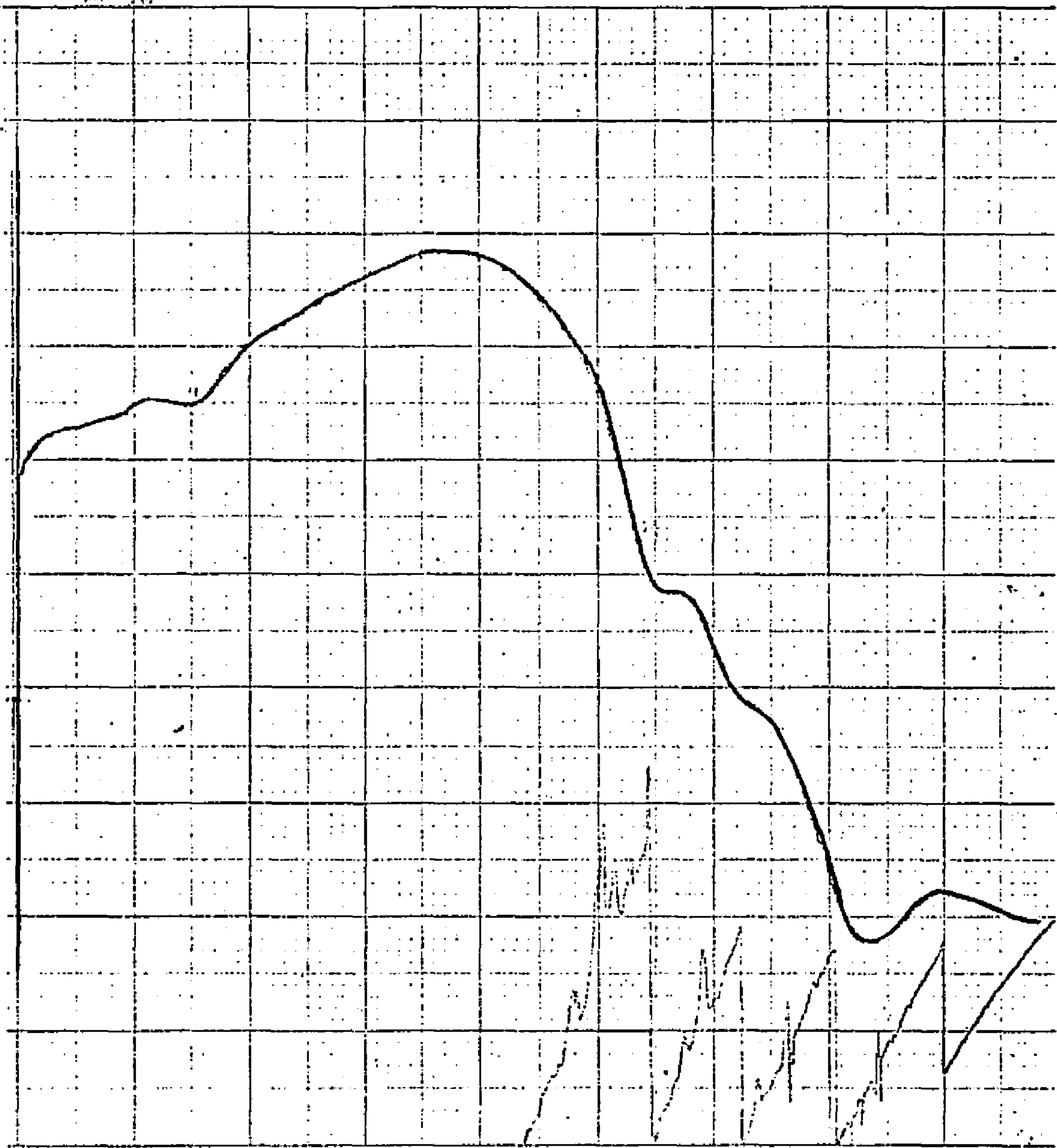

Figure Twenty Two

2nd harmonic voltage (y axis) vs D.C. voltage (forward bias) for Sn-Ge, $\mu_F = 40$ mv at 1.5^{o}K with H field strong enough to make the Sn non-supercon ducting.

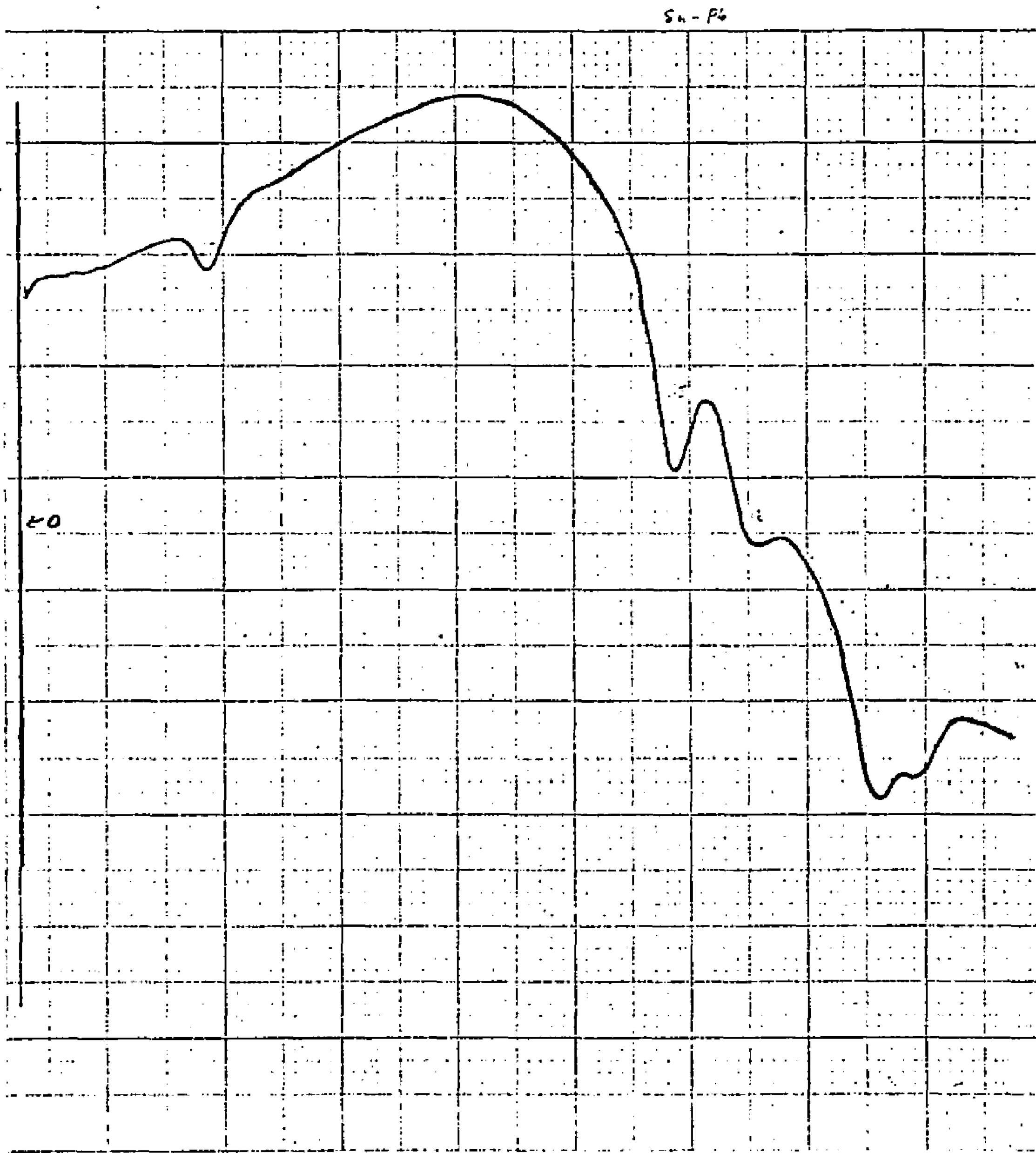
Sn - Pb

Figure Twenty Three

2nd harmonic voltage (y axis) vs D.C. voltage (forward bias) for Sn-Ge, $\mu_F = 40$ mv at 1.5°K with Sn superconducting.

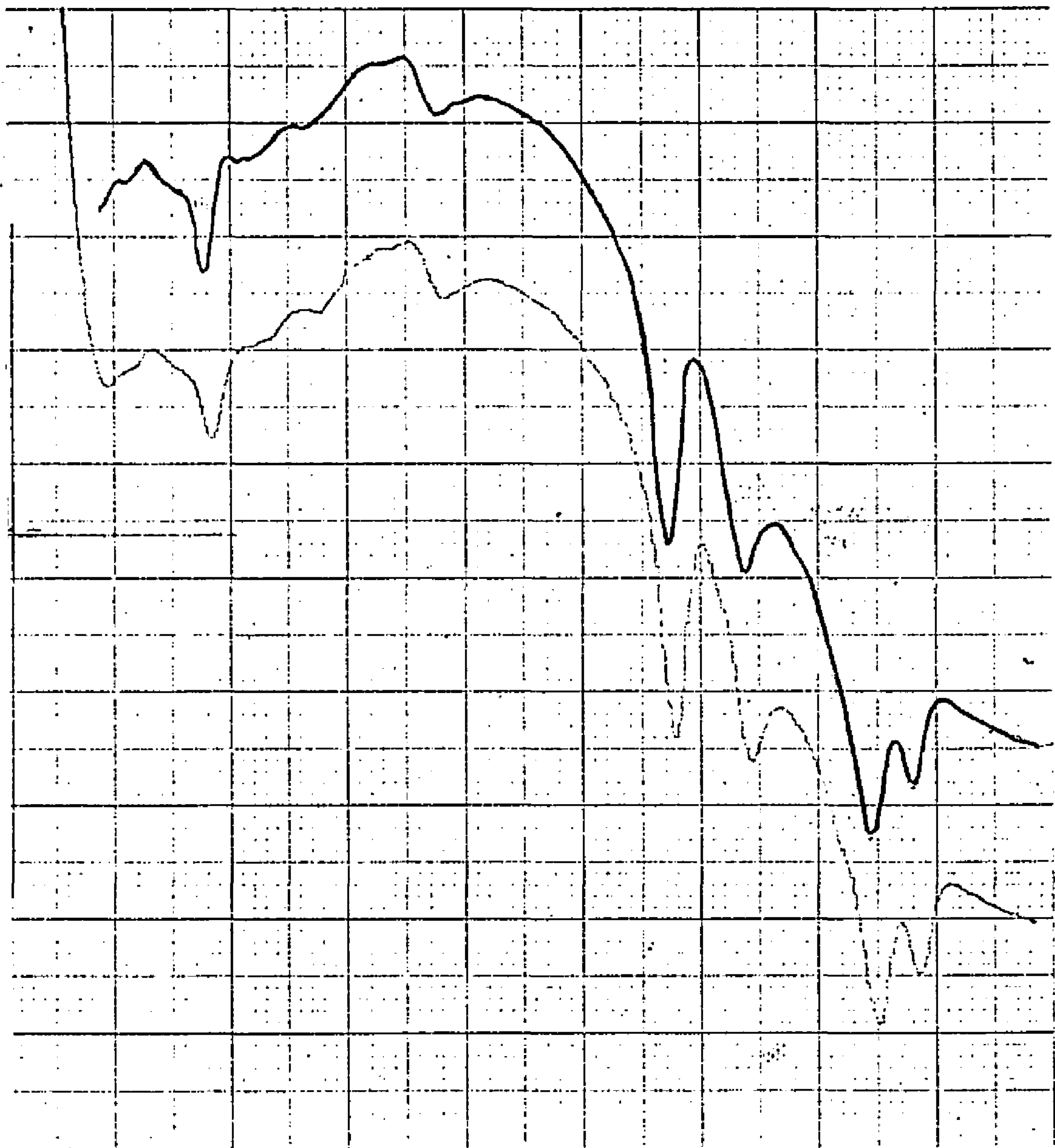

Figure Twenty Four

2nd harmonic voltage (y axis) vs D.C. voltage (forward and reverse bias) for Sn-Ge, μ_F = 29mv

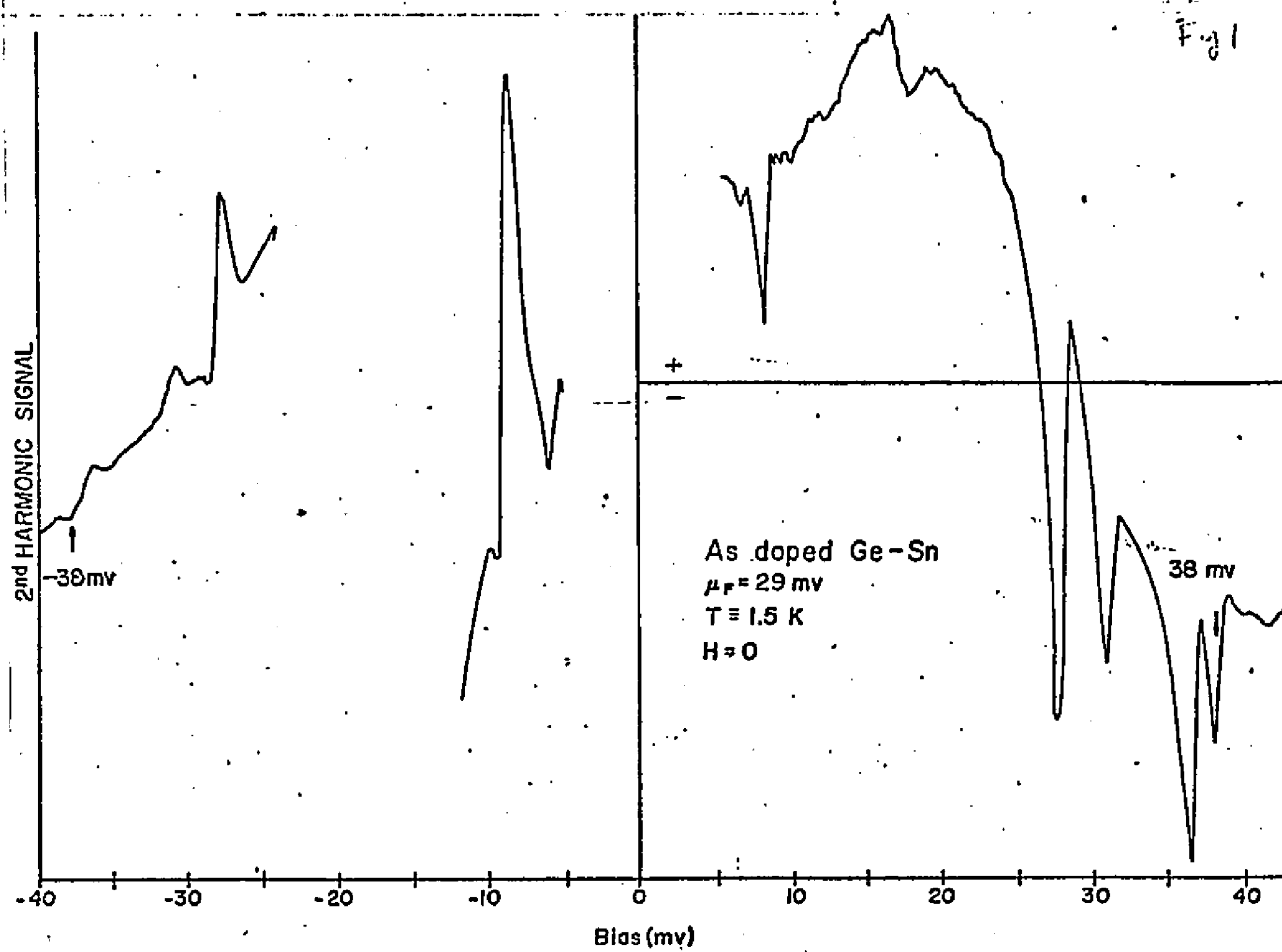
Fig 1
2nd HARMONIC SIGNAL
-38mv
38 mv
+
−
As doped Ge−Sn
μ_F = 29 mv
T ≡ 1.5 K
H = 0
-40
-30
-20
-10
0
10
20
30
40
Bias (mv)

Figure Twenty Five

Incremental conductance vs Voltage for Au-Si
The minimum in incremental conductance corresponds to a sample resistance of about 22 K ohms. The horizontal scale is 10 mv per box.

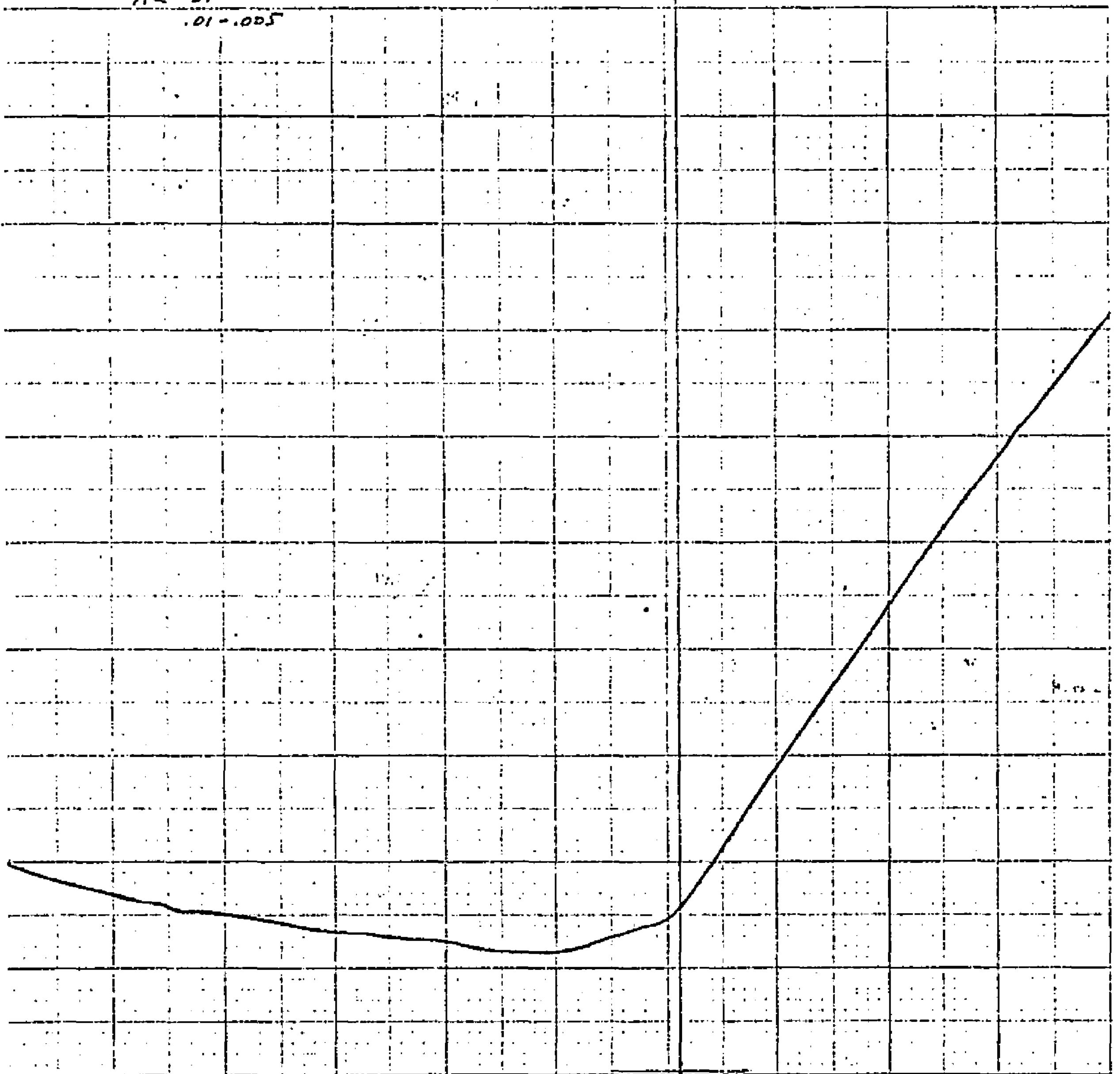
Au - Si
.01 - .005

Figure Twenty Six

2nd harmonic voltage (y axis) vs D.C. voltage for Au-Si sample in Fig. 25. Horizontal scale is 10 mv per box.

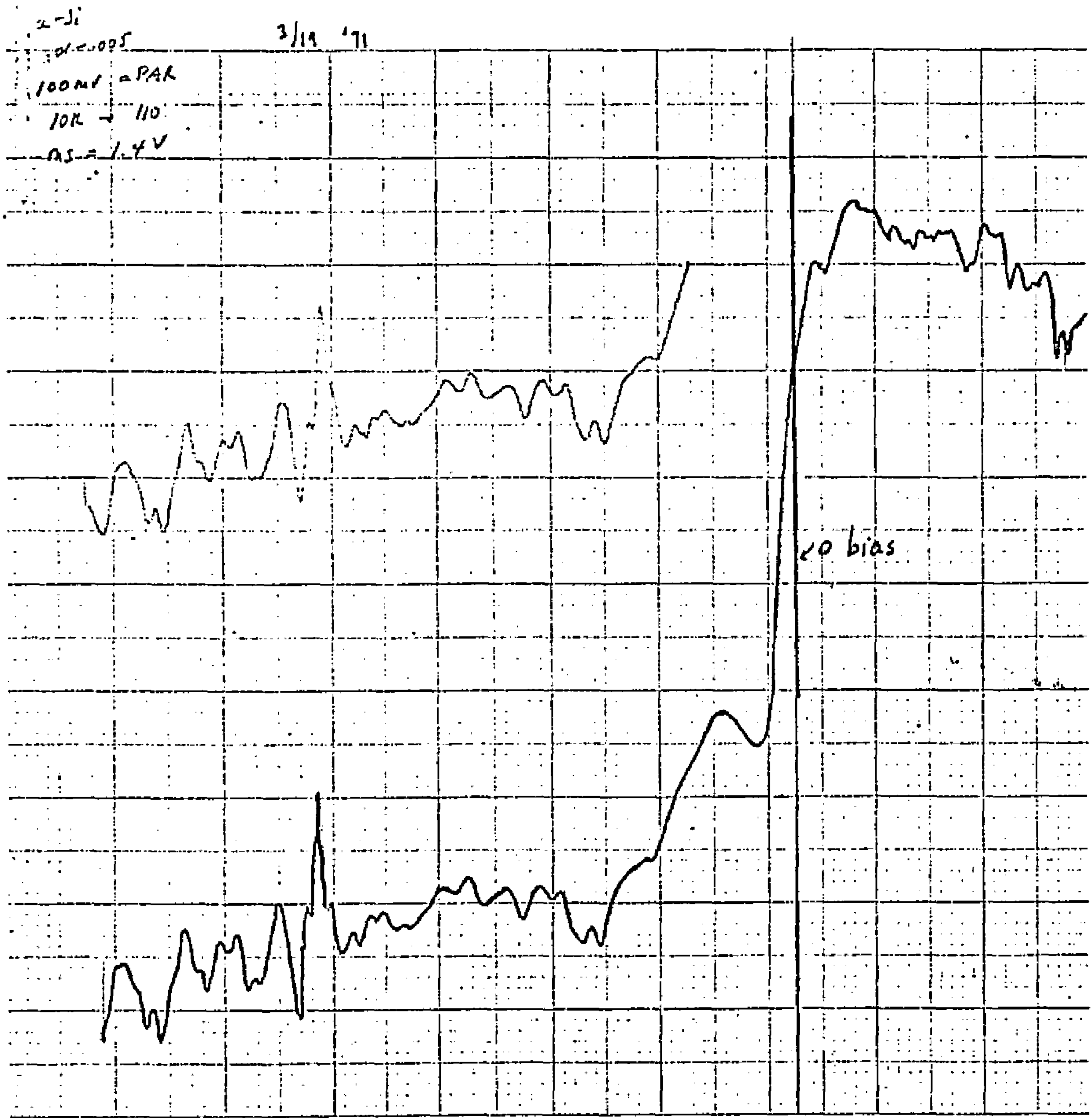

a-Si
3/19 '71
100mV = PAR
10R → 110
AS = 1.4V
← 0 bias

Figure Twenty Seven

Fig. a is incremental conductance vs D.C. voltage for a Cr-Si junction. The same silicon was used as for the Au-Si junction shown in Fig. 25. The minimum in incremental resistance corresponds to a sample resistance of 64.5 ohms. The horizontal scale is 10 mv per box. Fig. b is a plot of the voltage across the sample (which should be a constant if the measured A.C. current through the sample were to reflect the incremental conductance).

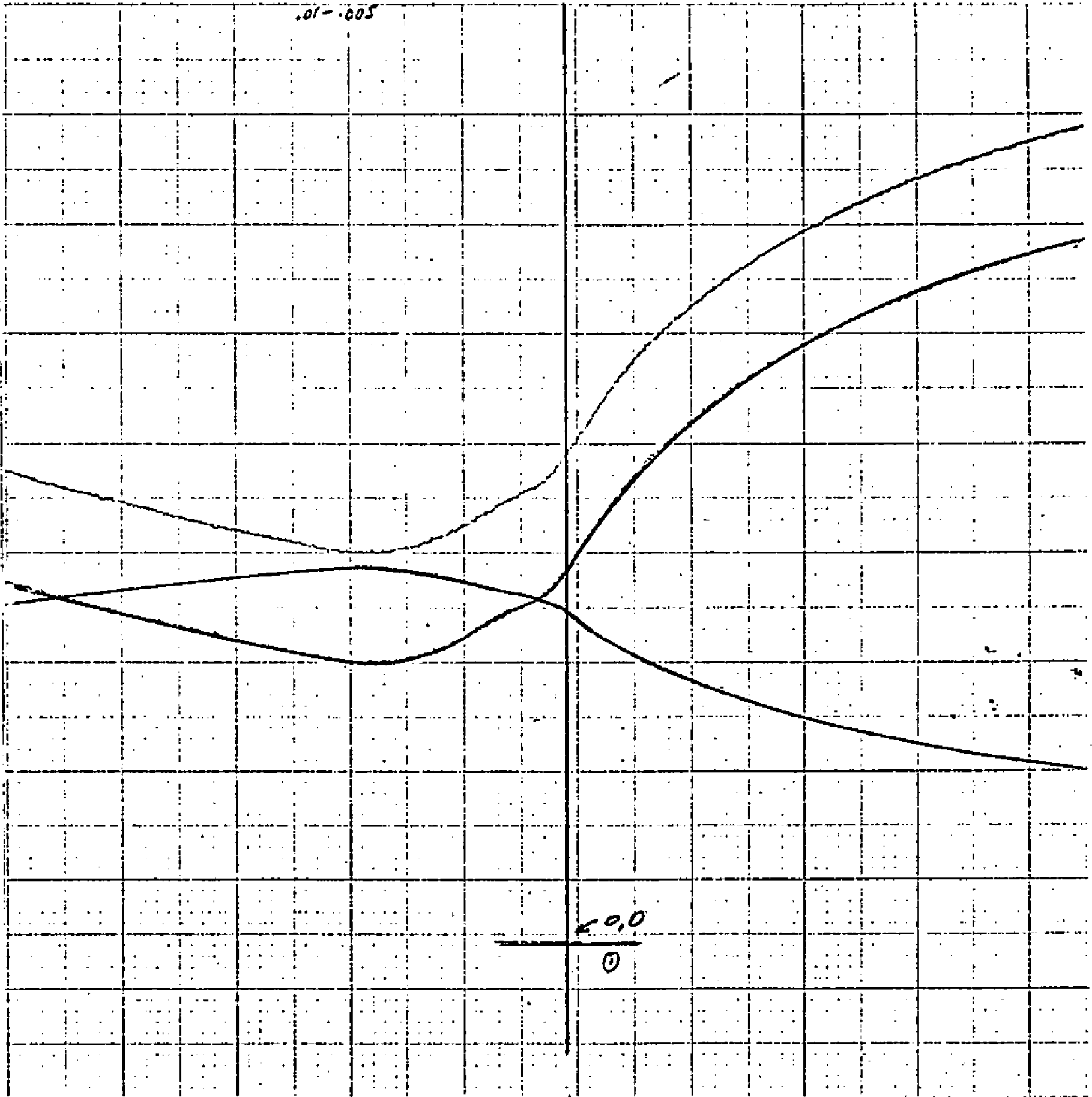
Cr-Si 2
.01-.005
0,0
0

Figure Twenty Eight

2nd harmonic voltage (y axis) vs D.C. voltage for Cr-Si junction. Plots were taken twice to prove that the structure was not noise. The arrow indicates the position of the Si TA phonon.

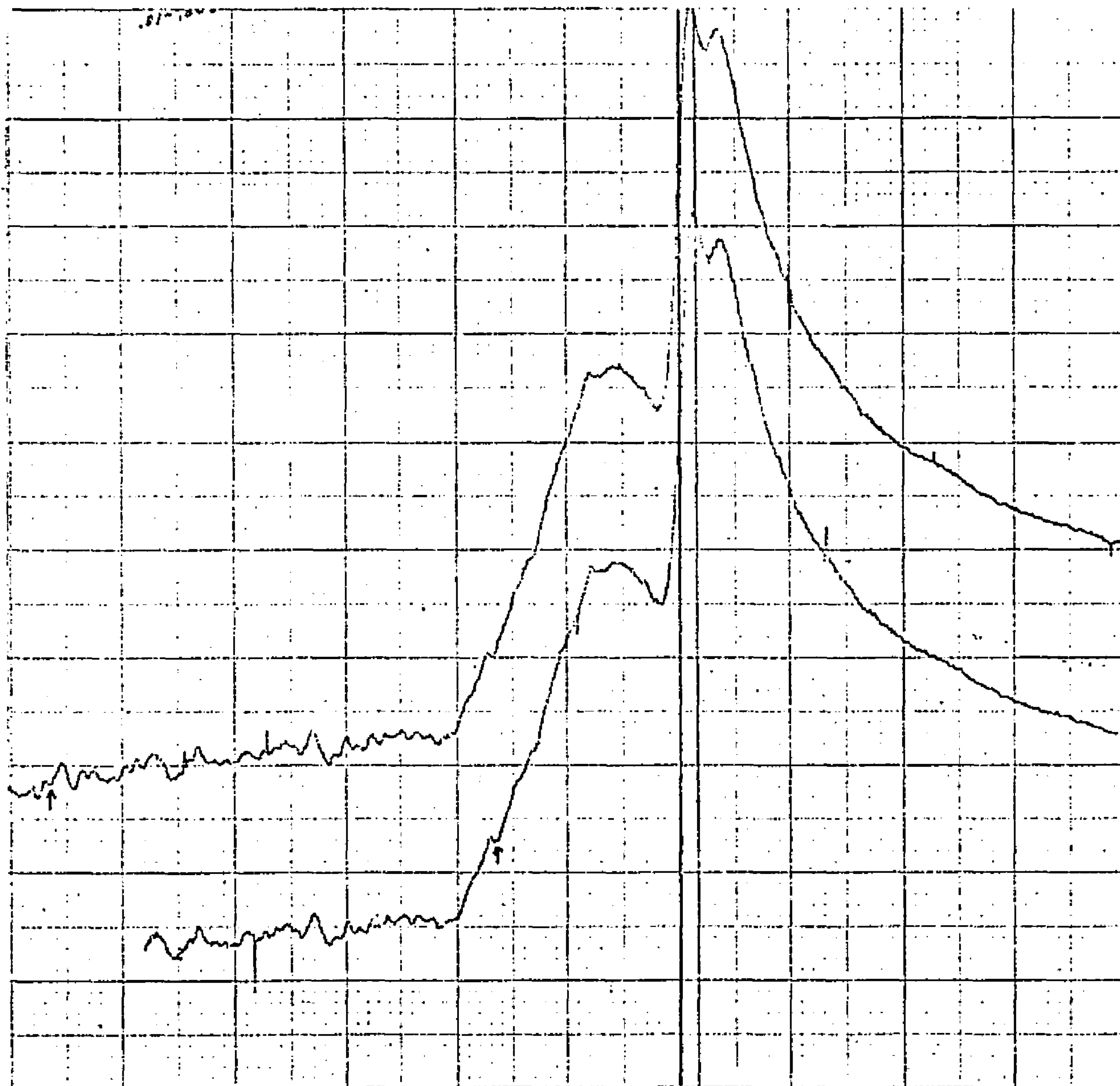

Figure Twenty Nine

2nd harmonic voltage (y axis) vs D.C. voltage for a low resistance Au-Si junction. Forward bias is to the left.

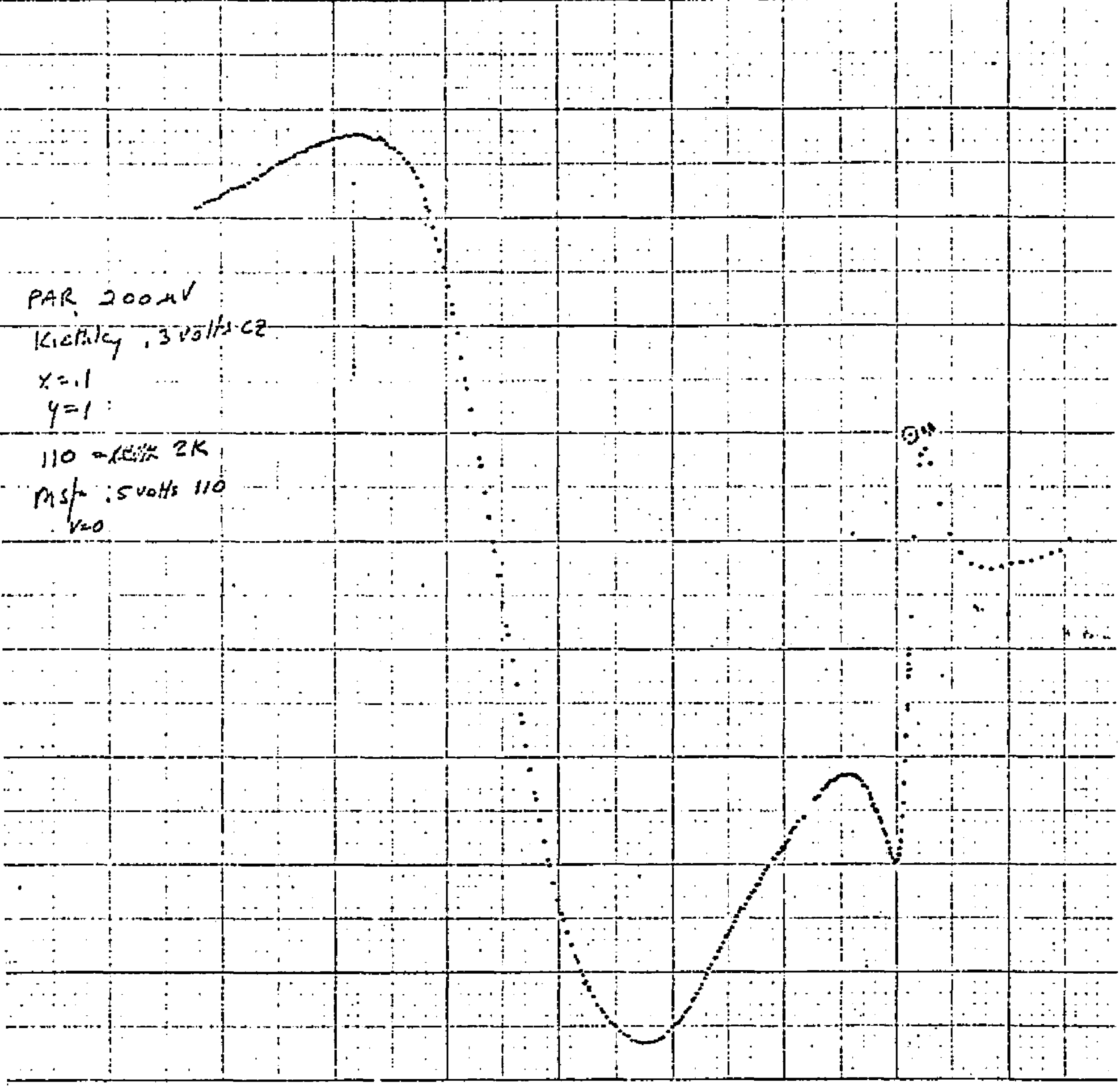
PAR 200 μV
Kiethley .3 volts·cz
x=.1
y=1
110 ohms 2K
msf .5 volts 110
V=0

Figure Thirty

2nd harmonic data of Tsui and Dunkleburge on low resistance Au-Si . Forward bias is to the right.

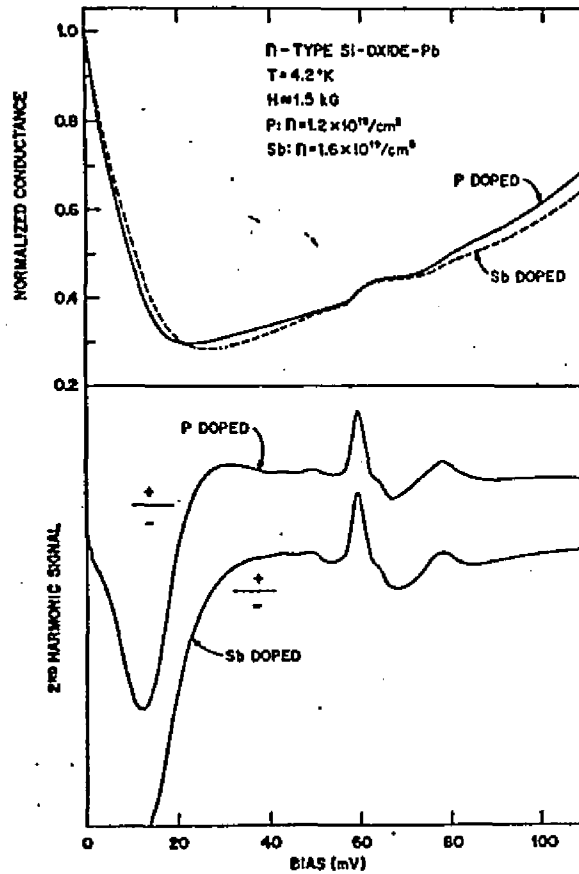

FIG. 3. Tunneling characteristics of a P-doped ($n \approx 1.2 \times 10^{19}/\text{cm}^3$) Sb-doped ($n \approx 1.6 \times 10^{19}/\text{cm}^3$) Si-oxide-Pb junctions in the Pb(+) bias ($T = 4.2\,°\text{K}$ and $H \approx 1.5\,\text{kG}$). (a) Conductance normalized at zero bias; (b) the second harmonic signal.

Conclusion

In this section we will compare our data to theory. We will first discuss the phonon-assisted tunneling that is found in Ge m-s junctions. As was previously mentioned this phonon-assisted tunneling is thought to take place by an electron making a transition from $L \rightarrow \Gamma_2'$ with the emission of a phonon. Once in this state the electron tunnels through the barrier and into the metal. The L state has an effective mass of about .08 while the effective mass of the Γ_2' state is about .034. We can use our data to qualitatively test the theory. We can determine, at least, whether the electron that tunnels via phonon-emission does so with a different effective mass than the electron that tunnels directly. Assume that the tunneling can be represented by some type of WKB approximation. The dependence of the probability on the effective mass goes as $e^{-A\sqrt{m}}$ where A is a factor that reflects the barrier properties. For a given barrier we can see that the tunneling probability is higher for electrons with small effective mass. Further, an electron tunneling with a large mass is more greatly affected by a change in barrier shape than an electron of small mass (i.e. Ratio= $e^{-\sqrt{m}(A_1-A_2)}$). The theory states that the inelastic tunneling takes place with a smaller effective mass than the direct tunneling. As the barrier width is decreased the direct tunneling should then decrease more rapidly than the phonon-assisted tunneling. This then would be observable as a decrease in importance of the inelastic process relative to the direct process. By reference

to Fig. 4 and Fig. 13 we can see that the increase in the Fermi level results in the theoretically expected relative decrease of the phonon-assisted tunneling. We can make a more quantitative test of the theory. Fig. 31 is a plot of the ratio of TA to LA phonon-assisted conductance as a function of Fermi degeneracy. Notice that as the Fermi degeneracy is increased the strength of the TA phonon increases relative to the LA phonon. Does the theory of Davis and Steinrisser predict this increase? Fig. 32 is a representation of how inelastic tunneling is theoretically expected to occur. An electron is thought to make a transition from L to a virtual Γ_2' state and then to tunnel through the barrier. There are two reasons why such a process should have a high probability of occurence. For on thing, the small effective mass of the inelastically tunneling electron gives it a high transmission probability. Perhaps even more importantly the electron does not have to emit the phonon in the barrier region. An electron that emits a phonon (and then enters a virtual Γ_2' state) may do so outside the junction and then tunnel toward the junction under a barrier $V_{\Gamma_2'}$ shown in Fig. 32 . This is a relatively small barrier and may not greatly decrease the transmission pobability of the electron. A great increase in the probability of phonon emission results since electrons may emit phonons not only in the junction but outside it as well. This is compared with a process in which an electron goes from

by the emission of a phonon. In this process the size of the barrier dictates that phonon-emission occur only in the junction. For an LA phonon, the transition $L \to \Gamma_{2'}$ is allowed. For a TA phonon on the other hand, such a transition is not allowed. The transition that is being made however is not $L \to \Gamma_{2'}$ but to a virtual $\Gamma_{2'}$ state. Once again returning to our two band Hamiltonian we have

$$\begin{pmatrix} \Delta_\Gamma + \hbar k^2/2m & \hbar/m\, k\cdot p \\ \hbar/m\, k\cdot p & \hbar^2 k^2/2m \end{pmatrix}$$

which has eigenvalues

$$E = \frac{1}{2}\Delta_\Gamma + \left[(\hbar^2 k^2/2m) \pm \tfrac{1}{2}\eta\right]$$

where

$$\eta = \left[\Delta_\Gamma^2 + (\Delta_\Gamma \hbar^2 k^2/m_\Gamma)\right]^{1/2}$$

and

$$U_k^{\Gamma_2'} = (2\eta)^{-1/2}\left\{(\eta + \Delta_\Gamma)^{1/2} U_0^{\Gamma_2'} + (\eta - \Delta_\Gamma)^{1/2} U_0^{\Gamma_{25}'}\right\}$$

The virtual $\Gamma_{2'}$ state then contains some $\Gamma_{25'}$. The extent of this admixture is $\left\{\dfrac{|(\eta - \Delta_\Gamma)^{1/4}}{|(\eta + \Delta_\Gamma)^{1/2}|}\right\}^2$. For energies reasonably close to $\Gamma_{2'}$, $\eta > \hbar^2 k^2/2m$ and $E \cong \frac{1}{2}\Delta_\Gamma + \frac{1}{2}\eta$

Then for a virtual state an energy $V_{\Gamma_{2'}}$ from $\Gamma_{2'}$ and $V_{\Gamma_{25'}}$ from Γ_{25}' we have $E = V_{\Gamma_{25'}}$ and $\Delta\Gamma - E = V_{\Gamma_2'}$. Then $|(\eta - \Delta_\Gamma)/(\eta + \Delta_\Gamma)| = V_{\Gamma_2'}/V_{\Gamma_{25}'}$.

In other words the virtual state at Γ_2' contains a k=0 Γ_2' part and a k=0 Γ_{25}' part whose magnitudes go as the distance (in energy) between them and the virtual state. Now the transition is forbidden (at k=0) but the transition can be made to the Γ_{25}' part of the virtual state. As the Fermi degeneracy is increased, the virtual state moves closer to the Γ_2' state. Between a Fermi degeneracy of 20 mv and 40 mv the virtualstate

only moves by 20 mv. This is a small number compared to the direct band gap (910mv). The relative strength of the TA and LA phonons depends basically on the ratio of $V_{\Gamma_{25'}}/V_{\Gamma_{2'}}$ in the $\Gamma_{2'}$ virtual state. But we have shown that this ratio is relatively independent of Fermi degeneracy. Hence the theory would predict that the ratio of TA to LA phonon strength should hardly depend on carrier concentration. Reference to Fig. 31 shows that, in fact, it is a strong function of carrier concentration. We have assumed that both the TA and LA phonons are emitted outside the barrier. In fact as was mentioned, the high probability of the two step tunneling process is owed to the possibility of phonon emission in the bulk. Hence we do not feel that the electrons emit phonons in the barrier. We find a very similar effect taking place with respect to the TO phonons. As the Fermi degeneracy is increased the strength of these phonons also increases relative to the LA phonons. Fig. 31 is a plot of this behavior.

We have also measured the absolute conductance due to the LA phonon as a function of Fermi degeneracy. This is shown in Fig. 33 . Also shown in that Fig. is the theoretical prediction of Davis and Steinrisser. We conclude from Fig. 33 that the theoretical prediction seems generally to describe the phonon process. The relative strengths of the phonons, are not, however, well described by the theory.

Recently there has been work on phonon-assisted tunneling in m-s junction of silicon. Schein and Compton have used

a theory of impurity mediated phonon assisted tunneling. We have not seen any calculation of this type of tunneling applied to Ge. However, we do not believe that this type of tunneling is responsible for the effects that we see. In this process the electron would start in the L band and scatter without k conservation again into the L band. As the impurity concentration is increased there is no reason to expect that the phonon-assisted process would decrease in strength relative to the direct process since they both tunnel in the L band. Thus this process cannot either explain our results. It may be that different processes are responsible for the TA and LA assisted tunneling.

We will next discuss the origin of the structure that was seen at the k=0 LO phonon energy. This structure, in other semiconductors,[40,41,13,42] has been the subject of much work, both experimental and theoretical. Our experiment did not try to get a detailed line shape for this structure. Our main concern is, therefore, with the general features that we have observed. We will try to explain why structure of this type has been attributed to an electron-phonon self energy effect which causes a modification of the density of states of the semiconductor. We will also try to explain why the structure is anti-symmetric about zero bias (see Fig. 24) and why it has a threshold (see Fig. 34).

First we try to calculate the E(k) relation due to the electron-optical phonon interaction. We have[5], by second

order perturbation theory for the ground state,

$$E = E_0 + \langle 0 | H_{ep} | 0 \rangle + \sum_n \frac{\langle 0 \, H_{ep} \, n \rangle \langle n \, H_{ep} \, 0 \rangle}{E_0 - E_n}$$

where H_{ep} represents the electron phonon interaction

$$H_{ep} = \sum_{q,k} V_q \, a^\dagger_{-q} \, c^\dagger_{k+q} c_k$$

we look at processes of the form

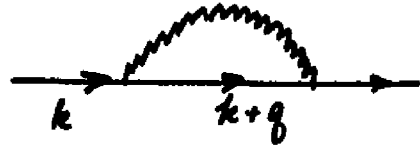

in which an electron at k emits a phonon of momentum q and scatters into a virtual state of energy k+q. Then it re-absorbs the phonon and goes back to the original state. (We will only consider phonon emission processes because we will assume T=0. Assuming a finite temperature would complicate things a little without really adding to what we want to show) The term $\langle 0 | H_{ep} | 0 \rangle = 0$ since $\langle 0 | a^\dagger_{-q} | 0 \rangle$ gives zero. The second term gives $\sum_{kq} |V_q|^2 n_k (1 - n_{k+q}) / \epsilon_k - \epsilon_{k+q} - \hbar\omega_q$ This is the change in the ground state energy of the system when the interaction is turned on. This, however is of small interest to us. The question of interest is really how much energy does it take to put an electron in a state k_0 above the Fermi level. In the absence of the electron-phonon interaction this would just be $E(k_0) = \hbar^2 k_0^2/2m$ but now putting an electron at k_0 does two things. Firstly that electron can do what all the other electrons were doing. That is, it can engage in a process of the form

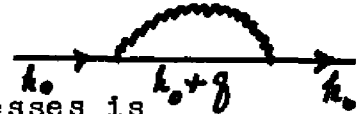

Its increase in energy due to these processes is

$$\sum_q \frac{|V_q|^2 (1 - n_{k_0+q})}{E(k_0) - (E(k_0+q) + \hbar\omega)} = \sum_{k' > k_F} \frac{|V_q|^2}{E(k_0) - (E(k') + \hbar\omega_q)}$$

Also however the electron prevents electrons below the Fermi level from making transitions of the form 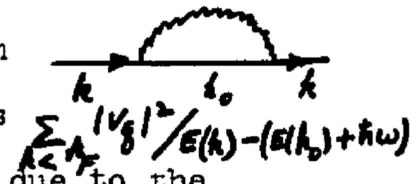

These terms must then be subtracted i.e. terms $\sum_{k<k_F} |V_g|^2 / E(k)-(E(k_0)+\hbar\omega)$ must be subtracted. Thus the change in energy due to the electron phonon interaction is $\sum_{k'<k_F} \frac{|V_g|^2}{E(k_0)-E(k')+\hbar\omega} + \sum_{k'>k_F} \frac{|V_g|^2}{E(k_0)-E(k')-\hbar\omega}$

This is true for k_0 both above and below the Fermi surface. We can use this formula to get a curve of $E(k_0)$ versus k_0^2. Consider a term due to k_0 below the Fermi surface. The second sum has no singularities since $E(k_0) < E(k') + \hbar\omega$ for all k'. The first sum on the other hand has a singularity at $E(k_0) = E(k') - \hbar\omega$. This is illustrated in the drawing.

$0 \quad \overbrace{k_0 \quad k'}^{\hbar\omega_0} \quad k_F$ Actually however for k a little less than k' the terms are large and positive while for k a little greater than k' the terms are large and negative. The singularity at k' is approached in the following way

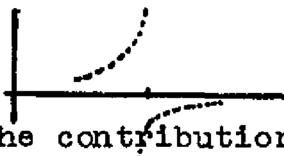

. This cancellation pretty much reduces the contribution of these terms to the sum. This happens for all terms except for terms around k_F. Here the situation looks like $0 \quad \overbrace{k' \, k_F \quad k_0}^{\hbar\omega_0}$. There are few negative terms to cancel the many positive ones. We can work similarly for $k_0 < k_F$. A plot of E vs. k^2 would then look like [41]

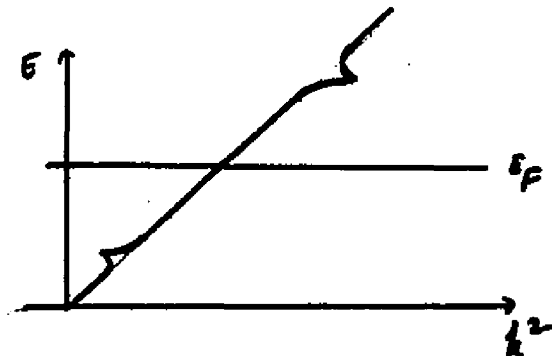

From this dispersion relation we can see that the density of states has anti-symmetric structure around the Fermi energy. The polaron effects in tunneling are ascribed to this anti-symmetric change in the density of states. Hence it would be expected that the tunneling current would reflect this anti symmetric property. The incremental conductance dI/dV is anti-symmetric and d^2I/dV^2 the derivative of dI/dV gives symmetric structure. In contrast to the structure seen for phonons this structure is symmetric and is usually taken to be a strong indication of polaron effects. To try more exactly to correspond the experimental tunneling curves to these theoretical predictions would require a knowledge of barrier penetration probabilities as well as a more exact knowledge of the electron phonon matrix element $V_{kk'}$ (i.e. screening). One interesting thing is predicted by the first term in the sum. If the Fermi degeneracy of the semiconductor is less than the phonon energy there are no singularities in the sum and hence there are no polaron type effects. This would then predict a threshold for the process. In tunneling into Ge where $\mu_F < \hbar\omega_0$ we would not expect to see this polaron type structure, otherwise we would. We do see a threshold but our threshold occurs at $\mu_F = 29mv$ (whereas $\hbar\omega_0 = 40mv$) It is possible that the Fermi degeneracy is not at the postion of the incremental resistance maximum. Thus, what we call $\mu_F = 29mv$ may really correspond to a Fermi degeneracy of 40mv. This does not seem likely. It is also possible that there exists a band tail

on the conduction band.[7] If this band tail did not effect the position of the resistance maximum but did enter self energy calculations it could explain a threshold at instead of $\mu_F = 40mV$. (see below)

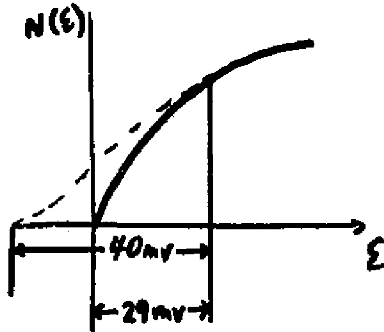

Figure Thirty One

Ratio of TA to LA phonon conductance (at onset) is plotted against Fermi level. The circles were measured directly from curves of dI/dV, while the crosses were measured by integrating measurements of d^2I/dV^2 on the same samples. The lower line is the theoretical prediction of Steinrisser and Davis.

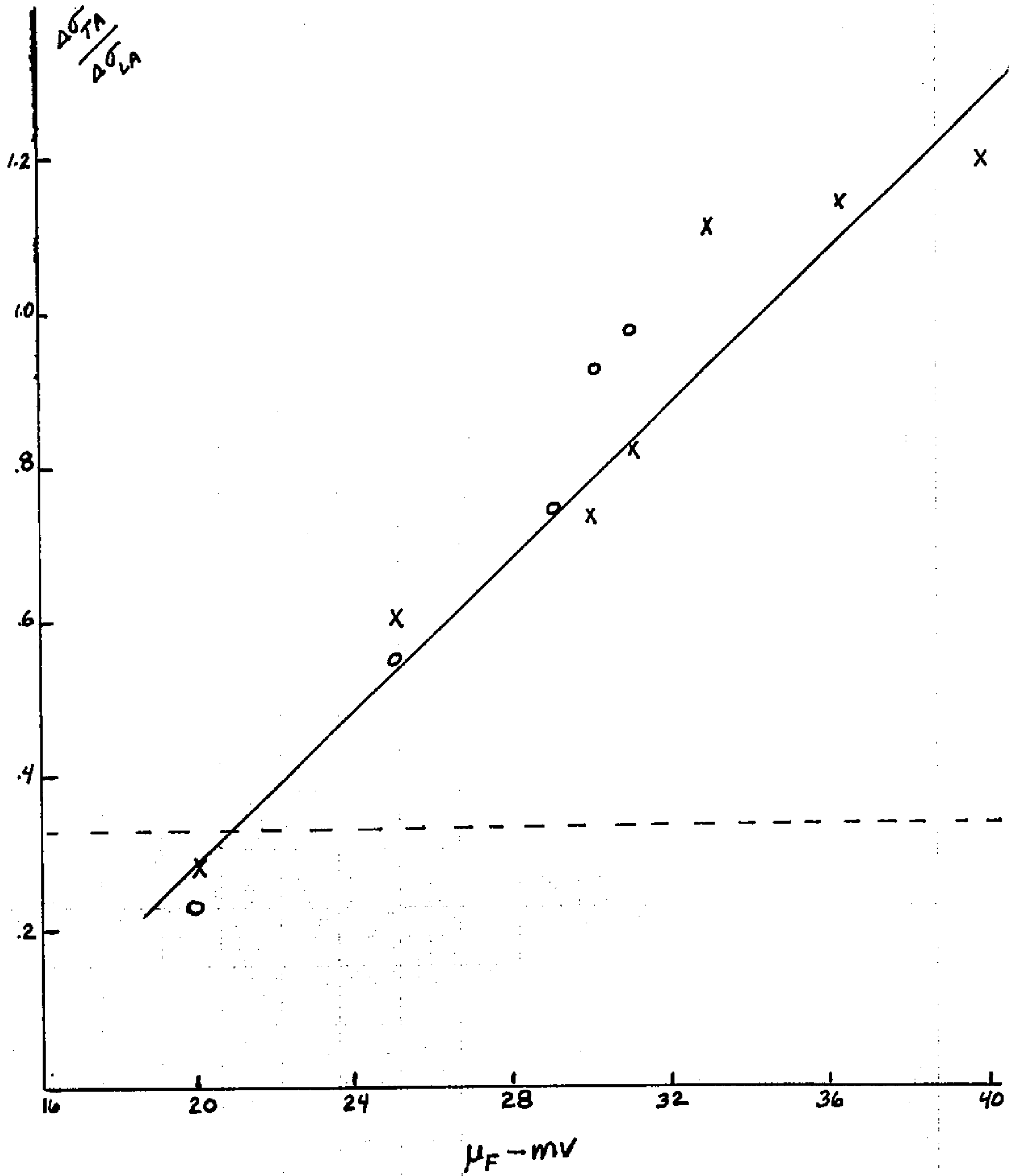

$\Delta\sigma_{TA}/\Delta\sigma_{LA}$
1.2
1.0
.8
.6
.4
.2
16
20
24
28
32
36
40
μ_F → mv

Figure Thirty Two

Schematization, following Davis and Steinrisser, of inelastic phonon-assisted tunneling. For a "first order process", the phonon emission takes place in the depletion region (solid circle) as the electrons at the semiconductor Fermi level (in an L_1 state) drop to the metal Fermi level (in a Γ_{25}' state), at onset. For a "second order process" the phonon emission can take place in the semiconductor (open circles) as the electron (in L_1) transfers to a virtual state (Γ_2') and tunnels to the metal at the metal Fermi level.

Fig 2.

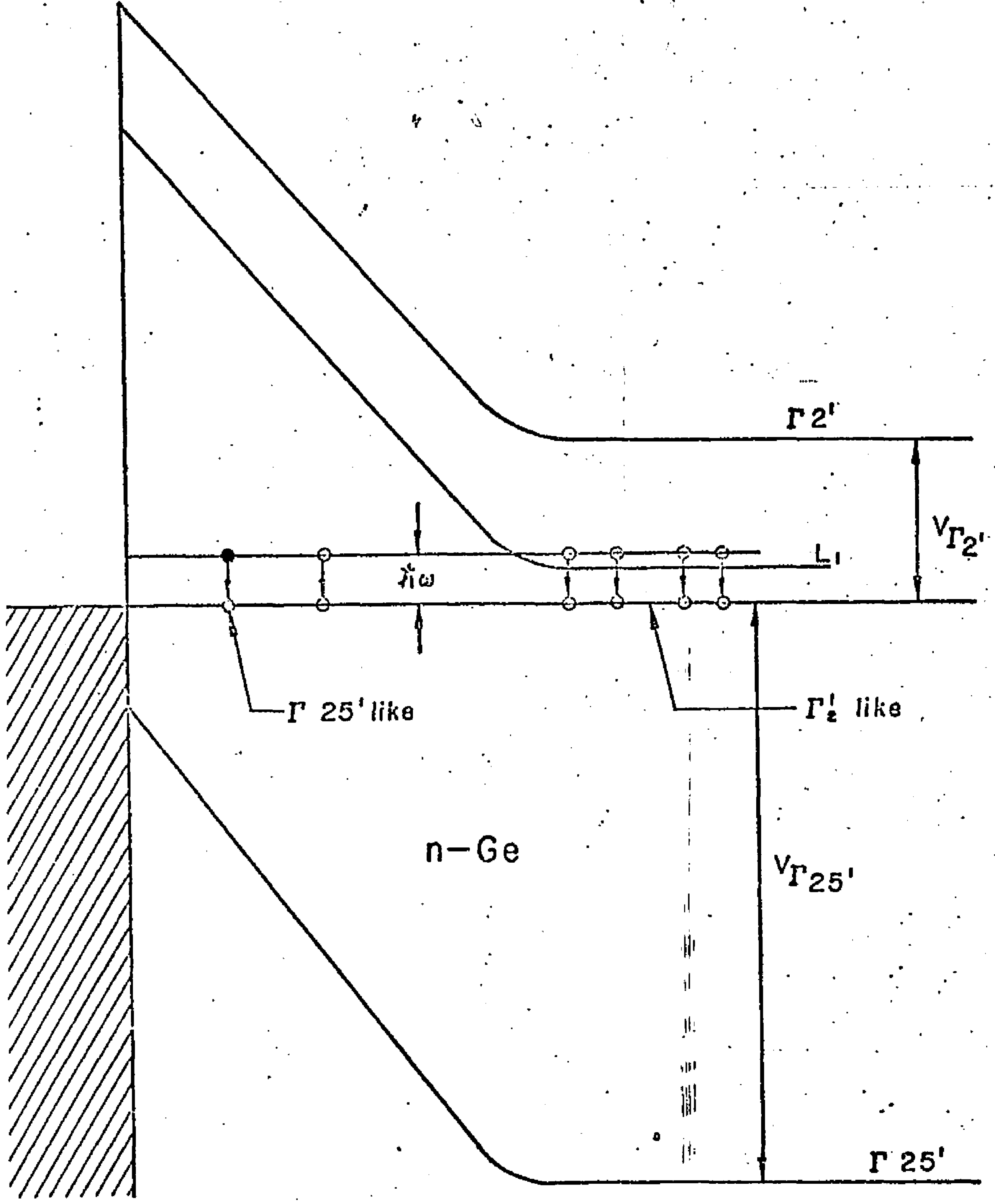

Figure Thirty Three

Absolute phonon conductance as a function of Fermi level for a junction area of 2.5×10^{-4} cm^2. Crosses are experimental points. The solid line is the theoretical prediction of Davis and Steinrisser.[18]

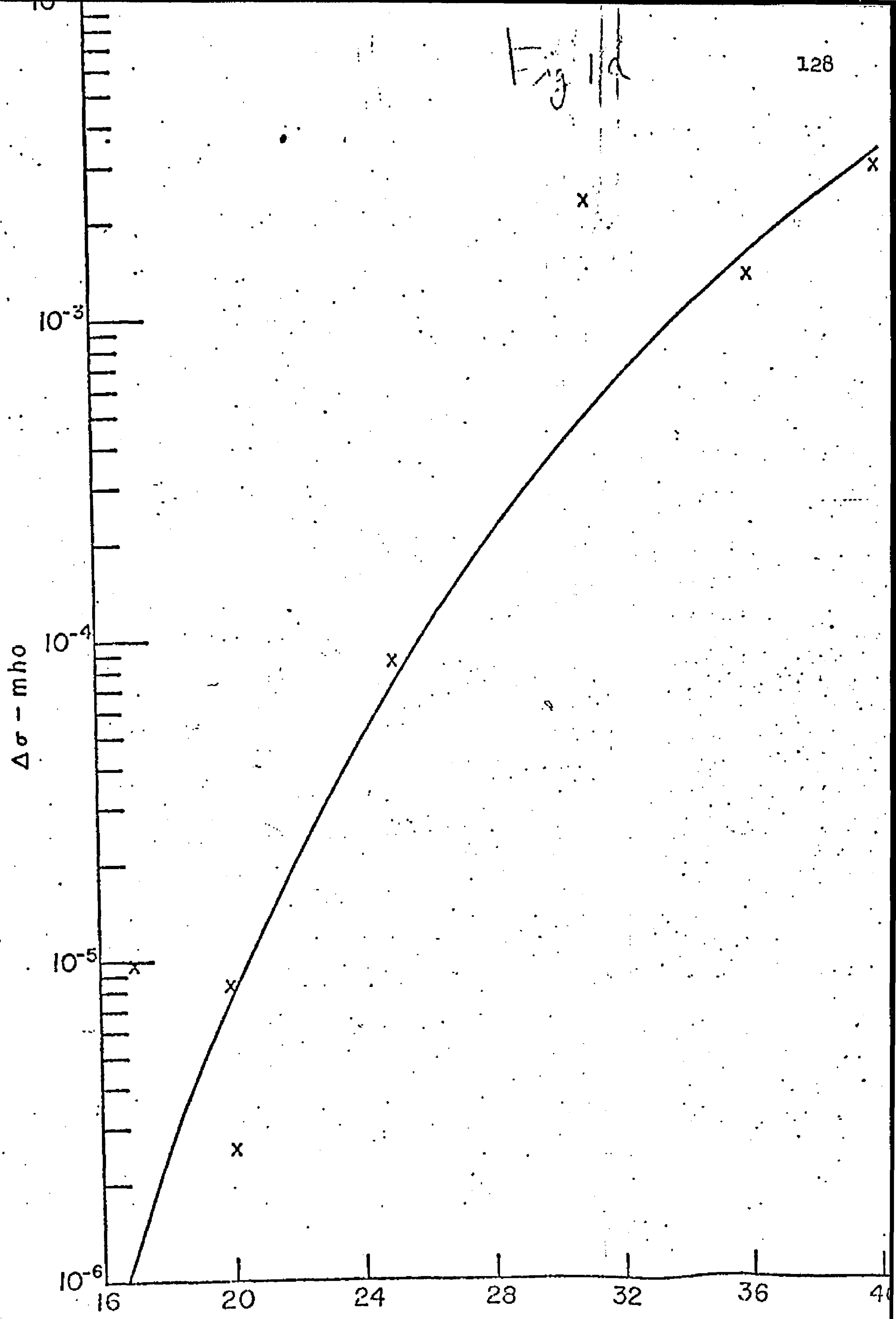

Fig 11d

Figure Thirty Four

Fractional change in conductance, due to the $k=0$ optical phonon, as a function of Fermi level

Fig 29

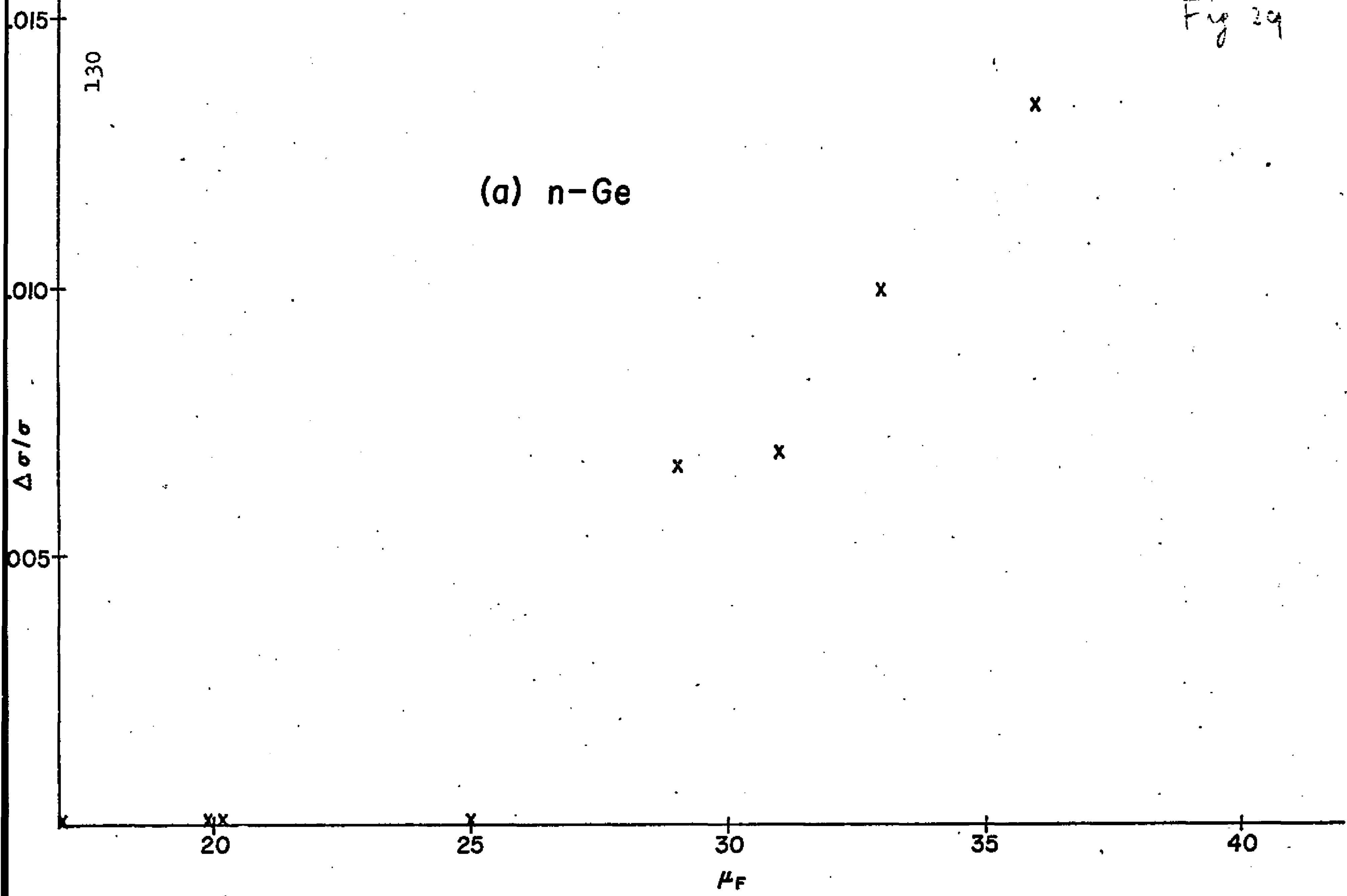

Tunnling Study of the Γ_2' Level in Ge

We have recently been taking measurements at large reverse bias (120mv-170mv) in Ge m-s junctions. The purpose of these measurements was to get a better idea of the participation of the Γ_2' state in m-s semiconductor[17] tunneling as well as the observation of possible band tailing effects seen in optical measurements.[44] Because of the preliminary nature of these results I thought it would be best to include them in a separate section. Since our observations depend greatly upon the technique that we used to take data I would like to explain what we actually measured before discussing any possible conclusions.

We took incremental resistance plots. There was no experimental difficulty associated with these. We also took plots of the incremental resistance as a function of magnetic field. To do this we use the same circuit that we had used for taking incremental resistance plots. In this circuit the D.C. voltage is fed to the sample through a large resistor. Unfortunately this type of circuit has a difficulty associated with it. As a magnetic field is applied to the sample its D.C. and incremental resistance changes. We keep the A.C. current in the circuit constant so that a change in sample incremental resistance is measured as a change in A.C. voltage across the sample. We would like to know this change in incremental resistance as a function of magnetic field, at various fixed D.C. voltages. Actually though, a change in sample resistance also reflects itself in a change in the

D.C. resistance of the sample. Since in our circuit we have a constant D.C. current through the sample, the D.C. voltage across it will depend upon its resistance. Thus as we change the magnetic field the D.C. voltage across the sample changes. Thus, our measurements of the change in incremental resistance due to a magnetic field must be corrected for the change in D.C. bias which accompanies our measurements and influences the change in resistance that we measure. We will give the data in the uncorrected form and explain what influence the corrections would have.

Fig. 35 is a plot of incremental resistance as a function of D.C. bias. Notice in this plot the inflection at 133mv. This decrease in resistance is caused by the ability of the electron to tunnel not only into the L band but into the Γ_1' band as well. This extra channel causes a drop in resistance. We also plot a second derivative curve, for this sample, (Fig. 36) that reflects the slope of the incremental resistance. Notice in this curve that the onset to the band is not sharp. The reason for this may lie in the fact that the density of states of the Γ_1' band is very small near the band edge. Thus tunneling to states at the band edge would be expected to be small and the onset would be consequently smeared. We have also plotted the fractional incremental resistance change as a function of magnetic field (parallel to current direction) at a given D.C. bias (which as we mentioned was not maintained exactly constant). This is shown in Fig. 37. Forgetting,

for the while, about the absolute magnitude of the incremental resistance changes we can see inflections in this curve. These inflections have been seen in p-n junctions and have been attributed to Landau levels. In figure 38 we plot the voltage at which these inflections occur as a function of the magnetic field. The curves that we get are consistent with an intepretation of this structure as being due to Landau levels. By drawing the curves for Landau levels of different order we can extrapolate these curve back to a position of zero field. This is similar to a technique that has been used in optical measurements of the absorption due to the Landau level structure of n-Ge.[43] When we perform this extrapolation we get the band edge. We could also have gotten the band edge by observing, on the plot of incremental resistance, for this sample, the onset ot the Γ_2' band. These two techniques for finding the band bottom agree reasonably well. We have also plotted (Fig. 39) the change in A.C. voltage (for a given magnetic field) as a function of D.C. bias. For this data we have re-set the A.C. voltage across the sample to be 500 microvolts at each measured D.C. bias. As we mentioned earlier the fractional change in incremental resistance reflects in part a change in A.C. resistance due to magnetic field and in part a change in resistance due to the changed D.C. voltage across the sample. One thing that can be noticed is that the fractional change begins to increase at an earlier value than the value of 124mv that would be predicted for the band bottom. We believe this increase

can be attributed to band tailing, already seen in optical work. However, the general shape of the change in fractional incremental resistance is not what we would expect from a simple qualitative model. When we apply a magnetic field we form Landau levels in the conduction band (Γ_1'). If the zero'th order Landau level is 8 mv above the bottom of the band edge (as is expected for H=50Kg, and the g factors of these electrons) we would expect that there would be an ever increasing change in resistance until the zero'th Landau level is reached. Once this Landau level is reached we might expect that the curves with and without magnetic field might tend to approach one another. This might occur due to the increased density of states found in the zero'th Landau level or to a lifetime broadening of the Landau levels. Anyway we might expect that the curve for change in resistance as a function of D.C. voltage would increase, achieve a peak near the Landau level and then decrease. This is the type of behavior that is found in p-n junctions.[9,10] The derivative of this plot with respect to voltage is the change in incremental resistance as a function of D.C. voltage. This plot should then show an increase, then a maximum, go through zero to a negative minimum and finally become zero again. Our incremental resistance plots show no such behavior. Even when we apply the corrections due to changed D.C. bias, we do not alter this basic behavior.

Further, our plots show structure for which we can not account. Although the necessary corrections do somewhat change the shape of this curve they do not eliminate this structure (see Fig. 40)

Magnetic fields have previously been used to investigate surface states. In that experiment[45] the junction had an accumulation layer. The accumulation layer acted like a potential well for the electrons. The electron would be free to move parallel to the surfact but would be confined perpendicular to it. It energy parallel to the surface would not be quantized but the energy due to perpendicular motion would be quantized. Applying a magnetic field perpendicular to the surface would also quantize the motion of the electron parallel to the surface. Thus sharp energy levels would be seen. On the other hand, if the field were directed parallel to the surface it would not cause any further quantization of the electron's energy.

It was found that when the magnetic field was applied parallel to the junction it did not have any effect upon the accumulation layer states. When it was applied perpendicular to the junction it had a pronounced effect. On the other hand the Landau level structure formed by the magnetic field in the bulk conduction band was found not to be sensitive to a change in direction of magnetic field. This is a little strange since in p-n junctions of Ge[9,10] and InSb[8] there are no Landau levels observed for a direction of magnetic field

parallel to the junction. In this case it is thought that the strong electric field in the junction causes a broadening of the Landau levels.which makes them difficult to observe. We felt, therefore, that we could get more information on our junctions by changing the direction of the magnetic field. We therefore modified our sample holder so that we could apply the magnetic field at various angles to the current direction. We found (in the one sample that we measured this way) that the structure depended on the direction of the magnetic field. We are investigating this further.

In other tunneling experiments, structure has often been associated with scattering from impurities.[47] To see whether this was the case in our junctions we took data also in the forward bias direction at these bias voltages. Usually the effect of impurity scattering turns out to be stronger in forward bias. We did not see any structure, so it is unlikely that impurity scattering is the cause of our structure. We also checked the possibility that the structure might be due to the higher conduction band along <100>. If these bands contributed to this structure, they should also affect the tunneling in the absence of a magnetic field. We found no effect at these voltages for zero magnetic field, as measured on a second derivative plot d^2V/dI^2. We thus do not believe that these bands are associated with the structure.

As of the present we do not have an understanding of what is responsible for the magnetic field behavior of these

junctions. We are continuing our experiments taking data which require less corrections and on more samples with different magnetic field orientations.

Figure Thirty Five

Reverse bias plot of incremental resistance as a function of D.C. bias for a Pb-Ge junction. The arrow indicates an inflection on the curve which is taken to indicate the onset of the Γ_2' level. The horizontal scale is 15 mv per box and the point 96.7 mv is indicated on the curve.

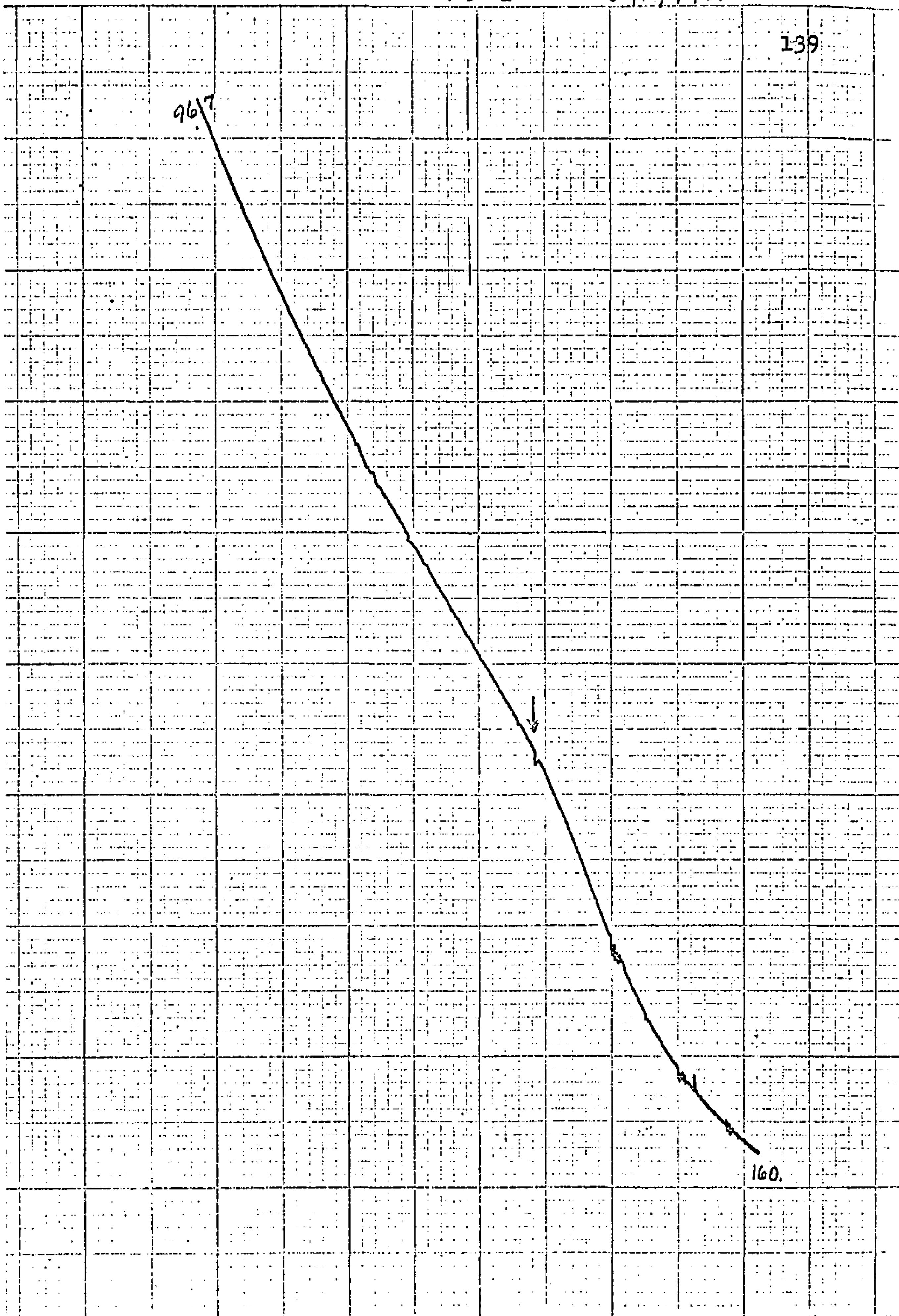
Pb-Ge 5/17/72
139
96.7
160.

Figure Thirty Six

Reverse bias plot of 2nd harmonic voltage vs D.C. voltage for a Pb-Ge junction. This plot shows, more clearly than Fig. 35, the onset of the Γ_2' level (arrow). Horizontal scale is 15 mv per box.

Pb-Ge

2nd derivatieplot f

PAR 500mv

X = 15 mv/"

110 = 1K

R_{DC} = 10K

R_{ac} = 330K

1.2mv | 96.8mv = M

96.8

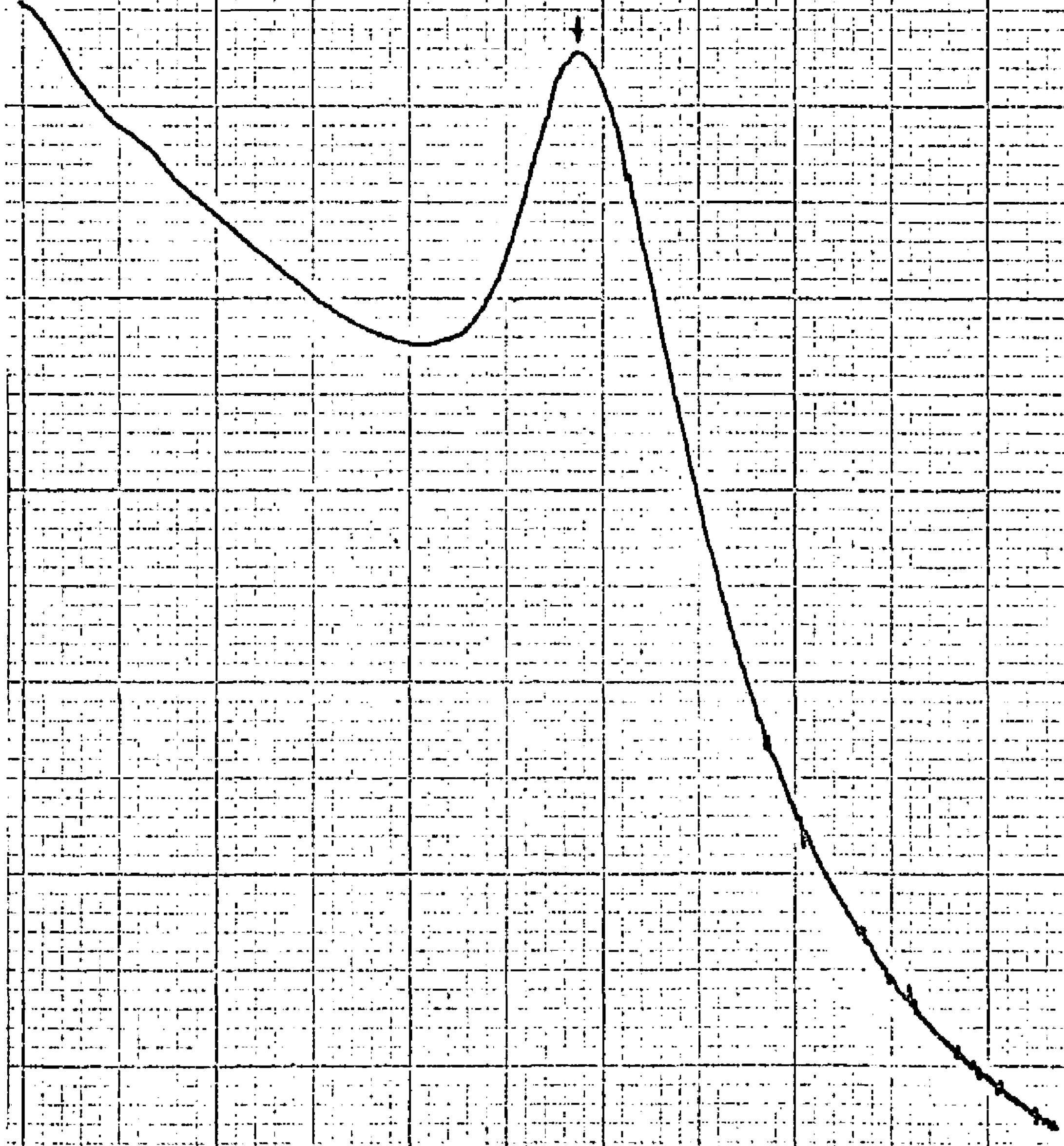

Figure Thirty Seven

Fractional change in resistance (y axis) as a function of magnetic field for large reverse bias (-140mv;Pb-Ge) Each inch in the vertical scale stands for a change of one part in 500. The positions of Landau levels are noted at H=3.4 and H=5.9 .

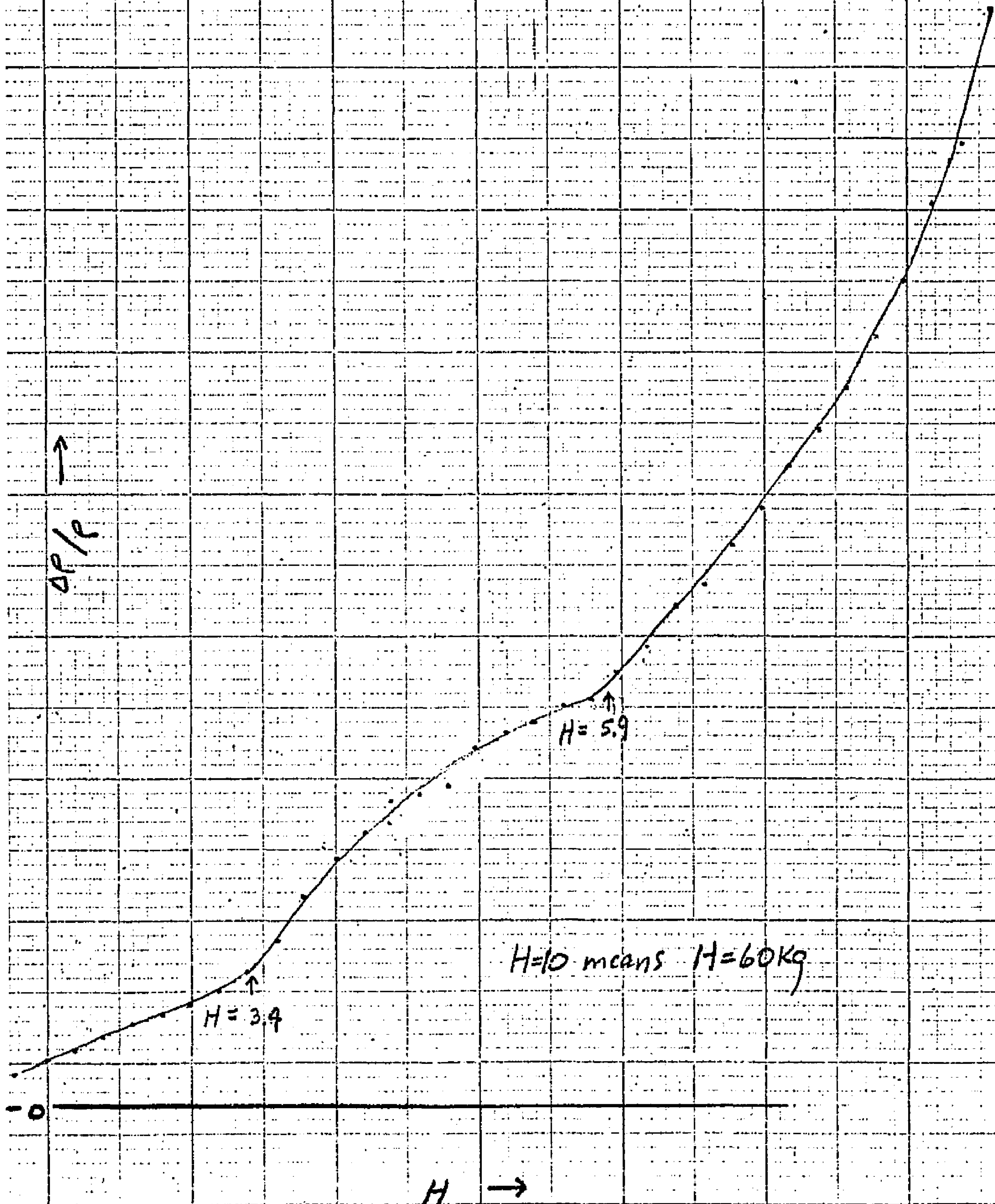
D.C. Bias = 140 mv at H=0
Δρ/ρ
H = 3.4
H = 5.9
H=10 means H=60Kg
0
H

Figure Thirty Eight

Position of Landau levels (for Γ_2' state) is plotted against D.C. voltage. The points were taken from curves such as Fig. 37.

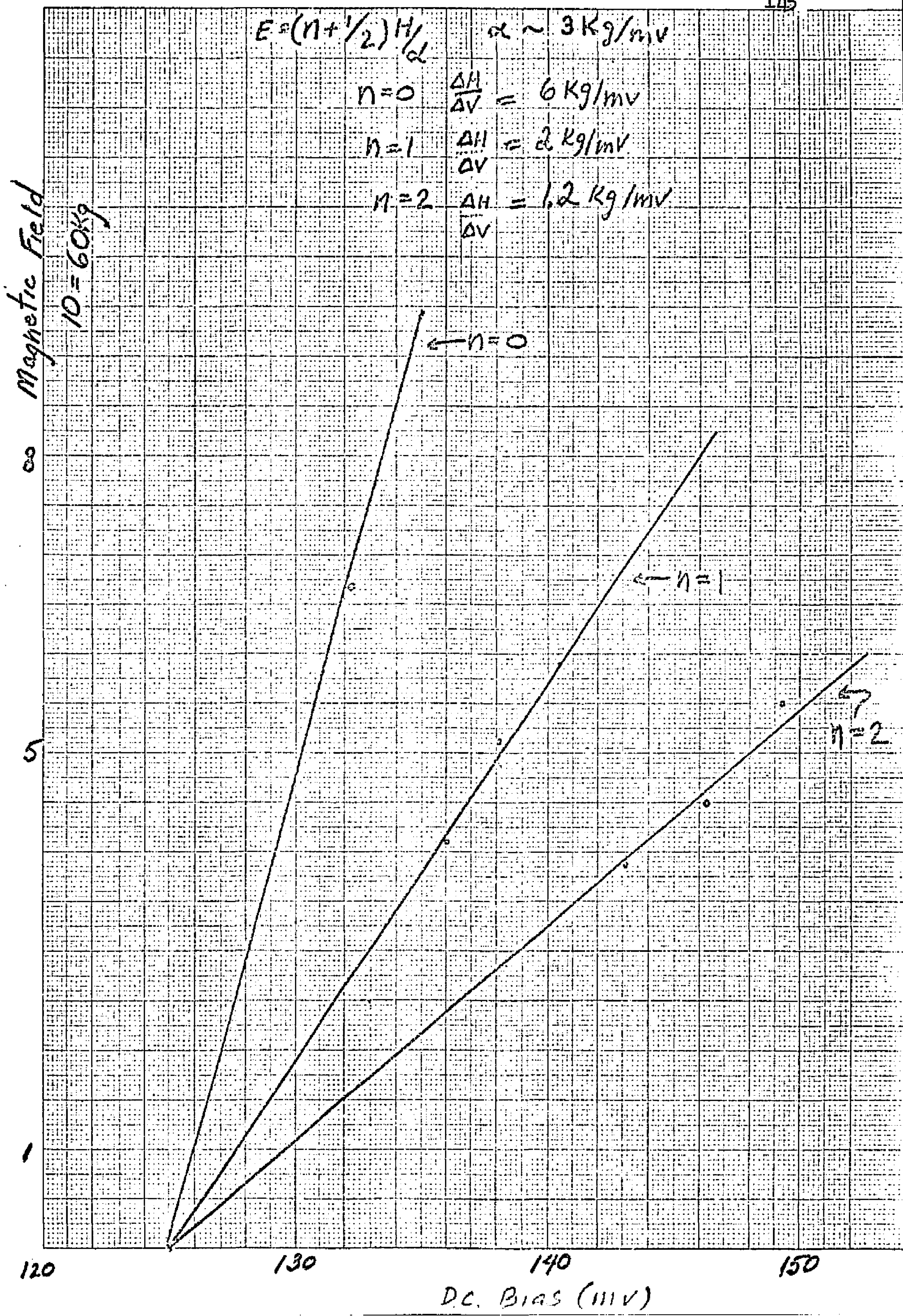

E=(n+1/2)H/α   α ~ 3 Kg/mv
n=0 ΔH/ΔV = 6 Kg/mv
n=1 ΔH/ΔV = 2 Kg/mv
n=2 ΔH/ΔV = 1.2 Kg/mv
Magnetic Field
10 = 60Kg
←n=0
←n=1
n=2
8
5
1
120
130
140
150
D.C. Bias (mV)

Figure Thirty Nine

Fractional change in incremental resistance (for various magnetic fields) is plotted against D.C. bias, for a Sn-Ge junction in reverse bias. One box on the vertical scale means a fractional change of one part in 500.

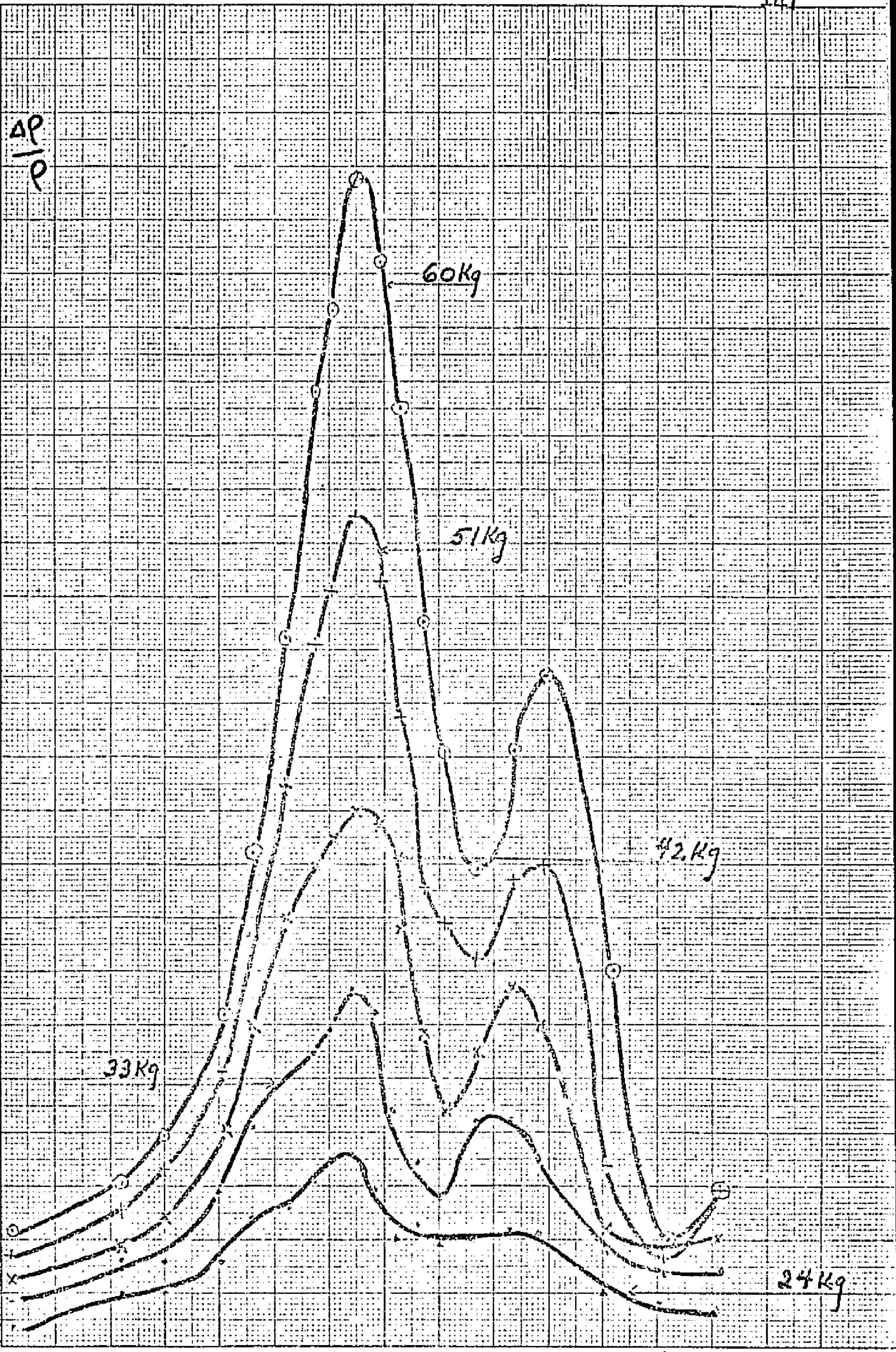
μV
Δρ/ρ
20
10
60Kg
51Kg
42Kg
33Kg
24Kg
100
120
140
160
Bias Voltage.

Figure Forty

Fractional change in incremental resistance, for a Pb-Ge junction in reverse bias, is plotted as a function of D.C. bias for a magnetic field of 45Kg. The upper curve was taken with a constant D.C. bias while in the lower curve the D.C. bias was not kept constant.

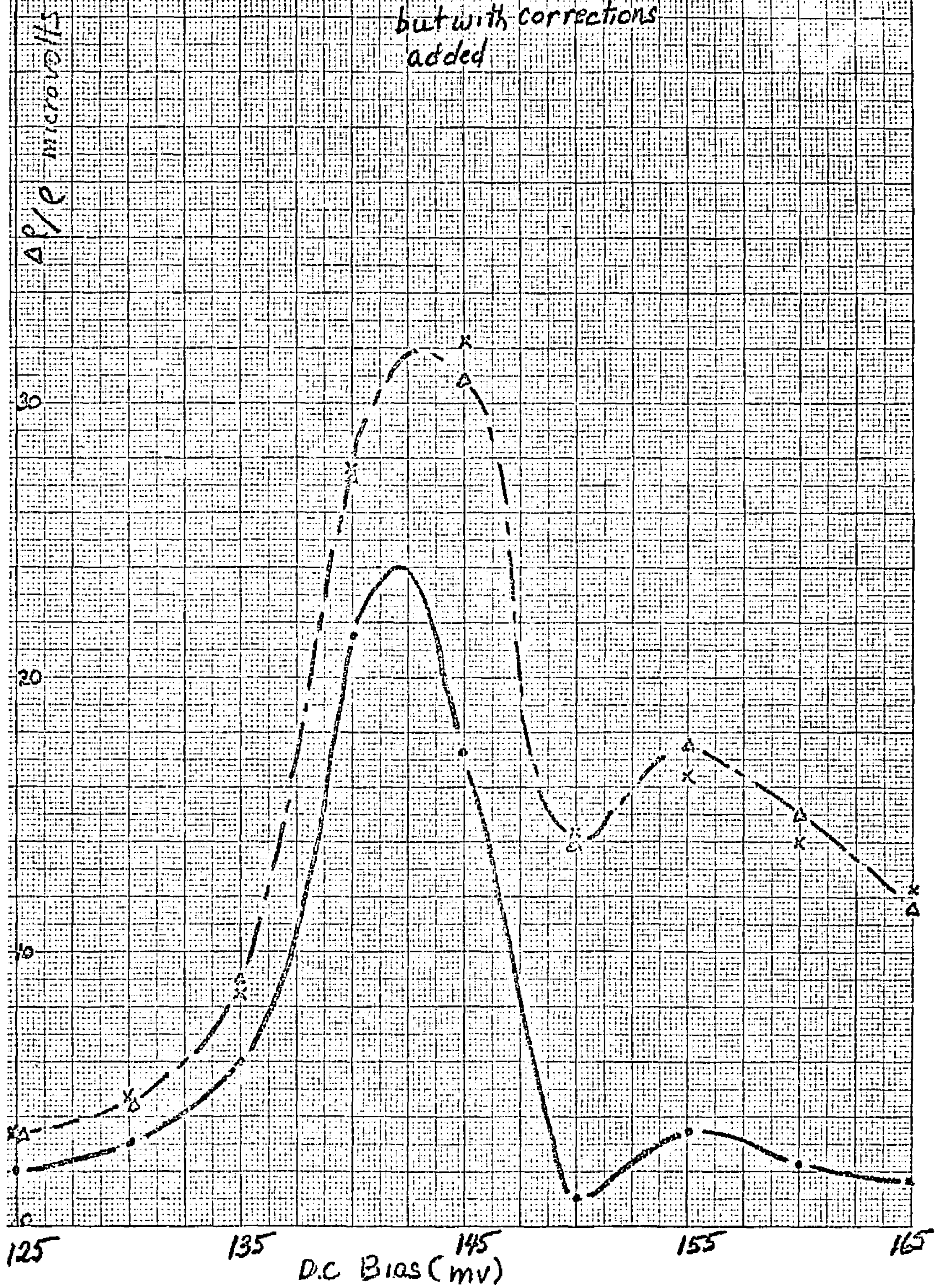

. D.C. Bias not constant
Δ D.C. Bias constant
x D.C Bias not constant but with corrections added
ΔP/e microvolts
30
20
10
0
125
135
145
155
165
D.C Bias (mv)

References

1 A.F.G. Wyatt, Phys. Rev. Letters 13/ 401 (1964)

2 J.M. Rowell and L.Y.L. Shen Phys. Rev. Letters 17/ 15 (1966)

3 Ivar Giaver and Karl Megerle Phys. Rev 122/ 1101(1961)

4 W.A. Harrison Phys. Rev., 123/ 85 (1961)

5 W.A. Harrison Solid State Theory Mcgraw Hill (1970)

6 John P Mckelvey Solid State and Semiconductor Physics Harper and Row (1966)

7 E.O. Kane Phys. Rev 131/ 79 (1963)

8 Chynoweth A.G., Logan R.A. and Wolff P.A. Phys. Rev. Lett. 5/ 548 (1960)

9 H. Roth, W. Bernard, W.D. Straub and J.E. Mulhern Jr Phys. Rev. 145/ 667 (1966)

10 W.Bernard, S.Goldstein, H. Roth,W.D. Straub and J.E. Mulhern Jr. Phys. Rev 166/ 785 (1968)

11 R.T. Payne Phys. Rev. 139/ A570 (1965)

12 Many, Goldstein, Grover Semiconductor Surfaces North-Holland (1965)

13 J.W. Conley and G.D. Mahan Phys. Rev. 161/ 681 (1967)

14 C.B. Duke Solid State Physics Supplement 10 (Tunneling in Solids P 221) Academic Press (1969)

15 A.M. Andrews, H.W. Korb, N. Holonyak, Jr., C.B. Duke and G.G. Kleiman Phys. Rev. B5/ 2273 (1972)

16 J.W. Conley,C.B.Duke, G.D. Mahan and J.J. Tiemann Phys. Rev. 150/ 466(1966)

17 J.W. Conley and J.J. Tiemann J. Appl. Phys
38/ 2880 (1967)

18 L.C. Davis and F. Steinrisser Phys. Rev B 1/ 614 (1970)

19 C.B. Duke S.S. Physics Supp. 10 Chapt. 4

20 Leonard Kleinman Phys Rev. 140/ A637 (1965)

21 Burstein and Lundqvist Tunneling Phenomena in Solids
Chapt. 13 (L. Kleinman) Plenum (1969)

22 D.C. Tsui and L.N. Dunkleberger Appl. Phys. Lett.
18/ 200 (1971)

23 E.L. Wolf and D.L. Lŏsee Phys. Rev. B 2/ 3660 (1970)

24 E.O. Kane J. Appl. Phys. 32/ 83(1961)

25 R.A. Logan and A.G. Chynoweth Phys. Rev. 131/ (1963)

26 L.B. Schein and W.Dale Compton Phys. Rev. B 4/ 1128 (1971)

27 R.C. Jaklevic and J. Lambe Phys Rev. Letters 17/1139 (1966)

28 L.B. Schein and W. Dale Compton Appl. Phys. Lett.
17/ 236 (1970)

29 White Exp. Techniques in Low Temp. Physics, Oxford,
Clarendon Press, 1959

30 R.J. Archer and M.M. Atalla Annals N.Y. Academy of Sciences
101/ 697 (1963)

31 E.L. Wolf and W. Dale Compton Rev. Scientific Instr.
40/ 1497 (1969)

32 G.W. Gobeli and F.G. Allen J. Phys. Chem. Solids 14/23(1960)

33 R.N. Hall Proceedings of the International Conference
on Semiconductors, Prague, 1960

34 D.E. Thomas and J.M. Rowell Rev. Sci. I. 36/ 3701 (1965)

35 G.R. Branner, E.M. Friar, and G. Medicus
Rev. Sci. Instr. 34/231 (1963)

36 J.M. Rowell Tunneling phenomena in Solids Plenum (1969)

37 C.B. Duke and G.G. Kleiman Phys. Rev. B2 1270 (1970)

38 Y. Hsia and Tien-Fan Tao paper presented at Electronic
Density of States Conf. 1969 Maryland

39 A.G. Chynoweth, R.A. Logan and D.E. Thomas Phys. Rev.
125/ 877 (1962)

40 E.L. Wolf, Phys. Rev. Letters 20/ 204 (1968)

41 L.C. Davis and C.B. Duke Phys. Rev. 184/ 764 (1969)

42 D.E. Cullen, E.L. Wolf and W. Dale Compton Phys. Rev.
B 3157(1970)

43 Zwerdling, S., Lax. B, and Roth L.M., Phys. Rev.
108/ 1402 (1957)

44 Pankove, J. Optical Processes in Semiconductors
Prentice Hall (1971)

45 D.C. Tsui Phys. Rev. B 4/ 4438 (1971)

46 G.D. Mahan and J.W. Conley Applied Phys. Letters
11/29 (1967)

47 N. Holonyak Jr., D.L.Keune, R.D. Burnham and C.B. Duke
Phys. Rev. Letters 24/ 589 (1970)

48 R.A. Logan Tunneling Phenomena in Solids Plenum(1969)